Biogeochemistry of the Amazonian Floodplains: Insights from Six End-Member Mixing Models*

Vincent Bustillo*,+,# Reynaldo Luiz Victoria,+,@ Jose Mauro Sousa de Moura,+ Daniel de Castro Victoria,& Andre Marcondes Andrade Toledo, and Erich Collicchio+,++**

+Centro de Energia Nuclear na Agricultura, Laboratório de Geoprocessamento e Tratamento de Imagens, Piracicaba, Brazil
#Université François-Rabelais de Tours, UMR CNRS/INSU 6113 Institut des Sciences de la Terre d'Orléans, Université d'Orléans, Tours, France
@USP–ESALQ, NUPEGEL, Piracicaba, Brazil
&Embrapa Monitoramento por Satélite, Campinas, Brazil
**Universidade Federal de Mato Grosso, UFMT, Campus de Rondonópolis, Rodovia Rondonópolis-Guiratinga, Rondonópolis, Brazil
++Universidade Federal do Tocantins, AgroUnitins, Palmas, Brazil

Received 10 January 2010; accepted 29 May 2010

ABSTRACT: The influence of Amazonian floodplains on the hydrological, sedimentary, and biogeochemical river budget was investigated along the Vargem Grande–Óbidos reach, by applying six mixing models based on variable regional and/or variable hydrological sources. By comparing the output of many different models designed for different purposes, the nature and the magnitude of processes linking water and biogeochemical budgets of the Amazonian

* Supplemental information related to this paper is available at the Journals Online Web site: http://dx.doi.org/10.1175/2010EI326.s1.

* Corresponding author address: Vincent Bustillo, Université François Rabelais de Tours, Parc Grandmont, UFR Sciences et Techniques, Bâtiment E, 37200 Tours, France.
E-mail address: bustillovincent@hotmail.com

DOI: 10.1175/2010EI326.1

floodplains were clarified. This study reveals that most of the chemical baseline of the Amazon River basin is acquired before the studied 2000-km Amazonian reach. However, the tight connection between the hydrograph stage of the river and the chemical signals provides insightful information on the dynamics of its floodplains. The chemical expression of biotic and abiotic processes occurring in the Amazonian floodplains can be particularly perceived during falling waters. It appears delayed in time compared to the maximum extension of submerged area, because the alternating water circulation polarity (filling versus emptying) between the main channel and the adjacent floodplains determines delayed emptying of floodplains during falling waters. It results also in a longer time of residence in the hydrograph network, which strengthens the rate of transformation of transiting materials and solutes. Biotic and biologically mediated processes tend to accentuate changes in river water chemistry initiated upstream, in each subbasin, along river corridors, indicating that processes operating downstream prolong those from upstream (e.g., floodplains of the large tributaries). Conversely, the flood wave propagation tends to lessen the seasonal variability as a result of the water storage in the floodplains, which admixes waters of distinct origins (in time and space). The morphology of floodplains, determining the deposition and the diagenesis of the sediments as well as the variable extension of submerged areas or the chronology of floodplains storage/emptying, appears to be the main factor controlling the floodplains biogeodynamics. By coupling classical end-member mixing models (providing insight on hydrological source) with a variable regional contribution scheme, relevant information on the biogeochemical budget of the Amazonian floodplains can be achieved.

KEYWORDS: Amazon River; Floodplains; Biogeochemical cycles; Sediment dynamics; Diagenesis; CO_2 outgassing

1. Introduction

This paper is dedicated to the study of coupled biogeochemical, sedimentary, and hydrological budgets of the Amazonian floodplains along a 2000-km reach extending between the stations of Vargem Grande (VG) and Óbidos (Óbi).

1.1. Preliminary work

Based on the chemical data of the Carbon in the Amazon River Experiment (CAMREX), biogeochemical mass balances over the studied reach were calculated at 10 sampling sites, well spatially distributed, by comparing incoming and outgoing signals and fluxes (Bustillo 2007) with respect to 44 physicochemical parameters. This approach, based essentially on empirical observations instead of modeling outputs, emphasized that the anomalies of mass balances were mainly related to hydrograph stages and to the hydrological balance of the floodplains. Geochemical and hydrological information were treated in a lumped way, providing thus a pertinent insight on the complex hydrological and chemical linkages normally present between floodplains and river channels. Deliberately based on facts instead of modeling outcomes, this preliminary work raised many intriguing questions with respect to the structure of flux and signal anomalies (e.g., the coarse fraction of particulate organic carbon is very significantly ^{13}C enriched during falling waters). The calculations of mass balances were performed in an exhaustive

way, at the 10 monitoring stations, involving 44 physicochemical parameters over 8 sampling cruises. However, the determinants of flux imbalances remain to be identified.

1.2. Research objectives and challenges

This study aims at deciphering the nature and magnitude of underlying processes driving the transport of particulate and dissolved species toward the ocean and the gaseous exchanges at the river–atmosphere interface, with a special focus on floodplain–channel linkages. This last component is especially significant in large river systems and is highly relevant to contemporary international debates on the human modification of floodplain land use, flood control, and the construction of levees and reservoirs, which all act to decouple floodplains from stream channel environments. Spatially linking tributary streams and longitudinal shifts in hydrology, water chemistry, and sedimentology is therefore a very challenging issue. Achieving this purpose requires testing the validity of the interpretative statements inspired by the empirical observations (preliminary work). The question addressed in this paper can be formulated as follows: what is the actual impact of the floodplains and of their hydrological functioning on the biogeochemical budget of the Amazon River basin?

To these ends, six hydrochemical modeling strategies, based on end-member mixing concept and using tracer-based separation methods, were implemented. These approaches aim to link hydrological pathways and chemical signals in order to couple hydrological and biogeochemical budgets. Comparing the outputs of these different models designed for different purposes is expected to provide a better sense of the whole by better constraining the range of possible interpretations given to the flux imbalances.

1.3. On the use of end-member mixing models

End-member mixing models provide comprehensive understanding of runoff generation processes with a special focus on hydrological pathways, contributive areas, and retention times (Gonzales et al. 2009). However, the direct measurement of each contributive runoff in a continuous way and at a sufficient number of locations is practically impossible (Tardy et al. 2004; Bustillo 2005). Hydrograph separation methods can be divided in two main categories: tracer-based and nontracer-based separation methods. Nontracer-based separation methods are based on the analysis of hydrographs, including a large variety of procedures, including graphical analysis of recession curves, low-pass filtering, unit hydrograph modeling with extrapolation to rising limb of hydrographs, and rating curve methods linking groundwater levels and river flow. Tracer-based separation methods are based on a mass balance approach determined by the conservative mixture in variable proportions of compositionally constant end members (or at least sufficiently stable and distinct from one end member to another to make the procedure achievable). They are usually recognized to deliver valuable information about the groundwater contribution to the river discharge, provided that adequate tracers are selected. The procedure proposed by Hooper et al. (Hooper et al. 1990), which was called end-member mixing analysis and based on the identification of end members by principal component analysis (PCA), was widely applied for studying the hydrology of small

catchments. Its implementation supposes that the water chemistry within each hydrological component is known. At the scale of very large river basins, no such input data can be measured, particularly because of spatial heterogeneities of tracer concentrations and because the fluxes supplied by hydrological reservoirs are not systematically conservative because of in-stream processes and fluvial filtering in river corridors and floodplains (Meybeck and Vörösmarty 2005).

The synthesis of Mortatti (Mortatti 1995) attempted to provide new insights into Amazon River hydrology by gathering biogeochemical and hydrological approaches. However, the hydrograph separation is based on two reservoirs only; although it is very interesting, it proved to be insufficient, particularly because it did not allow capture of the very significant influence of the floodplains on the biogeochemical budget of the Amazon River basin. Despite peculiar cases that are easily corrected case by case, it appears that most large river basins, whatever their morphology and hydroclimatology, are reasonably modeled using the hydrograph separation concept, dividing the total discharge into—at least—three reservoirs.

1.4. Organization of the manuscript

To overcome the difficulties mentioned above, we proposed to investigate the hydrologic function of the Amazon River floodplains, between Vargem Grande (before the confluence of Rio Içá) and Óbidos (the outlet of the studied area), by applying six complementary modeling approaches (including end-member mixing models) to the successive sampling stations located along the main stem of the Amazon. These are based on 1) variable regional sources with (model M2) and without (model M1) correction of inputs by small tributaries; 2) variable hydrological sources with three end members (model M3) to determine their individual compositional evolution, with contrasted response depending on hydrograph stage, throughout their course in the floodplains; 3) variable hydrological sources with three end members, including a correction on the baseflow to account for in-stream biogenic transformations (model M4); and 4) mixed approaches (models M5 and M6) combining the regional variability of chemical signals (between river basins) and the variability related to hydrological source (between contributing runoffs or end members), taking into consideration the defaults of floodplains water balance.

The compositional changes of the chemical baseline in each individual reservoir, set in evidence by comparing their composition within incoming (tributaries) and outgoing (Amazon River reach) runoffs, are more particularly analyzed. By determining hydrological sources and the magnitude of their individual compositional changes, this approach delivers a valuable and original insight on the main factors [hydrological source, water budget of the floodplains, nature of hydrobiological pattern (e.g., photosynthesis versus mineralization, air–water gaseous exchanges, etc.)] driving the biogeochemical and sedimentary budgets of Amazonian floodplains.

2. Study area and dataset

The main physiographic structural elements of the basin include (i) the Precambrian, highly weathered Guyana and Brazilian shields; (ii) the Andean mountains to the west; (iii) the Andean alluvial foreland; and (iv) a large alluvial plain along the Amazon main stem. Soils in the lowlands are generally deep and highly weathered, with widespread covers of sandy podzols in the shields. The soils in floodplains (and alluvial

regions around main stems draining the Andes) are much less weathered because of the continuous input of fresh sediments delivered by physical erosion. The Amazon River and most of its large tributaries have developed extensive floodplains, which are integral parts of the river systems (Richey et al. 1997). After leaving the Andean foothills, the tributaries of the Amazon converge into a large sedimentary plain, where they deposit large volumes of sediments (e.g., Guyot 1993) and inundate the floodplains via an extensive network of drainage channels called paranas. Two distinct types of floodplain channels are (i) tributary channels that drain upland terraces and (ii) distributary channels that transport main-stem Amazon water and sediment to floodplain lake basins. A synthetic view of the Amazon River basin upstream from Óbidos, including the delineation of major subbasins, the location of the sampling station along the Amazon River main stem, and the geographical repartition of small tributaries ungauged during the CAMREX project, is presented (Figure 1).

The samples were collected during the CAMREX project over the period 1982–84 (eight cruises), during contrasted hydrographic stages, completed by five additional cruises between 1985 and 1991 focusing on specific topics, for which an exhaustive dataset is not available (thus not considered in this paper). The objective of CAMREX project was to define by mass balances and direct measurements the processes that control the distribution of bioactive elements (C, N, P, and O) in the main stem of the Amazon River in Brazil. The CAMREX dataset represents a time series unique in its length and detail for very large river systems. The dataset, extracted from Pre-Large-Scale Biosphere-Atmosphere Experiment in Amazonia (PreLBA) compilation (Marengo and Victoria 1998; Richey et al. 2008), consists in representative flux-weighted water samples for comprehensive chemical analysis measured over 18 different sites within a 2000-km reach of the Brazilian Amazon main stem, including seven major tributaries. This dataset constitutes, until that date, the basis of more than 130 CAMREX publications, which have focused on understanding physical and biogeochemical dynamics throughout the basin using a large variety of approaches (e.g., Richey et al. 1990). Monitoring stations are located a few kilometers upstream of the confluence of the seven major tributaries with the Amazon River, Iça, Japura, Jutai, Jurua, Purus, Negro, and Madeira, and along the Amazon River at the 11 following stations: Vargem Grande (VG), Santo Antonio do Içа (SAI), Xibeco (Xib), Tupe (Tup), Jutica (Jut), Anori (Ano), Itapeua (Ita), Manacapurú (Man), São Jose da Amatari (SJA), Paurá (Pau), and Óbidos (Óbi; 4 619 000 km^2; the outlet of the studied area). Thus, it becomes possible to compare the inputs from tributaries and the outputs of the Amazon River at different locations along the longitudinal profile of the main stem.

3. Modeling strategy

Six mixing models of increasing complexity are implemented (Table 1). They belong to three distinct categories. The first category (models M1 and M2) accounts the variable contribution of the subbasins to the biogeochemical budget. The second category relies on end-member mixing models (models M3 and M4), which allow the identification of source reservoirs, supposed to have constant composition but contributing in variable proportion to the river flow. A third category of model, taking into account the variability related to regional contrasts and hydrological source, is also explored (models M5 and M6).

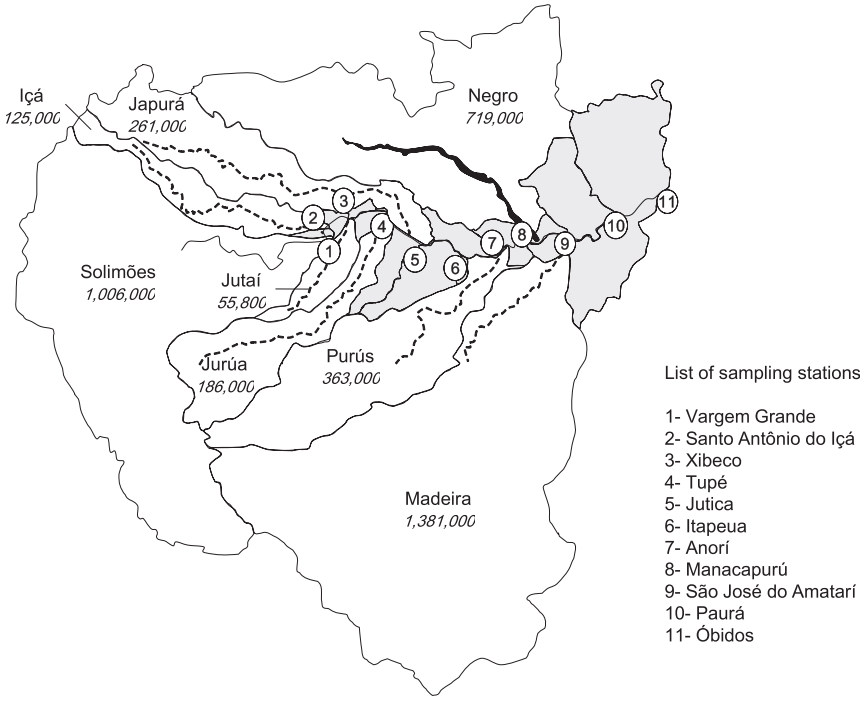

Figure 1. Map of the Amazon basin upstream from Óbi showing the major tributaries and the geographical repartition of small tributaries (areas colored in gray) along the Amazon River main stem. Numbers in italics stand for the drainage area of major subbasins (expressed in km^2).

3.1. Variable regional source

The first model (M1) fundamentally relies on the comparison between calculated and observed longitudinal profiles of concentrations. Upstream, the chemical composition of Rio Solimões constitutes 1) the starting point. Along its course, in low plains, several tributaries join the principal river and modify its chemical composition: the rivers 2) Içá; 3) Jutai; 4) Japurá; 5) Juruá; 6) Purus; 7) Negro; and 8) Madeira, the last one before 9) Óbidos, the outlet of the Amazon River basin chosen in this study. Considering the concentrations C_i^j of each chemical species i, the total discharge Q_t^j of the jth confluent, and before the confluence with the tributary $(j + 1)$, the concentration $C_{i,\mathrm{tot}}^{j+1}$ in the Amazon River after the $(j + 1)$th confluent is established as follows:

$$C_{i,\mathrm{tot}}^{j+1} = \left(C_{i,\mathrm{tot}}^{j} \times \sum_{k=1}^{k=j} Q_t^k + C_i^{j+1} \times Q_t^{j+1} \right) \Bigg/ \sum_{k=1}^{k=j+1} Q_t^k. \tag{1}$$

Subscripts i and superscripts j correspond to the parameter analyzed and to the number of tributaries contributing to the Amazon River flow at each station considered (from $j = 1$ standing for Santo Antonio do Içá to $j = 8$ designating the station

Table 1. Modeling of the Amazon River composition along a 2000-km longitudinal profile. Main principles and rules of calculations of six distinct mixing models: M1 and M2 are based on the variable contribution of regional sources to water and biogeochemical budgets; M3 and M4 rely on the variable contribution of hydrological sources (viz., forwarded direct runoff RS, delayed direct runoff RI, and baseflow RB) with a correction for M4 taking into account the influence of the river processes; and M5 and M6 are composite models taking into account the combined effects of the variable contributions relative to the regional and hydrological sources. Note that *i* is the index of the chemical species ($n_i = 44$), *j* is the index of the monitoring station ($n_j = 10$), and *k* is the index of the sample ($n_k = 8$).

Model	Principle	Rule of calculation
M1	Variable contribution of major tributaries	$\mathrm{C}(ijk) = \Sigma\Sigma\Sigma\,[\mathrm{C}ijk, t \times Q(jk, t)/Q_t(jk)]$
M2	Step 1: Variable contribution of major tributaries Step 2: Mean concentration of the additional flow (small tributaries and alluvial aquifers)	$C(ijk) = C(ijk)$, M1 $\times\, Q_{\mathrm{in}}(jk)/Qo(jk) + Cij(v) \times [Qo(jk) - Q_{\mathrm{in}}(jk)]/Qo(jk)$
M3	End-member mixing models: Three reservoirs RS: forwarded direct runoff; RI: delayed direct runoff; RB: baseflow	$C(ijk) = Cij(\mathrm{RS}) \times Q\mathrm{RS}\,(jk)/Q_t(jk) + Cij(\mathrm{RI}) \times Qjk(\mathrm{RI})/Q_t(jk) + Cij(\mathrm{RB}) \times Q\mathrm{RB}(jk)/Q_t(jk)$
M4	Step 1: Variable contribution of major tributaries Step 2: End-member mixing models taking into account biotic processes	$Cijk(\mathrm{RB}) = Cij(\mathrm{RB}),\, 0 + K_{\mathrm{BIO}}(ij) \times I_{\mathrm{BIO}}(jk)$
M5	Step 1: Variable contribution of major tributaries Step 2: End-member mixing models calibrated on the relative differences ($\Delta\mathrm{C}ijk$)	$\Delta\mathrm{C}ijk = f$ (3 covariates) $\Delta(Q\mathrm{RS}/Q_t)$, $\Delta(Q\mathrm{RI}/Q_t)$, and $\Delta Q_t(\mathrm{I} - \mathrm{O})$
M6	Step 1: Variable contribution of major tributaries Step 2: End-member mixing models calibrated on the relative differences ($\Delta Cijk$)	$\Delta Cijk = f$ (2 covariates) 1) River discharge Q_t 2) Default of water balance $\Delta Q_t(\mathrm{I} - \mathrm{O})$

of Óbidos), respectively. Assuming conventionally that $Q^{j}_{\text{tot}} = \sum_{n=1}^{n=j} Q^{n}_{\text{tot}}$ and $Q^{j+1}_{\text{tot}} = \sum_{n=1}^{n=j+1} Q^{n}_{t}$, one obtains

$$C^{j+1}_{i,\text{tot}} = (C^{j}_{i,\text{tot}} \times Q^{j}_{\text{tot}} + C^{j+1}_{i} \times Q^{j+1}_{t})/Q^{j+1}_{\text{tot}}. \tag{2}$$

After the jth confluent, $C^{j+1}_{i,\text{tot}}$ becomes $C^{j}_{i,\text{tot}}$, and the cumulative runoff changes from Q^{j+1}_{tot} to Q^{j}_{tot}.

For each parameter, the concordance between theoretical (i.e., calculated) and observed longitudinal profiles is appreciated by analyzing the fitting capability of the simple linear model,

$$C^{j}_{i}(\text{obs}) = \alpha^{j}_{i} \times C^{j}_{i}(\text{calc}) + \beta^{j}_{i}. \tag{3}$$

The correlation coefficient r^2 is calculated for each parameter ($n_i = 44$) and each station ($n_j = 10$). The results of calibration are given in the appendix (Table A2). Then, the slope α^{j}_{i} (ideally close to 1) and the intercept to origin β^{j}_{i} (ideally close to 0) are considered. Finally, the mean bias B is calculated as follows:

$$B^{j}_{i} = \frac{\sum_{k=1}^{k=Nk} C^{j}_{i,k}(\text{calc}) - \sum_{k=1}^{k=Nk} C^{j}_{i,k}(\text{obs})}{N^{j}_{i,k}}, \tag{4}$$

where k indexes the number of the sample and $N^{j}_{i,k}$ for the number of samples for each station and each parameter. This bias, calculated on average discharge-weighed values, allows estimating the mean chemical composition of floodplains and small tributaries $C^{j}_{i}(\upsilon)$, assuming that measured biases depend on their variable contribution to river flow. The model M2 corrects M1 by taking into account the mean composition of small tributaries and floodplains. The composition of the additional flow (small tributaries plus alluvial aquifers), noted $C^{j}_{i}(\upsilon)$, is estimated by the analysis of differences (composition and flow) between the sum of major tributaries (calculated input), $\Phi^{j}_{i}(\text{in}) = C^{j}_{i}(\text{in}) \times Q^{j}_{t}(\text{in})$, and the output (measured output), $\Phi^{j}_{i}(\text{out}) = C^{j}_{i}(\text{out}) \times Q^{j}_{t}(\text{out})$, corresponding to the river water composition at the considered station:

$$\begin{aligned} C^{j}_{i}(\upsilon) &= \left[\Phi^{j}_{i}(\text{out}) - \Phi^{j}_{i}(\text{in})\right]/Q^{j}_{t}(\upsilon) \\ &= \left[C^{j}_{i}(\text{out}) \times Q^{j}_{t}(\text{out}) - C^{j}_{i}(\text{in}) \times Q^{j}_{t}(\text{in})\right]/[Q^{j}_{t}(\text{out}) - Q^{j}_{t}(\text{in})]. \end{aligned} \tag{5}$$

Finally, the concentrations obtained through the model M2 for each cruise are given by

$$C^{j}_{i,k}(\text{M2}) = \left\{C^{j}_{i,k}(\text{M1}) \times Q^{j}_{t,k} + C^{j}_{i}(\upsilon) \times \left[Q^{j+1}_{t,k} - Q^{j}_{t,k}\right]\right\} \Big/ Q^{j+1}_{t,k}. \tag{6}$$

To test the model fitting capability, linear equations comparable to those presented above for M1 are also calibrated for M2. By averaging the estimations of all the

samples, it must be reminded that $B_i^j = 0$ for each station and each parameter in the case of M2.

3.2. Variable hydrological source

The third model (M3) relies on the hydrograph separation into three components: the superficial runoff RS, the interflow RI, and the baseflow RB. These reservoirs are meant as the expression of spatially organized tributary basins with vertical (top–bottom in soils) and upstream–downstream gradients involving three mixing end members:

- RS tracking superficial and hypodermic pathways that arise more particularly in upstream areas, which provide most of the solid load transported by fluvial systems;
- RI tracking superficial and hypodermic pathways that arise more particularly in downstream areas where deep leached soils provide waters of low dissolved (except for organic matter) and solid loads; and
- RB tracking groundwater pathways, corresponding to the leaching of the soil horizon C (permeable saprolite) that occasionally emerge in the gleysols of lowlands, as inferred from the very characteristic ^{18}O enrichment of waters (Tardy et al. 2009).

The identification of these three components relies upon chemical tracing. The concentrations of Na^+ and fine suspended sediment [FSS] are selected as the best tracers (Tardy et al. 2005). The fluctuations of [Na^+] track the processes of dissolution and evaporation, which tend to generate a concentration gradient from the superficial layer of soil to groundwaters that are directly at the contact with the chemical front of alteration. On the other hand, the fluctuations of [FSS] track the soil erosion, which is almost specific of surface runoff. The chemical tracers in each reservoir determine the contribution of these source reservoirs to the total river flow Q_t by solving the system of equation composed of two equations of mass conservation for each tracer [Equation (7)] and the equation of flow conservation [Equation (8)],

$$C_{i,k}^j = C_i^j(\mathrm{RS}) \times Q\mathrm{RS}_k^j/Q_{t\,k}^{\ j} + C_i^j(\mathrm{RI}) \times Q\mathrm{RI}_k^j/Q_{t\,k}^{\ j} + C_i^j(\mathrm{RB}) \times Q\mathrm{RB}_k^j/Q_{t\,k}^{\ j} \quad \text{and} \tag{7}$$

$$Q\mathrm{RS}_k^j + Q\mathrm{RI}_k^j + Q\mathrm{RB}_k^j = Q_{t\,k}^{\ j}, \tag{8}$$

where j indexes the considered subbasin and i the parameter used as a chemical tracer.

Here [Na^+] and [FSS] within each reservoir correspond to the values established by Tardy et al. (Tardy et al. 2005). The next step consists in adjusting C_i^jRS, C_i^jRI, and C_i^jRB to the whole dataset (42 parameters, excluding the 2 tracers) by performing multilinear regressions. As a result, we define statistically the most probable composition of each reservoir RS, RI, and RB. End-member mixing models are calibrated for each of the 10 stations located along the Amazon River

main stem (from Saõ Antonio do Içá to Óbidos) but also for each of the eight major tributaries. Then, the decomposition of hydrograph is performed theoretically by cumulating the reservoir inflow Q_K of each tributary (trib) to each station ($1 \leq j \leq 8$),

$$Q_K^{j+1} = Q_K^j + Q_{K,\text{trib}}^{j+1}, \tag{9}$$

where K is the index for hydrological reservoirs, RS, RI, or RB. Consequently, for each hydrological node, two models of repartition are implemented. The first one is calibrated using chemical data measured at each of the 10 stations, whereas the second one is calibrated using a calculated pool of chemical data, corresponding to the variable spatial contribution of subbasins to the Amazon River discharge. It is expected that differences between the chemical characteristics of reservoirs are good indicators of floodplains biogeodynamics. A full dataset is provided in the appendix (Table A3).

3.3. Biologically mediated processes

The biological control of chemical factors in river, popularized by Redfield (Redfield 1958), is evaluated in the model M4 by testing the influence of biotic processes on the composition of the baseflow RB. The protocol of calculation for evaluating $Q\text{RS}(j)$, $Q\text{RI}(j)$, and $Q\text{RB}(j)$ is identical to that of the model M3. The composition of baseflow is supposed to be variable as a function of biological pathway tracked with the synthetic variable I_{BIO},

$$I_{\text{BIO}\,k}^{\ j} = [\text{O}_2]_k^j - [\text{CO}_2]_k^j. \tag{10}$$

In the case of intense photosynthesis, O_2 is actively produced while CO_2 is removed and consequently I_{BIO} increases. Conversely, when the decomposition prevails, CO_2 is actively produced while O_2 is removed and consequently I_{BIO} diminishes. The model M4 is formalized as follows:

$$\begin{aligned} C_{i,k}^j = {} & C_i^j(\text{RS}) \times Q\text{RS}_k^j / Q_{t\,k}^{\ j} + C_i^j(\text{RI}) \times Q\text{RI}_k^j / Q_{t\,k}^{\ j} \\ & + \left[C_i^j(\text{RB}) + K_{\text{BIO}\,k}^{\ j} \times I_{\text{BIO}\,k}^{\ j}\right] \times Q\text{RB}_k^j / Q_{t\,k}^{\ j}, \end{aligned} \tag{11}$$

with $K_{\text{BIO}\,i}^{\ j}$ corresponding to the rate of uptake or release of each bioactive element (i) for each station (j) associated to biologically mediated processes in the river water. If $K_{\text{BIO}\,i_j}^{\ j} > 0$, the concentration increases when the photosynthesis pathway prevails ($I_{\text{BIO}\,k}^{\ j} > 0$) and decreases when the mineralization predominates ($I_{\text{BIO}\,k}^{\ j} < 0$). The mineralization leads to the removal of dissolved O_2 and to the release of CO_2. That is the reason why I_{BIO} associated to mineralization paths is usually negative and potentially very negative. Therefore, $K_{\text{BIO}\,i}^{\ j} < 0$ indicates that the concentration increases when mineralization pathway prevails ($I_{\text{BIO}\,k}^{\ j} < 0$) and decreases when photosynthesis predominates ($I_{\text{BIO}\,k}^{\ j} > 0$). In the case of isotopic data ($\delta^{18}\text{O}$, $\delta^{13}\text{C}$) that are all negative, the interpretation of $K_{\text{BIO}\,i}^{\ j}$ is inverted. For simplification purposes, the signs of $K_{\text{BIO}\,i}^{\ j}$ associated to isotopic values were systematically inverted to homogenize the deciphering for all the parameters. Full model outcomes relative to M4 are presented in the appendix (Table A4).

3.4. Composite approach

The model M5 is a composite approach that integrates both variable spatial contribution (M1) and variable hydrological source (end-member mixing models). First, we establish for each cruise k ($Nk = 8$) each parameter i and each hydrological node j, the relative difference, noted $\Delta C_{i,k}^{j}$, between calculated (calc) and observed (obs) values, as follows:

$$\Delta C_{i,k}^{j} = \frac{C_{i,k}^{j}(\text{obs}) - C_{i,k}^{j}(\text{calc})}{C_{i,k}^{j}(\text{calc})} \tag{12}$$

The second step consists in relating this relative difference with several factors. We have selected three covariates corresponding to the relative differences $\Delta(Q\text{RS}/Q_t)$, $\Delta(Q\text{RI}/Q_t)$, and ΔQ_t:

$$\Delta C_{i,k}^{j} = \alpha_i^j \times \Delta(Q\text{RS}/Q_t)_k^j + \beta_i^j \times \Delta(Q\text{RI}/Q_t)_k^j + \gamma_i^j \times \Delta Q_{tk}^{\ j} + \delta_i^j, \tag{13}$$

with

$$\begin{cases} \Delta(Q\text{RS}/Q_t)_k^{\ j} = (Q\text{RS}/Q_t)_k^{\ j}, M_3/(Q\text{RS}/Q_t)_k^{\ j}, M_1 - 1 \\ \Delta(Q\text{RI}/Q_t)_k^{\ j} = (Q\text{RI}/Q_t)_k^{\ j}, M_3/(Q\text{RI}/Q_t)_k^{\ j}, M_1 - 1 \\ \Delta\, Q_{tk}^{\ j} = Q_{t\,k}^{\ j}, \text{obs}/Q_{t\,\text{tot},k}^{\ j} - 1 \end{cases}. \tag{14}$$

The term δ_i^j in Equation (13) stands for the residual relative difference $\Delta C_{i,k}^{j}$ when the three following conditions are fulfilled:

$$\text{(i) } \Delta(Q\text{RS}/Q_t)_k^{\ j} = 0\,;\ \text{(ii) } \Delta(Q\text{RI}/Q_t)_k^{\ j} = 0\,;\ \text{and (iii) } \Delta\, Q_{t\,k}^{\ j} = 0.$$

The coefficients α_i^j, β_i^j, and γ_i^j, estimated by multilinear regressions, provide qualitative information on river diagenesis in RS (surface runoff), RI (interflow), and Q_t (total runoff). If the coefficient is positive, it indicates that the concentration increases in the correspondent runoff as the individual discharge Q_K increases. Considering the total river flow Q_t, the sign of γ_i^j indicates whether the discharge of floodplains, roughly estimated by $\Delta Q_{t\,k}^{\ j} = Q_{t\,k}^{\ j}/Q_{t\,\text{tot},k}^{j} - 1$, contributes to increase or decrease the chemical concentration of the chemical parameter i in the river water at the station j. Values of QRS, QRI, QRB, and Q_t are given in the appendix (Table A1 and Figure A1), with M3 corresponding to model-derived data and M1 corresponding to data calculated from upstream subbasins. A complementary approach (M6) consists in evaluating the combined effect of the total discharge $Q_{t\,k}^{\ j}$ and its excess or deficit $\Delta Q_{t\,k}^{\ j}$,

$$\Delta C_{i,k}^{j} = \alpha_{2\,i}^{\ j} \times \Delta Q_{t\,k}^{\ j} + \beta_{2\,i}^{\ j} \times Q_{t\,k}^{\ j} + \gamma_{2\,i}^{\ j} \times Q_{t\,k}^{\ j} \times \Delta Q_{t\,k}^{\ j} + \delta_{2\,i}^{\ j}. \tag{15}$$

The calibration of these four coefficients ($\alpha_{2\,i}^{\ j}, \beta_{2\,i}^{\ j}, \gamma_{2\,i}^{\ j}$, and $\delta_{2\,i}^{\ j}$) for each sampling station and each parameter leads to synthetic 3D diagrams (see Figure A2),

which allow describing the compositional fluctuations of the river water as a function of the river discharge $Q_{t\,k}^{\,j}$ and the default of water balance $\Delta\, Q_{t\,k}^{\,j}$.

4. Results and discussion

After a brief comparison of the five models in term of statistical resolution capability, the information supplied individually by each method is analyzed. The analysis of their mutual consistency is more particularly performed.

4.1. Compared performance

The agreement between calculated and observed water composition is very significant for most of the parameters. The cumulative distribution of correlation coefficient for five tested models is presented in Figure 2. This indicates that 50% of the parameters modeled by M1 exhibit $r^2 > 0.75$. Unexpectedly, M1 provides better results than M2, suggesting that floodplains are not of constant composition, contrary to the assumption underlying the approach M2. The comparison between M3 and M4 reveals a significant improvement of the performance of end-member mixing models by taking into account the "hydrobiological index" I_{BIO}, which allows identifying the parameters influenced by in-stream processes. The level of performance remains deficient (threshold arbitrarily fixed to $r^2 < 0.60$) on 25% of parameters for M4 versus 50% of parameters for M3. Finally, the mixed approach (M5) combining variable spatial contribution and end-member mixing models constitutes a very convenient compromise, which provides the best results.

4.2. Variable regional contribution (M1 and M2)

The simple approach consisting in correlating incoming (theoretical and calculated) and outgoing (measured) concentrations (M1) provides insightful information. It appears that most of linear calibrations are very significant, except for SO_4^{2-}, HPO_4^{2-}, coarse fraction of suspended sediment (CSS), particulate organic carbon (POCC), nitrogen (PONC), and C/N (in all fractions). These deficiencies reveal that substantial modifications occur in the floodplains.

Table 2 delivers the mean values of α (slope), β (intersect of line for $x = 0$), r^2 (correlation coefficient), bias, and average for each parameter and for the 10 sampling stations located along the Amazon main stem. These linear calibrations indicate that the compositional fluctuations of river water in the Amazon reach might be greater than those impulsed by the tributaries inputs ($\alpha > 1$ and $\beta < 0$) for pH, K^+, Mg^{2+}, NO_3^-, CO_2, NaSil, KSil, CaSil, MgSil, dolomite, and FR. For example, when the inflow defines a low pH, the outflow is still more acidic and conversely, when the inflow defines an elevated pH, the outflow is more basic. Considering the parameters listed before, the open system dynamics along the Amazon main stem (and in its floodplains) accentuate the chemical perturbations initiated upstream, in the subbasins. Conversely, the compositional fluctuations generated in the tributaries tend to be buffered in the outflow ($\alpha < 1$ and $\beta > 0$) for other parameters such as Ca^{2+}, HCO_3^-, DIC, Cl^-, DOC, O_2, CSS, POCC, C/N (all the fractions), dissolved and particulate organic nitrogen, and [$CaCO_3$].

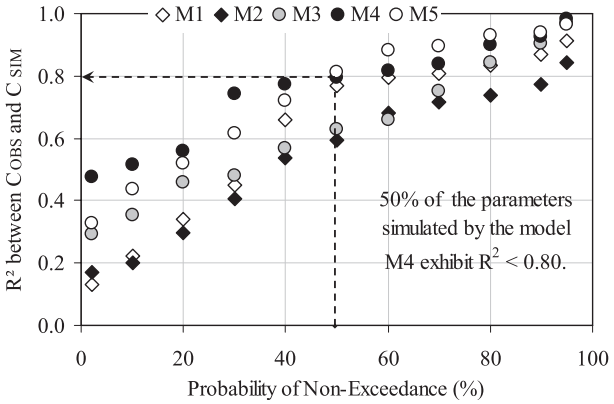

Figure 2. Compared performance of the five hydrochemical models (M1–M5) based on the probability of nonexceedance of the determination coefficient r^2 established by confronting simulated and observed concentrations (or isotopic values). Data represented are obtained by gathering the results of 42 chemical parameters for the station of Óbi, outlet of the studied reach.

A complementary analysis of Table 2 consists in assessing the bias between the concentrations in the inflow and in the outflow. Positive values (bias > 0) indicate that concentrations in the inflow are superior to those measured in the outflow and vice versa. Negative biases are observed for Ca^{2+}, HCO_3^-, Cl^-, O_2, CSS, PONF, PONC and $CaCO_3$. We observe also a decrease of $\delta^{13}C$ in all the carbon fractions: DIC, POCF, and to a lower extent POCC. In turn, positive biases are obtained for NO_3^-, CO_2, and C/N (in all the fractions), whereas $\delta^{18}O$ gets less negative. Globally speaking, the measured composition of the Amazon River (outputs) follows the chemical baseline imprinted by the tributaries (inputs). Thus, in-stream processes arising in the studied reach do not fundamentally modify the chemical composition acquired in the tributaries. The mitigation of compositional fluctuations is probably related to the contribution of ungauged rivers, which influence substantially the chemical signal measured in the Amazon River (e.g., Ca^{2+}, HCO_3^-, and Cl^-) because of the very low salinity of small rivers draining thick, sandy soils in central Amazonia. Conversely, the accentuation of trends observed downstream seems to be due to organic matter decay, which is expected to take place in the floodplain as water slowly enters the stream channel from temporary storage. This leads to the release of CO_2 (^{13}C depleted) and nitrogenous dissolved species (NO_3^- and DON) and symmetrically to the removal of O_2.

In the model M2, outputs are adjusted by prescribing ad hoc additional contribution of small rivers (whose average composition is not accurately known) that border the Amazon River. The reconstituted mean annual composition of small rivers and floodplains (Bustillo 2007) delivers reliable results for most of the parameters and provides valuable insight on the presumed impact of river processes. However, the correction proposed in the model M2, relying on the variable contribution but constant composition of small rivers and adjacent floodplains,

Table 2. Mean parameters of the linear equation (α, β, r^2, Bias) relating incoming and outgoing concentration (model M1) for 44 chemical parameters at 10 sampling stations (j) of the Amazon main stem. Data are presented for each chemical parameter (index i) and correspond to the mean values from 10 equations: $C_i^j(\text{obs}) = \alpha_i^j \times C_i^j(\text{calc}) + \beta_i^j (nj = 10)$. The mean biases and r^2 are also given.

		Cations (μmol L^{-1})				μeq L^{-1}		Anions (μmol L^{-1})						Mg L^{-1}	μmol L^{-1}		
k	pH	Na^+	K^+	Ca^{2+}	Mg^{2+}	S^+	S^-	HCO_3^-	Cl^-	NO_3^-	DOC^-	SO_4^{2-}	HPO_4^{2-}	DOC	DIC	CO_2	O_2
α	1.07	1.04	1.35	0.80	1.12	0.84	0.84	0.80	0.70	1.30	0.86	0.40	0.79	0.86	0.81	1.17	0.82
β	−0.59	−3	−9	25	−9	70	71	78	24	−2.6	1.9	23.4	0.23	0.35	98	−9	20
r^2	0.77	0.63	0.81	0.91	0.84	0.87	0.87	0.78	0.66	0.84	0.84	0.27	0.36	0.84	0.80	0.82	0.74
Bias	−0.08	−3	0	−37	−3	−84	−84	−67	−11	0.3	−1.3	−2.7	0.05	−0.24	−54	12	−12
Ave	6.99	144	27	273	55	827	827	618	92	11.2	20.1	42.1	0.76	3.76	759	141	159

	μmol L^{-1}	mg L^{-1}						δ^{13}C			δ^{18}O	C/N			Organic N (μmol L^{-1})		
k	SiO_2	FSS	CSS	TSS	POCF	POCC	POC	DIC	POCF	POCC	H_2O	POCF	POCC	DOC	PONF	PONC	DON
α	0.89	0.86	026	0.76	0.88	0.24	0.77	1.14	0.99	0.61	0.95	0.41	0.60	0.69	0.72	0.26	0.86
β	15	8	36	36	0.05	0.38	0.1	1.4	−0.6	−10.9	−0.12	6.6	11.1	24.6	3.7	1.2	1.9
r^2	0.82	0.91	0.39	0.83	0.79	0.10	0 68	0.92	0.69	0.50	0.98	0.34	0.21	0.21	0.81	0.15	0.49
Bias	1	−26	−13	−38	−0.25	−0.08	−0.22	−0.57	−0.28	−0.19	0.23	0.35	1.63	−1.50	−2.38	−0.37	0.00
Ave	136	227	59	286	2.59	0.53	3.11	−14.32	−27.19	−27.72	−6.10	10.97	24.91	28.26	19.80	1.83	11.17

	Silicates (μmol L^{-1})				Carbonates (μmol L^{-1})		Carbon cycle (μmol L^{-1})			Additional indexes	
k	NaSil	KSil	CaSil	MgSil	$CaCO_3$	Dolomite	CO_2 carb	CO_2 sil	CO_2 tot	FR	Re
α	1.67	1.35	1.67	1.67	0.76	1.45	0.96	1.29	0.80	1.93	0.34
β	−21	−8.54	−8	−7	13.55	−25.05	−31.63	−16.44	85.06	−0.40	1.53
r^2	0.34	0.81	0.34	0.34	0.67	0.80	0.79	0.26	0.79	0.64	0.14
Bias	8.0	0.0	3.2	2.6	−31.32	−5.73	−42.78	19.56	−65.99	−0.03	0.19
Ave	52.0	26.60	20.8	16.6	172.17	38.26	248.69	153.51	650.90	0.38	2.23

unambiguously fails (Figure 2). This may be due to several factors: 1) the area of flooded areas, on which direct precipitation falls, is variable; 2) the biotic transformations undergone by transiting materials are not the same depending if floodplains fill or dry up; and 3) the respective contributions of small rivers draining lowlands [low total dissolved solids (TDS)] and groundwater (high TDS) fluctuate along the hydrological cycle.

4.3. Hydrograph separation into three reservoirs (model M3)

The detailed modeling outcomes relative to M3 are presented in the appendix (Table A3). A simple comparison can be made between inputs (calculated) and outputs (observed). Mean values are more accurately examined (Figures 3a,b). Observed values are established by averaging the results obtained for nine sampling stations (excluding Vargem Grande and Santo Antonio do Içа, which are located at and close to the upstream boundary) located along the Amazon River main stem. Calculated concentrations ($\hat{C}_{i,k}$) are obtained as follows:

$$\hat{C}_{i,k} = 1/9 \times \left[C_{i,k}^{j=2} + C_{i,k}^{j=3} + 3 \times C_{i,k}^{j=5} + C_{i,k}^{j=6} + C_{i,k}^{j=7} + 2 \times C_{i,k}^{j=8} \right]. \qquad (16)$$

Notice that [C]RS $\times$ QRS/Q_t + [C]RI $\times$ QRI/Q_t +[C]RB $\times$ QRB/Q_t = [C]AVE for all the chemical parameters.

The agreement between both datasets is good, except for C/N, DON, HPO_4^{2-}, CO_2, O_2, and pH. Despite some unavoidable deviations resulting from the imprecisions of the chemical analyses and from simplifying assumptions required for modeling, the repartition of chemical species and isotopic signatures display the same pattern. The compositional contrasts between the three reservoirs tend to decrease in the outflow, suggesting that the intermittent storage of water in floodplains contributes to mix waters originating from different sources (e.g., hydrological reservoirs, subbasins). This tends to homogenize their chemical composition at the outlet of the system. The examples provided by CSS, $\delta^{18}O$, and DOC (Figure 3b) and by SO_4^{2-} and Cl^- (Figure 3a) are particularly explicit. The greatest deviations are observed for the sand fraction CSS whose transport in the Amazonian reach is considerably delayed compared to solutes and water.

Concerning the major chemical species (anions and cations), concentrations in RS and RI tend to be lower in the outflow: this effect of dilution is very marked for SO_4^{2-}, Cl^-, DOC, Ca^{2+}, and HCO_3^- (Figure 3a). This is consistent with the biogeochemical balance calculated for the floodplains (Bustillo 2007), which did not reveal any dissolution of carbonates in central Amazonia. It is likely that a part of Ca^{2+} is adsorbed on transiting clay suspensions, fulvic acids, and/or goethite (Weng et al. 2005), whereas HCO_3^- might be partly converted into CO_2 as a result of pH buffering of very acidic waters provided by small Amazonian rivers draining lowlands and Rio Negro. We observe also a very significant increase of weathering rate in the outflow (see CO_2 SIL), attributed to the baseflow RB. The consequence is the correlative decrease of the lithological index FR and $\delta^{13}C$ (DIC): $-9.6\,‰ \rightarrow -11.7\,‰$. However, the values established for $\delta^{13}C$ (DIC) and FR are not totally compatible, because a low contribution of carbonates on DIC release (FR low) should lead to a very negative $\delta^{13}C$ (DIC). The unexpected heavy signature of $\delta^{13}C$ (DIC) in the

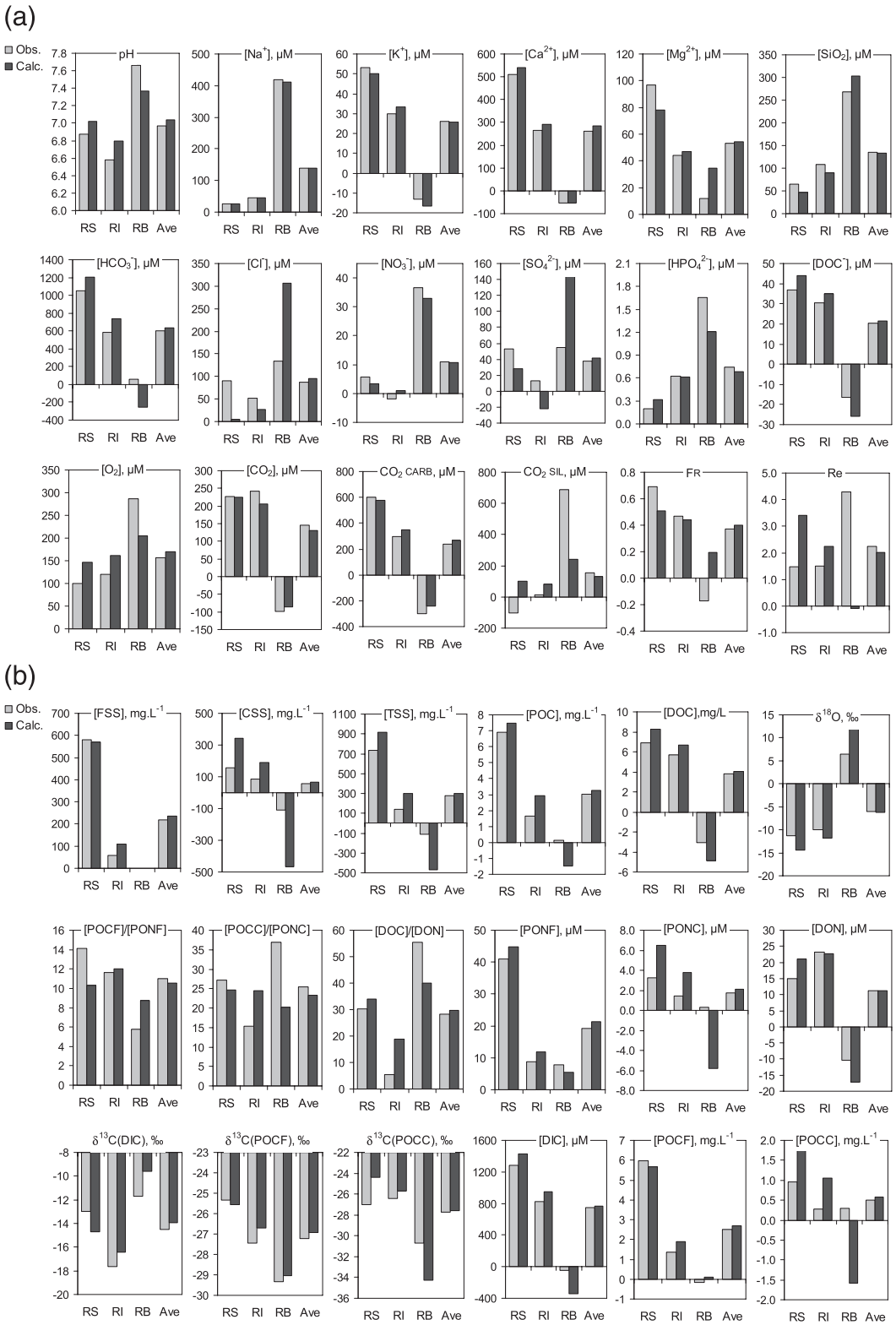
(a)
Obs.
Calc.
pH
[Na+], μM
[K+], μM
[Ca2+], μM
[Mg2+], μM
[SiO2], μM
[HCO3-], μM
[Cl-], μM
[NO3-], μM
[SO4 2-], μM
[HPO4 2-], μM
[DOC-], μM
[O2], μM
[CO2], μM
CO2 CARB, μM
CO2 SIL, μM
FR
Re
RS RI RB Ave
(b)
Obs.
Calc.
[FSS], mg.L-1
[CSS], mg.L-1
[TSS], mg.L-1
[POC], mg.L-1
[DOC],mg/L
δ18O, ‰
[POCF]/[PONF]
[POCC]/[PONC]
[DOC]/[DON]
[PONF], μM
[PONC], μM
[DON], μM
δ13C(DIC), ‰
δ13C(POCF), ‰
δ13C(POCC), ‰
[DIC], μM
[POCF], mg.L-1
[POCC], mg.L-1
RS RI RB Ave

baseflow (Figure 3b) might be the consequence of 1) CO_2 outgassing (Richey et al. 2002) and 2) aquatic photosynthesis, which both subtract preferentially ^{12}C and thus concentrate ^{13}C in the river water.

4.4. Focus on the sampling stations of Paurá and Óbidos

The outcomes of the end-member mixing model are more particularly analyzed downstream from the confluence of the eight major tributaries, at the monitoring stations of Paurá and Óbidos (Table 3). Chemical characteristics of the three reservoirs are almost similar for Paurá and Óbidos; they display distributions comparable to those resulting from the conservative mixing of the eight major tributaries. Even so, the statistical resolution might be deeply altered on specific parameters for one station and not for the other (e.g., Ca^{2+}, Mg^{2+}, and HCO_3^-). Small errors of chemical analyses might have large repercussions on the outcomes of the models, especially when the number of samples is low and when the variability of the chemical baseline is moderate. For the sampling stations located at the outlet of large fluvial basins, the compositional fluctuations of the river water are often attenuated because of the water storage in the floodplains and the slow motion of flood wave, which mixes waters having resided for a short or long time in the surface network. Even when r^2 values are low, the model outcomes are qualitatively very instructive to appreciate the dynamics within each reservoir and their heterogeneity. The similarity between the fictitious station (8 Rios) and the sampling stations (Paurá and Óbidos) indicates that the chemical composition (including isotopic composition) of the Amazon River water is essentially acquired before the waters supplied by tributaries reach the Amazonian floodplains. It seems that underlying processes driving biogeochemical budgets (chemical weathering, gas emissions toward the atmosphere, deposition versus remobilization of sediments, etc.) in the tributaries and in the Amazon main reach are of the same nature and define comparable chemical equilibria. The large-scale flooding of lowlands, occurring almost concomitantly over central Amazonia (Hamilton et al. 2002), provides autochthonous organic substrate for decomposition, leading subsequently

←

Figure 3. (a) Composition of (i) the three individual runoffs RS, RI, and RB and (ii) the river (AVE) obtained by averaging the model M3's outcomes of nine stations located on the studied Amazonian reach. Calculated data (calc; see Equation (16)) resulting from the discharge weighing of runoffs composition of the major tributaries are compared to observed data (obs) obtained by multilinear regression. Dissolved species and biogeochemical indices (see the appendix for a list of parameters). (b) Composition of (i) the three individual runoffs RS, RI, and RB and (ii) the river (AVE) obtained by averaging the model M3's outcomes of nine stations located on the studied Amazonian reach. Calculated data (calc; see Equation (16)), resulting from the discharge weighing of runoffs composition of the major tributaries, are compared to observed data (*obs.*) obtained by multilinear regression. Suspended sediments, organic carbon and nitrogen, C/N molar ratios, and isotopic signature of carbon ($\delta^{13}C$) and water ($\delta^{18}O$).

Table 3. Compared composition of the three individual runoff RS, RI, and RB for the eight major tributaries (8 Rios, calculated data from discharge weighing of the contributing reservoirs) and the stations of Pau and Óbi (data established from measured concentrations by multilinear regressions).

		mm yr^{-1}		Cations (μmol L^{-1})				μeq L^{-1}		Anions (μmol L^{-1})					
	k	QK	pH	Na^+	K^+	Ca^{2+}	Mg^{2+}	S^+	S^-	HCO_3^-	Cl^-	NO_3^-	DOC^-	SO_4^{2-}	HPO_4^{2-}
Pau	RS	358	6.66	28	39	250	69	706	706	584	52	10.0	26	17	0.02
	RI	490	6.34	33	21	102	21	302	302	232	17	0.6	28	12	0.41
	RB	317	7.66	308	17	205	57	848	848	535	134	24.6	8	71	1.56
	Ave	1165	6.80	106	25	176	46	575	575	423	60	10.0	22	30	0.60
	r^2		0.60	1.00	0.31	0.55	0.71	0.68	0.68	0.59	0.85	0.80	0.49	0.25	0.90
Óbi	RS	345	6.63	28	44	246	68	703	703	586	68	11.4	22	8	0.53
	RI	437	6.23	33	18	102	25	306	306	254	19	−2.2	25	5	0.68
	RB	341	7.52	285	19	188	51	782	782	476	99	27.4	14	80	0.98
	Ave	1122	6.75	108	26	172	46	573	573	423	58	11.0	21	28	0.73
	r^2		0.48	1.00	0.16	0.26	0.28	0.36	0.36	0.33	0.69	0.72	0.17	0.36	0.05
8 Rios	RS	344	6.59	28	41	302	57	789	790	628	3	3.9	41	57	0.07
	RI	433	6.36	33	22	120	25	351	350	284	10	0.4	39	8	0.30
	RB	340	7.81	280	11	185	62	788	787	490	196	25.2	−10	41	1.36
	Ave	1117	6.87	107	25	196	46	619	618	453	65	9.0	25	33	0.55
	r^2		0.73	1.00	0.69	0.80	0.90	0.85	0.85	0.75	0.98	0.82	0.76	0.83	0.46

		mm yr^{-1}	mg L^{-1}	μmol L^{-1}				mg L^{-1}						$\delta^{18}O$
	k	QK	DOC	DIC	CO_2	O_2	SiO_2	FSS	CSS	TSS	POCF	POCC	POC	H_2O
Pau	RS	358	4.9	820	237	116	123	620	58	679	5.77	0.57	6.34	−7.8
	RI	490	5.3	466	236	116	107	20	51	70	1.17	0.52	1.69	−7.3
	RB	317	1.5	494	−44	250	154	0	−24	−23	−0.43	−0.18	−0.61	−0.9
	Ave	1165	4.1	583	160	153	125	199	33	232	2.15	0.35	2.49	−5.7
	r^2		0.49	0.59	0.50	0.48	0.44	1.00	0.40	0.99	0.94	0.55	0.93	0.46
Óbi	RS	345	4.2	802	216	120	117	610	63	673	5.3	0.8	6.0	−7.1
	RI	437	4.9	519	264	90	128	15	59	73	2.0	0.4	2.4	−7.6
	RB	341	2.7	445	−30	262	144	0	−32	−31	−0.3	−0.3	−0.5	−1.6
	Ave	1122	4.0	583	160	151	129	193	33	226	2.3	0.3	2.6	−5.6
	r^2		0.17	0.43	0.49	0.67	0.17	1.00	0.52	0.99	0.85	0.85	0.89	0.39

8 Rios	RS	344	7.7	877	248	76	95	665	192	857	5.5	1.4	7.0	−10.3
	RI	433	7.4	522	234	105	101	20	48	68	1.0	0.5	1.5	−8.4
	RB	340	−2.0	389	−95	320	191	0	−94	−93	0.5	−0.6	−0.1	1.7
	Ave	1117	4.6	591	138	162	127	213	49	262	2.2	0.4	2.7	−5.9
	r^2		0.78	0.67	0.59	0.39	0.55	1.00	0.81	0.99	0.95	0.72	0.94	0.41

		mm yr^{-1}	δ^{13}C			C/N			Carbon cycle (μmol L^{-1})						
	k	QK	DIC	POCF	POCC	POCF	POCC	DOC	DIC	POCF	POCC	PONF	PONC	DOC	DON
Pau	RS	358	−14.5	−25.7	−28.5	7.5	28.8	22.9	810	480	48	55.3	2.15	404	8.5
	RI	490	−18.7	−27.8	−26.9	11.2	22.0	−10.1	461	98	44	6.5	2.00	438	25.1
	RB	317	−11.6	−28.0	−28.0	9.9	11.6	109.0	490	−36	−15	−4.7	−0.51	125	−9.5
	Ave	1165	−15.50	−27.22	−27.70	9.7	21.2	32.5	576	179	29	18.4	1.36	343	10.6
	r^2		0.67	0.61	0.68	0.51	0.11	0.81	0.60	0.94	0.55	0.91	0.30	0.49	0.67
Óbi	RS	345	−14.6	−27.4	−28.3	10.5	21.9	48.9	812	439	65	45.0	3.1	349	5.3
	RI	437	−19.3	−28.1	−27.5	12.9	17.2	3.6	525	169	35	11.7	1.9	408	24.3
	RB	341	−11.8	−26.1	−28.4	6.1	21.0	35.3	450	−22	−23	2.7	−1.1	224	4.1
	Ave	1122	−15.56	−27.26	−28.01	10.1	19.8	27.1	590	194	26	19.2	1.3	334	12.3
	r^2		0.46	0.29	0.17	0.57	0.08	0.29	0.43	0.85	0.85	0.76	0.79	0.17	0.41
8 Rios	RS	344	−17.0	−26.4	−25.7	6.8	24.4	41.1	882	461	119	54.2	5.2	642	15.6
	RI	433	−18.4	−27.4	−26.9	10.2	26.5	24.5	525	79	42	7.5	1.6	611	22.9
	RB	340	−8.2	−27.1	−29.9	11.3	16.1	22.3	392	41	−52	−0.1	−1.9	−163	−1.3
	Ave	1117	−14.86	−27.02	−27.47	9.5	22.7	29.0	594	185	37	19.6	1.6	385	13.3
	r^2		0.78	0.50	0.10	0.34	0.32	0.42	0.67	0.95	0.72	0.97	0.74	0.76	0.47

		mm yr^{-1}	Sil (μmol L^{-1})			Carb (μmol L^{-1})		CO_2 cycle (μmol L^{-1})				
	k	QK	NaSil	CaSil	MgSil	$CaCO_3$	Dolomite	CO_2 CARB	CO_2 SIL	CO_2 TOT	FR	Re
Pau	RS	358	−25	−10	−8	166	77	319	−21	619	0.56	1.45
	RI	490	16	7	5	68	16	100	61	261	0.37	1.73
	RB	317	174	70	56	62	2	66	440	571	0.07	3.89
	Ave	1165	46.7	18.7	14.9	96	31	158	139	456	0.35	2.23
	r^2		0.90	0.90	0.90	0.41	0.63	0.56	0.94	0.61	0.75	0.90

Table 3. (*Continued*)

		mm yr^{-1}	Sil (μmol L^{-1})			Carb (μmol L^{-1})		CO_2 cycle (μmol L^{-1})				
	k	QK	NaSil	CaSil	MgSil	$CaCO_3$	Dolomite	CO_2 CARB	CO_2 SIL	CO_2 TOT	FR	Re
Óbi	RS	345	−40	−16	−13	175	80	335	−53	621	0.60	1.46
	RI	437	14	6	4	71	21	113	52	278	0.38	1.44
	RB	341	187	75	60	40	−7	26	473	519	0.02	4.12
	Ave	1122	49.8	19.9	15.9	94	30	154	148	456	0.34	2.26
	r^2		0.91	0.91	0.91	0.50	0.39	0.45	0.97	0.35	0.78	0.76
8 Rios	RS	344	25	15	10	185	49	284	101	669	0.45	2.54
	RI	433	23	14	9	85	17	120	78	319	0.37	1.86
	RB	340	84	49	33	75	35	146	215	508	0.28	1.81
	Ave	1117	42.0	24.7	16.8	113	33	176	127	484	0.37	2.06
	r^2		0.89	0.89	0.89	0.57	0.86	0.69	0.88	0.74	0.44	0.53

to the creation of hypoxic and anoxic environments along river corridors. These reductive conditions influence considerably carbon and nutrient cycling resulting from the enhancement of gas emission (CH_4, CO_2, NO, N_2O, and N_2) toward the atmosphere and thus determine the isotopic signature of the dissolved inorganic carbon. The major chemical species released by chemical weathering in upstream reaches, where the bedrock outcrops, and in the floodplains, where coarse unweathered sediments deposit, seem to be transported (almost) conservatively within the river network.

4.5. Hydrobiological modeling (model M4)

The analysis focuses more particularly on the sign of the coefficient $K_{\mathrm{BIO}\,i}^{\,j}$ associated to the hydrobiological factor $I_{\mathrm{BIO}\,i}^{\,j}$. Model outcomes, on several characteristic parameters and for the 11 monitoring stations of the Amazon profile, are represented in Figure 4 (full dataset in Table A4 and electronic supplementary material; supplements are available online at http://dx.doi.org/10.1175/2010EI326..s1.). Chemical responses to the hydrobiological factor may be roughly grouped into three categories: 1) $K_{\mathrm{BIO}\,i}^{\,j} > 0$, indicating that concentrations (or values) increase concomitantly to I_{BIO} or that concentrations are higher when photosynthetic paths dominate; 2) $K_{\mathrm{BIO}\,i}^{\,j} < 0$, indicating that concentrations (or values) increase when the mineralization prevails on the photosynthesis; and 3) $K_{\mathrm{BIO}\,i}^{\,j} \ll \overline{C}_i^{\,j}$, indicating that hydrobiological processes do not significantly influence the chemical baseline. Among the parameters varying like $I_{\mathrm{BIO}\,k}^{\,j}$, we have the following: pH, K^+, NO_3^-, SO_4^{2-}, HPO_4^{2-}, O_2, $\delta^{13}C$ (DIC), $\delta^{13}C$ (POCF), and C/N (three fractions). Among the parameters varying in the opposite sense, we have the following: Ca^{2+}, HCO_3^-, DOC, DIC, CO_2, POCF, PONF, PONC, and DON. Other parameters do not exhibit any significant and reproducible correlation with $I_{\mathrm{BIO}\,k}^{\,j}$. A break is observed at Manaús, depending if we locate upstream or downstream from the confluent of Rio Negro. Roughly speaking, there is a loss of Ca^{2+}, Mg^{2+}, K^+, and HCO_3^- under photosynthetic regime and conversely a gain of these solutes after the confluent of Rio Negro. Similarly, the decrease of [DOC] is clearly observed downstream from Manaús but remains negligible upstream.

When the photosynthetic paths dominate ($I_{\mathrm{BIO}\,k}^{\,j} \gg 0$), CO_2 is removed while O_2 is released. As a result, the pH increases and influences the nature and magnitude of abiotic processes. First of all, the biological uptake of CO_2 operates a carbon fractionation, which tends to make heavier, by mass effect, the value of $\delta^{13}C$ (DIC) in the river water. Concomitantly, the decrease of [Ca^{2+}] and [HCO_3^-] supports the hypothesis that Ca^{2+} is adsorbed by clay minerals, which releases H^+ and leads to the subsequent protonization of HCO_3^- (which frees CO_2). After the confluence of Rio Madeira, the dynamics of Ca^{2+} is reversed: all other things being equal, [Ca^{2+}] and [HCO_3^-] tend to increase (photosynthetic path). The rise of pH and/or [O_2] related to photosynthetic paths might promote the side-chain oxidation of nitrogenous functions contained in dissolved organic molecules (Aufdenkampe et al. 2001; Aufdenkampe 2002). Their condensation makes them get more hydrophobic (Tardy et al. 2009) and leads presumably to their sorption onto fine suspended sediments to form diagenetic POCF. The rise of POCF/PONF and POCC/PONC reflects the genesis of autochthonous molecules, which progressively obliterates the signal of

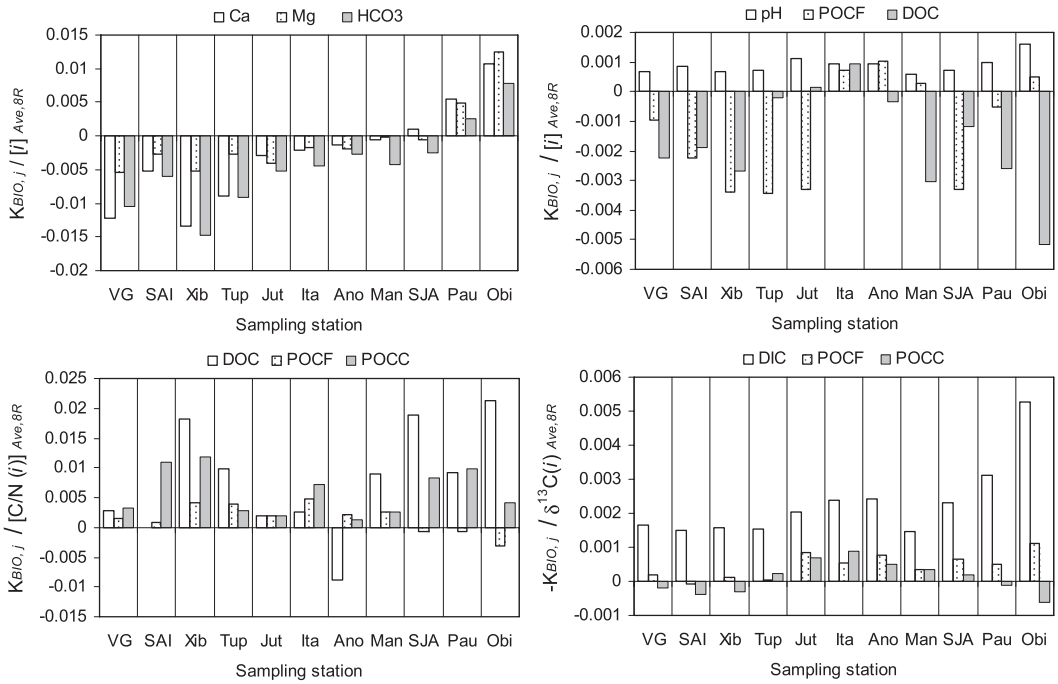

Figure 4. Influence of the hydrobiological regime, appreciated by $K_{\mathrm{BIO}\,i}^{\,j}/(i)_{\mathrm{AVE},8R}$ for 12 chemical parameters (noted *i*) at the 11 sampling stations (noted *j*) over the Amazon River longitudinal profile: VG, SAI, Xib, Tup, Jut, Ita, Ano, Man, SJA, Pau, and Óbi (the outlet of the studied reach); $(i)_{\mathrm{AVE},8R}$ is the mean concentration of *i*, calculated by discharge weighing the inputs of the eight major tributaries upstream from Óbi; $K_{\mathrm{BIO}\,i}^{\,j}$ is a calibrated parameter (outcomes of the model M4; see Equation (11)) corresponding to the rate of uptake or release of each bioactive element (*i*) for each station (*j*) associated to biologically mediated processes in the river water and describing thus the response of chemical parameters to $I_{\mathrm{BIO}\,k}^{\,j} = [\mathrm{O_2}]_k^j - [\mathrm{CO_2}]_k^j$. Here, $K_{\mathrm{BIO}\,i}^{\,j} > 0$ means that C_i^j rises with photosynthetic pathways $(I_{\mathrm{BIO}\,k}^{\,j} > 0)$, decreases with mineralization pathways $(I_{\mathrm{BIO}\,k}^{\,j} < 0)$ and vice versa.

soil-derived substances. Actually, riparian grasses and floating aquatic plants that grow in the floodplains exhibit a high atomic ratio C/N, evaluated to 42 by Victoria et al. (Victoria et al. 1992), suggesting that the uptake of NO_3^- is rather low and does not totally counterbalance the input associated to the sorption of DOM. However, the most significant rise is observed for [DOC]/[DON] because of the diagenesis of DOM, which tends to release NO_3^- and to concentrate carbon in DOM.

Conversely, when the mineralization paths prevail on photosynthesis ($K_{\mathrm{BIO}\,i}^{\,j} \ll 0$), low $^{13}C/^{12}C$ source of DIC is released in the river while O_2 is consumed. The chemical signals associated to mineralization are, roughly speaking, symmetrical to those imprinted by the photosynthesis. The Andean soil-derived POCC, mainly mobilized in surface runoff, is exposed to increasing temperature as transported downstream and subjected to mineralization in lowland environments (McClain

et al. 1995). This source of unstable carbon provides a significant amount of carbon substrate that fuels the heterotrophic metabolism of the river, after deposition of large quantities of carbon. In addition to allochthonous POCC, the mechanism locally named ''terras-caídas,'' corresponding to the large-scale bank erosion during flood periods (Irion et al. 1997), promotes the large-scale destruction of well-developed floodplain forest communities (Junk and Piedade 1997) and provides large amounts of highly unstable organic substrate. The contribution of grass várzeas to the carbon budget of floodplains, appreciated by the isotopic composition of várzea sediments (Victoria et al. 1992; Martinelli et al. 2003), increases as we move downstream. This suggests that the impact of aquatic vegetation on the carbon budget of floodplain progressively increases (Quay et al. 1992). Because of preservation mechanisms during decomposition (such as adsorption-linked protection), the fine fraction POCF is clearly refractory: $K_{\mathrm{BIO}}{}_i^j \ll$ [POCF] AVE and does not appear to be significantly influenced by in-stream mineralization.

4.6. The composite approaches (M5 and M6)

The model M5 exhibits an unexpected high performance for all monitoring stations and all chemical parameters, as shown in the appendix (Table A5). The reconstitution of isotopic signatures is very convincing for δ^{18}O (SMOW) and δ^{13}C (DIC), whereas the lowest levels of confidence are observed for POCC, CSS, PONC, and C/N atomic ratios for POCC and POCF. The significant improvement compared to M1 and M3 denotes the influence of floodplains on the chronological variations of the Amazon River composition, mainly because of 1) the polarity of water circulation in the floodplains and 2) the variable contribution of each individual runoff to the water budget of floodplains. The chemical response of river to the polarity of water circulation in the floodplains can be approached by analyzing the magnitude and the sign of γ_i^j [cf. Equation (13)] corresponding to the variation of concentration in the river water associated to the water balance of floodplains $\Delta\, Q_t{}_k^j$. The complete dataset compiling the values of γ_i^j is supplied in the electronic supplementary materials (Table A5); several selected values are represented in Figure 5. Despite some variations between stations, the magnitude and the sign of γ_i^j match quite well. The model M5, taking into account simultaneously the variables $\Delta\, Q_t{}_k^j$, $\Delta Q\mathrm{RS}/Q_t$, and $\Delta Q\mathrm{RI}/Q_t$, although providing reliable outcomes, might sometimes be difficult to interpret, notably because of covariations between variables. For example, $\Delta\, Q_t{}_k^j$ and $\Delta Q\mathrm{RI}/\, Q_t$ exhibit a positive correlation simply because the drainage of floodplains principally involves the hydrological reservoir RI. Moreover, the simple interpretation of γ_i^j does not allow investigating the additional impact of the river flow, whose magnitude influences floodplain dynamics.

To facilitate the deciphering process, the model M6 was implemented. The calibration of the four parameters [see Equation (15)] leads to the determination of 3D diagrams with spatial representation realized for $600\ \mathrm{mm\ yr^{-1}} \leq Q_t{}_k^j \leq 1600\ \mathrm{mm\ yr^{-1}}$ (average = $1122\ \mathrm{mm\ yr^{-1}}$) and $-0.05 \leq \Delta\, Q_t{}_k^j \leq 0.30$ (average = 0.134). These figures, available in full in the appendix (Figure A2) for the station of Óbidos, represent the variations of concentration (or isotopic value) as a function of the river outflow and as a function of the water balance of floodplains, tracked by $\Delta\, Q_t{}_k^j$. The mean concentration of each parameter, calculated in the inflow (for eight cruises), is centered on $Q_t{}_k^j = 1\ 122\ \mathrm{mm\ yr^{-1}}$ and $\Delta\, Q_t{}_k^j = 0.134$. The isolines

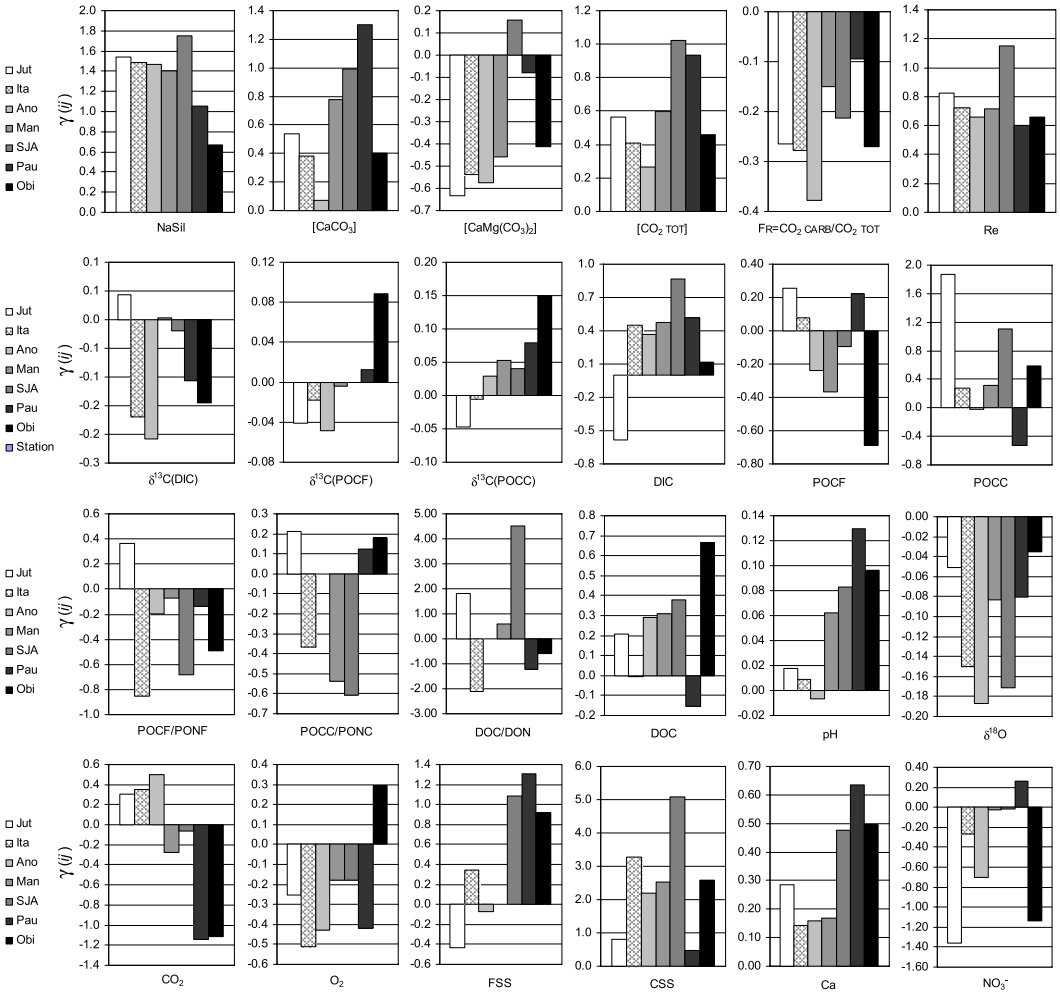

Figure 5. Variation of the coefficients γ_i^j over the Amazon River (longitudinal profile between Jut and Óbi) obtained by the model M5 for a sample of 24 chemical parameters (*i*) and 7 sampling stations (*j*): Jut, Ita, Ano, Man, SJA, Pau, and Óbi (the outlet of the studied reach). The coefficients γ_i^j enable tracking of the influence of floodplains water balance on the compositional changes of water chemistry for a given parameter (*i*) at a given station (*j*): $\gamma_i^j > 0$ indicates that concentrations are higher (all other things being equal) when the floodplains drain $[\Delta Q_{tk}^{\ j} > 0]$ and vice versa. For example, $\gamma_i^j = 0.92$ for fine suspended sediments (FSS) at Óbi, indicating that (FSS) in the outgoing flow increases by 92% compared to (FSS) in the incoming flow (data calculated by discharge-weighing chemical signals from the eight tributaries upstream from Óbi) when $\Delta Q_{tk}^{\ j} = 100\%$ (i.e., outflow = 2 × inflow).

represent the changes of chemical characteristics as we stray from the central point, assuming that the chemical composition of the inflow remains constant, whatever $Q_{t\,k}^{\,j}$ and $\Delta Q_{t\,k}^{\,j}$ are. In this section, the objective is not to predict the chemical composition of the outflow but rather the deviation to the inflow. As a consequence, the following diagrams must be read and interpreted only in terms of relative values. In each diagram are identified the main sequence of hydrological cycle: 1) lowest waters, characterized by low Q_t and excess of outflow; then 2) rising waters, exhibiting intermediate Q_t and a severe deficit of outflow; then 3) highest waters, with high Q_t and moderate deficit of outflow; then 4) falling waters, with intermediate Q_t and excess of outflow; and back to 1) lowest waters.

4.6.1. Major chemical species and chemical weathering

Concerning the major chemical species, a dilution effect is observed during the phase of water storage while concentrations rise when the waters stored in the floodplains join back the main channel. The influence of the circulation polarity is greater after the confluence of Rio Japurá, as the Amazon valley widens. Considering the poles of chemical erosion, it is noticeable that the apparent rate of chemical alteration is substantially greater (both for silicates and carbonates) when the floodplains empty, with the exception of dolomite, all other things being equal (Figure 5). On average, the lithological index *F*R (cf. list of parameters) exhibits lower values during the emptying of floodplains. It suggests that submerged low plains drain areas where the alteration of sedimentary minerals mimics the weathering of crystalline rocks. It is likely that chemical weathering in floodplains manifests itself sequentially, when the floodplains dry up: that is, when the water stored in low plains joins back the main channel. Following Johnsson and Meade (Johnsson and Meade 1990), these model outcomes support the idea that the chemical weathering of the additional flow is mainly driven by the diagenesis of unweathered sediments that are deposited during the filling of floodplains (Martinelli et al. 1993). The decrease of lithological index *F*R during the emptying of floodplains coincides with lower δ^{13}C (DIC), compared to the stage of filling (Figure 6a). The parallel evolution of δ^{13}C (DIC) and *F*R confirms that the isotopic signal of dissolved inorganic carbon is fundamentally determined by the pattern of weathering processes (synthesized by *F*R). Because of the hydrological dynamics of floodplains, following an annual immutable cycle, the chemical expression of weathering processes is sequential as well. It should also be noticed that the index Re (SiO_2/Al_2O_3 in altered products inferred from the chemistry of river water; Tardy et al. 2004) is much higher during the emptying of floodplains, suggesting that SiO_2 might be picked up and converted into a particulate form because of the growth of diatoms, which is encouraged in adjacent lakes and flooded areas.

4.6.2. Budget of sediments

The sand fraction CSS exhibits systematically lower concentrations during the phase of water storage (γ_i^j values are all positive in Figure 5) than during the emptying stage (Figure 6b). This result supports the idea that the sediments tend to deposit as the river inundates the low plains and tend to be remobilized as the extension of submerged areas lessens. The greatest contrasts are observed between Itapeua and São José da Amatari and the lowest is accredited to Paurá, after the

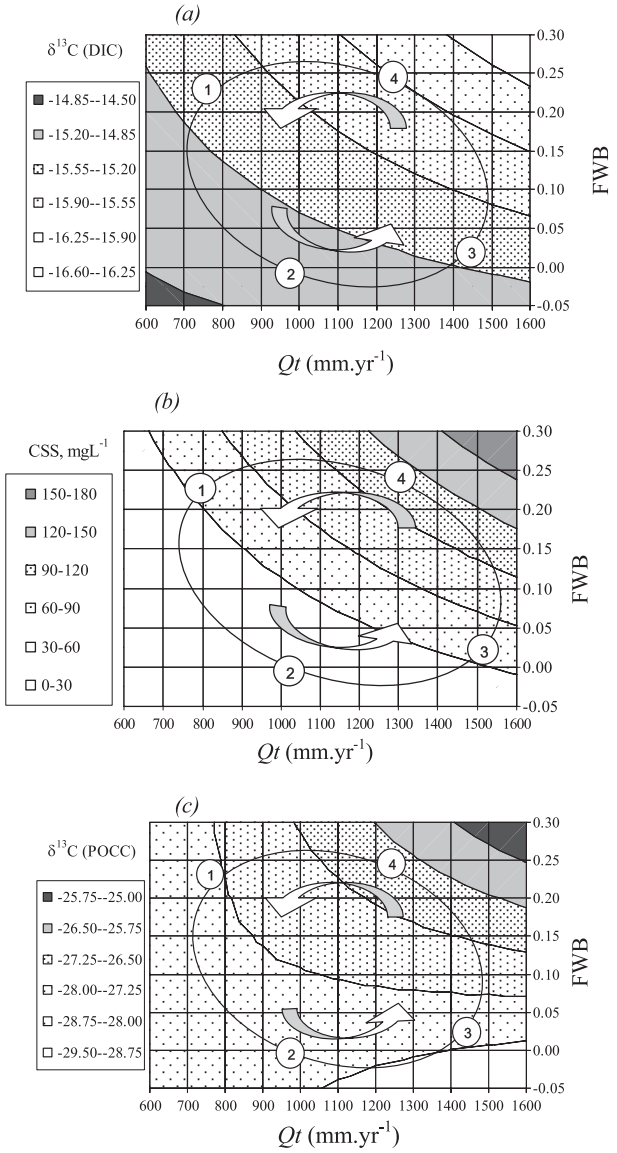

Figure 6. Mean simulated variations of (a) δ^{13}C (DIC), (b) (CSS), and (c) δ^{13}C (POCC) as a function of the river outflow (Q_t) and the floodplain water balance (FWB) = $\Delta Q_{t\,k}^{\,j} = Q_{t\,k}^{\,j}, \mathrm{obs}/Q_{t\,\mathrm{tot},k}^{\,j} - 1$. The fluctuations modeled by M6 over an annual cycle, at the station of Óbi, are represented by arrows, showing (a) ^{13}C/^{12}C depletion during falling waters (path 3 → 4); (b) sedimentation patterns on the 1 → 2 → 3 paths and remobilization patterns on the 3→ 4 → 1 paths; and (c) the exportation of the várzeas grasses (^{13}C/^{12}C enriched) toward the main channel during the falling water stage (3 → 4 path). The hydrological sequence is 1) lowest waters with outflow = inflow (FBW = 0); then 2) rising waters, with outflow < inflow (FBW < 0); then 3) highest waters, with outflow = inflow (FBW = 0); then 4) falling waters, with outflow > inflow (FBW > 0); and then 1) lowest waters.

confluence of Rio Madeira, which provides large amounts of coarse sediments. The trends for the silt–clay fraction are less explicit. Considering the silt–clay fraction FSS, no clear tendency can be outlined on the Vargem Grande–Manacapurú reach. In turn, between São José da Amatari and Óbidos, the pattern is very similar to the one described for CSS, suggesting that the flushing action of Rio Negro (Meade et al. 1985; Dunne et al. 1998) might promote the remobilization of fine sediments when the floodplains drain.

4.6.3. River metabolism

Considering the gaseous composition of the river, the computed γ_i^j values indicate higher [CO_2] during the emptying of flooded area on the upstream reach and lower [CO_2] on the downstream reach (from Manacapurú to Óbidos). All other things being equal, pH appears to be higher during the emptying of floodplains while [O_2] is lower.

Considering nitrogenous species, the evolutions are the following: while the floodplains dry up, a generalized drop of [NO_3^-] and a gain of [PONC] and [DON] are observed. The exceptions are Paurá and São José da Amatari, where sorption processes of dissolved organic matter arise (Aufdenkampe et al. 2001; Tardy et al. 2009).

Considering organic carbon species, γ_i^j values highlight a gain of POCF and POCC during the emptying of floodplains and conversely a deficit of DOC. The major exception corresponds to the station of Paurá, which is highly influenced by the forwarded contribution of Rio Madeira, which reverberates directly on the chronological evolution of processes.

As the waters stored in the floodplains join back the main channel, the atomic ratio POCF/PONF rise, whereas DOC/DON and POCC/PONC drop drastically. The drift observed along the Amazon profile involves the increasing contribution of submerged areas to the water budget of the Amazon River, as we move downstream. This amplifies the imprint of river diagenesis on the organic matter. As heterotrophic processes operate more and more intensely, the maturation of organic matter is accelerated and leads to lower and lower POCF/PONF in the water draining floodplains. The effects of these processes on the isotopic signature of carbon are not appreciable. Concerning POCC, the concentrations tend to be higher during the emptying of the floodplains. The effects on the isotopic signal of $\delta^{13}C$ (POCC) are noticeable, leading unequivocally to a ^{13}C enriched signature when the water stored in the floodplains rejoins the main channel (Figure 6c). The presumed influence of aquatic grasses, whose isotopic signature is heavy (−13 ‰, according to Victoria et al. 1992), on the isotopic composition of POCC, seems to be confirmed here.

The amounts of DOM, both those observed at Óbidos and those reconstituted by modeling (model M6), exhibit a drastic decline of [DON] and a correlative increase of [DOC]/[DON] when the inundation of the floodplains occurs: that is, during rising water stage. At this stage, the chemical nature of DOM, mobilized by surface runoff (Tardy et al. 2005), is mainly soil derived and refractory (Hedges et al. 1986). Low C/N molecules, conveyors of positive charge (e.g., amino acids) or hydrophobic (humic acids), are recognized to be the best candidates to sorption onto fine sediments (Aufdenkampe et al. 2001), leading subsequently to rising C/N in the remaining DOM fraction. Conversely, the emptying of floodplains coincides

with a rise of [DOC] and [DON] and a decrease of [DOC]/[DON]. This supports the idea that additional DOC and DON observed during the emptying of floodplains is autochthonous and is released by the decay of aquatic biomass, which contains high proportion of amino acids (low C/N) compared to soil-derived DOM (Hedges et al. 1994). The high variability of C/N tends to confirm that, along a complete hydrological cycle, distinct pools of molecules (allochthonous soil derived versus autochthonous river derived) exhibiting contrasted reactivity and very dissimilar elemental composition are exported by the Amazonian rivers (Amon and Benner 1996a; Amon and Benner 1996b).

5. Summary and concluding remarks

The six hydrochemical models that were tested provide a valuable insight on the main factors [hydrological source, water budget of the floodplains, nature of hydrobiological pattern (e.g., photosynthesis versus mineralization, air–water gaseous exchanges, etc.)] controlling the biogeochemical and sedimentary budgets of the Amazonian floodplains. The influence of floodplain and additional flow (small rivers, alluvial groundwater, and direct precipitation) could be shown for most of the studied parameters (Bustillo 2007). Unfortunately, because of the lack of reliable data concerning the water chemistry of small tributaries, the influence of variable additional input (involving variable contribution of small rivers and alluvial groundwaters to the river flow) cannot be distinguished from the effects of the diagenesis operating in the floodplains. At the light of the results provided by the six mixing models, three main issues dealing with the biogeochemistry and hydrology of the floodplains are addressed:

1) coupling between sediment deposition and biogeochemical diagenesis;
2) organic metabolism of the river and its effects on the nature and intensity of biotic processes; and
3) nature and intensity of abiotic processes, involving notably the sorption of DOM, the evaporation of wetlands, and the river outgassing.

A companion paper (V. Bustillo et al. 2010, unpublished manuscript) aims to investigate more in detail these three topics, which are intrinsically related and which determine most of the biogeochemical budget relative to Amazonian floodplains.

The magnitude and polarity of water exchanges between the Amazon River and its floodplains strongly influence the sedimentary and chemical signals measured in the river waters. The floodplains constitute widespread sites where major biotic and abiotic processes affecting the dynamics of transiting materials occur: sedimentation, remobilization of sediments, organic matter decay, CO_2 outgassing, etc.

Unexpectedly, the chemical trends observed upstream are sometimes accentuated downstream, as shown by the model M1. It supports the idea that the processes operating downstream are of the same nature as those occurring upstream, prolonging therefore the imprint given by upstream rivers to the chemical baseline. Because of the increase in floodplain size as we move downstream, the impact of floodplain filling and draining on the biogeochemical qualities of the water are therefore amplified downstream. Taking into account the additional contribution of ungauged areas, using ad hoc constant characteristics to close the river budget

(model M2) does not improve the performance of modeling compared to the simplest possible model M1. It means that the composition of the ''additional'' flow is probably very variable, particularly because the alluvial groundwaters draining unweathered sediments deposited alongside the Amazon River (high TDS) and the small tributaries draining thick, sandy soils (intensively leached, low TDS) do not contribute synchronously to the river flow (Bustillo 2007) and exhibit very distinct chemical characteristics.

The mixing model M3 shows a decrease of compositional differences between hydrological reservoirs as we move downstream. This homogenization might be the result of the mixture of waters having resided more or less durably in the hydrographic network. The main differences between incoming and outgoing compositions are attributable to the baseflow RB and, to a lesser extent, to the delayed direct runoff RI. This would be the result of in-stream biogeochemical processes: the aquatic photosynthesis impacts RB, whose contribution to river flow is at maximum during lowest waters stage (i.e., when autotrophic regime prevails), whereas organic matter decay more particularly impacts RI ($\uparrow$ CO_2, $\downarrow$ pH, $\downarrow$ O_2, $\downarrow$ δ^{13}C-DIC, $\downarrow$ DON, $\downarrow$ DOC, and $\downarrow$ DOC/DON), whose contribution is maximum when the emptying of floodplains (where heterotrophic regime prevails) occurs.

The model M4, which is also based on variable hydrological source, involves the hydrobiological index $I_{\mathrm{BIO}}{}_k^j = [\mathrm{O_2}]_k^j - [\mathrm{CO_2}]_k^j$, used as a tracer of autotrophic versus heterotrophic regime. This improves considerably the performances of the simulations, compared to M3. The model M4 enables us 1) to identify the parameters significantly influenced by in-stream processes and 2) to determine their response, depending on the nature and magnitude of hydrobiological regime. Globally speaking, the hydrobiological regime promotes large variations of pH and $[O_2]$, which have direct repercussions on the biodynamics of other chemical variables. The autotrophic regime is dominant ($I_{\mathrm{BIO}} > 0$) during lowest waters stage, when 1) the river turbidity is minimum, 2) when the river–floodplain connectivity is interrupted, and 3) when the rate of incoming solar radiation reaching the water body is at maximum (flow concentrated within the well exposed main channel). The rises of pH and $[O_2]$ directly induced by aquatic photosynthesis coincide with losses of organic nitrogen to the benefit of mineral nitrogen, increases of $^{13}C/^{12}C$ for DIC (isotopic fractionation induced by aquatic photosynthesis), and losses of Ca^{2+} and HCO_3^-. The heterotrophic regime is dominant over the annual cycle, except during lowest waters stage. The heterotrophic signal is hugely amplified when the waters stored in the floodplains rejoin the main channel. Falling waters constitute privileged moments to appreciate the biogeodynamics of the floodplains, because their discharge in the main channel is intermittent. The decrease of pH and $[O_2]$ related to the heterotrophic regime coincide with increase of $[CO_2]$; decrease of δ^{13}C(DIC); decrease of [DOC]/[DON]; and rise of δ^{13}C(POCC), which is interpreted as the result of the sequential release of autochthonous carbon (C4 aquatic grasses).

The models M5 and M6 enable the impact of floodplains water balance (filling versus emptying) on the differences of chemical concentrations between the tributaries and the Amazon River to be tested more specifically. This test appears to be very conclusive, showing that chemical signals observed in the Amazon River waters are thoroughly influenced by the magnitude and polarity of water exchanges between the Amazon River main channel and its floodplains.

Acknowledgments. This work was funded by the Brazilian FAPESP agency by way of a postdoctoral fellowship (2005/58884-5) associated to the project entitled "A large-scale synthetic model applied to the hydroclimatology and eco-geodynamics of the Amazon River basin." This study benefited from insightful comments from two anonymous referees, whose very careful review and far-reaching vision contributed indeed to substantially improve the quality of the language and the clarity of the thinking.

Appendix

List of parameters

The full results of the end-member mixing models are provided in the appendices. Table A1 and Figure A1 report the simulated fluctuations of the three runoff components for monitoring [(11)] and virtual [(7)] stations. Tables A2–A5 show the detailed results (calibrated parameters and performance criteria) of the models M1, M3, M4, and M5, respectively. The results of the model M6 are presented synthetically in Figure A2. The list of parameters shown below is intended to facilitate the self-exploration of the appendices.

a. Indexes

i	chemical species
j	sampling station
k	number of the sample.

b. Hydroclimatic features

RS	forwarded direct runoff
RI	delayed direct runoff
RB	baseflow
Q_K	discharge of each individual runoff with K standing for RS, RI, or RB

c. Geochemical characteristics (for full details, see Tardy et al. 2004)

Re: SiO_2/Al_2O_3 in altered products	stoechiometry of clays formed by chemical weathering
CO_2 CARB	CO_2 consumed by the alteration of carbonated rocks
CO_2 SIL	CO_2 consumed by the alteration of crystalline rocks
CO_2 TOT: CO_2 SIL + 2.CO_2 CARB	DIC released by geochemical alteration
FR: CO_2 CARB/CO_2 TOT	lithological index is the part of DIC originating from the dissolution of carbonates
WR	chemical weathering rate (m Ma^{-1})
FCO_2	rate of CO_2 consumption (TC km^{-2} yr^{-1})

d. Hydrochemical modeling

$I_{\mathrm{BIO}\,k}^{\,j}$	hydrobiological index based on the gaseous composition of the river water
$K_{\mathrm{BIO}\,i}^{\,j}$	rate of uptake or release of chemical species associated to hydrobiological path
$(\Delta Q_t/Q_t)_k^j$	index of hydrograph stage (>0 during rising water, <0 during falling water, and $=0$ for highest waters and lowest waters)
$\Delta Q_{t\,k}^{\,j} = Q_{t\,k}^{\,j}/Q_{t\,\mathrm{tot},k}^{\,j} - 1$	water balance of floodplains (<0 if filling and >0 if emptying)
α_i^j	variation of concentration in the river water associated to the variation of $Q\mathrm{RS}/Q_t$ in the main channel
β_i^j	variation of concentration in the river water associated to the variation of $Q\mathrm{RI}/Q_t$ in the main channel
γ_i^j	variation of concentration in the river water associated to the water balance of floodplains $\Delta Q_{t\,k}^{\,j}$
δ_i^j	residual variation of concentration in the river water, for $\Delta Q\mathrm{RS}/Q_t = \Delta Q\mathrm{RI}/Q_t = \Delta Q_t = 0$

Table A1. Total discharge and river flow components (superficial runoff RS, interflow RI, and baseflow RB) as calculated by chemical tracing (model 3); in-long profile of discharge established for each individual cruise (n = 8) and for averages; and observed values on the Amazon River main stem (10 stations) compared to theoretical in-long profile (nine virtual stations) by cumulating the inputs and inflows.

		Cruise 1										
		mm yr^{-1}				m^3 s^{-1}				QK/Q_t		
Station	km	QRS	QRI	QRB	Q_t	QRS	QRI	QRB	Q_t	QRS	QRI	QRB
SAI	90	394	1187	334	1914	13 724	41 371	11 634	66 729	0.206	0.620	0.174
Xib	231	411	1310	363	2084	14 516	46 278	12 835	73 629	0.197	0.629	0.174
Tup	372	461	1287	382	2130	17 240	48 109	14 280	79 629	0.217	0.604	0.179
Jut	628	450	1044	403	1897	24 263	56 223	21 725	102 212	0.237	0.550	0.213
Ita	808	473	1076	349	1897	26 362	60 020	19 437	105 819	0.249	0.567	0.184
Ano	923	469	1085	344	1897	26 578	61 548	19 497	107 623	0.247	0.572	0.181
Man	1026	484	1085	307	1876	33 437	74 980	21 182	129 598	0.258	0.579	0.163
SJA	1553	419	1396	237	2052	38 524	128 290	21 784	188 598	0.204	0.680	0.116
Pau	1744	298	1120	244	1662	40 980	154 047	33 571	228 598	0.179	0.674	0.147
Óbi	2000	284	882	330	1496	41 757	129 683	48 560	220 000	0.190	0.589	0.221

		mm yr^{-1}				m^3 s^{-1}				QK/Q_t		
Station	km	QRS	QRI	QRB	Q_t	QRS	QRI	QRB	Q_t	QRS	QRI	QRB
Solimões	0	456	1479	380	2315	13 738	44 535	11 428	69 700	0.197	0.639	0.164
+ Içá	90	490	1328	384	2202	17 032	46 212	13 356	76 600	0.222	0.603	0.174
+ Jutai	372	481	1374	386	2241	17 728	50 649	14 223	82 600	0.215	0.613	0.172
+ Jur + Jap	628	454	1211	366	2031	24 030	64 032	19 338	107 400	0.224	0.596	0.180
+ Jur + Jap	808	454	1211	366	2031	24 030	64 032	19 338	107 400	0.224	0.596	0.180
+ Purus	1026	413	1214	343	1970	26 698	78 539	22 163	127 400	0.210	0.616	0.174
+ Negro	1553	352	1489	314	2154	30 425	128 837	27 137	186 400	0.163	0.691	0.146
+ Madeira	1744	333	1086	319	1738	43 355	141 479	41 565	226 400	0.191	0.625	0.184
Σ Rios	2000	333	1086	319	1738	43 355	141 479	41 565	226 400	0.191	0.625	0.184

Cruise 2

Station	km	mm yr^{-1}				m^3 s^{-1}				QK/Q_t		
		QRS	QRI	QRB	Q_t	QRS	QRI	QRB	Q_t	QRS	QRI	QRB
SAI	90	86	589	331	1006	3009	20 538	11 532	35 079	0.086	0.585	0.329
Xib	231	68	798	334	1199	2410	28 180	11 789	42 379	0.057	0.665	0.278
Tup	372	174	678	340	1192	6505	25 342	12 732	44 579	0.146	0.568	0.286
Jut	628	269	874	444	1587	14 485	47 084	23 909	85 478	0.169	0.551	0.280
Ita	808	359	813	414	1587	20 043	45 355	23 097	88 495	0.226	0.513	0.261
Ano	923	341	781	465	1587	19 327	44 291	26 385	90 003	0.215	0.492	0.293
Man	1026	287	1000	332	1619	19 832	69 096	22 935	111 863	0.177	0.618	0.205
SJA	1553	363	1009	284	1656	33 329	92 721	26 113	152 163	0.219	0.609	0.172
Pau	1744	227	733	245	1206	31 256	100 866	33 741	165 863	0.188	0.608	0.203
Óbi	2000	246	598	253	1097	36 180	87 918	37 202	161 300	0.224	0.545	0.231

Station	km	mm yr^{-1}				m^3 s^{-1}				QK/Q_t		
		QRS	QRI	QRB	Q_t	QRS	QRI	QRB	Q_t	QRS	QRI	QRB
Solimões	0	137	599	317	1053	4122	18 035	9 543	31 700	0.130	0.569	0.301
+ Içá	90	129	682	310	1121	4487	23 715	10 797	39 000	0.115	0.608	0.277
+ Jutai	372	133	672	312	1118	4905	24 779	11 516	41 200	0.119	0.601	0.280
+ Jur + Jap	628	97	837	282	1216	5115	44 277	14 908	64 300	0.080	0.689	0.232
+ Jur + Jap	808	97	837	282	1216	5115	44 277	14 908	64 300	0.080	0.689	0.232
+ Purus	1026	88	806	269	1163	5716	52 110	17 373	75 200	0.076	0.693	0.231
+ Negro	1553	38	1056	241	1335	3270	91 406	20 824	115 500	0.028	0.791	0.180
+ Madeira	1744	99	648	245	992	12 836	84 466	31 898	129 200	0.099	0.654	0.247
$\sum$ Rios	2000	99	648	245	992	12 836	84 466	31 898	129 200	0.099	0.654	0.247

Cruise 3

Station	km	mm yr^{-1}				m^3 s^{-1}				QK/Q_t		
		QRS	QRI	QRB	Q_t	QRS	QRI	QRB	Q_t	QRS	QRI	QRB
SAI	90	913	170	446	1529	31 812	5924	15 550	53 285	0.597	0.111	0.292
Xib	231	1054	197	464	1715	37 236	6952	16 397	60 585	0.615	0.115	0.271
Tup	372	1097	135	457	1690	41 022	5065	17 098	63 185	0.649	0.080	0.271
Jut	628	996	−4	518	1510	53 653	−221	27 927	81 359	0.659	−0.003	0.343

Table A1. (*Continued*)

		Cruise 3										
		mm yr^{-1}				m^3 s^{-1}				QK/Q_t		
Station	km	QRS	QRI	QRB	Q_t	QRS	QRI	QRB	Q_t	QRS	QRI	QRB
Ita	808	950	3	558	1510	52 958	155	31 118	84 231	0.629	0.002	0.369
Ano	923	963	−4	552	1510	54 604	−224	31 287	85 667	0.637	−0.003	0.365
Man	1026	761	13	398	1172	52 583	888	27 464	80 935	0.650	0.011	0.339
SJA	1553	530	61	343	935	48 739	5648	31 548	85 935	0.567	0.066	0.367
Pau	1744	347	145	301	793	47 720	19 902	41 413	109 035	0.438	0.183	0.380
Óbi	2000	321	220	295	836	47 155	32 380	43 365	122 900	0.384	0.263	0.353

		mm yr^{-1}				m^3 s^{-1}				QK/Q_t		
Station	km	QRS	QRI	QRB	Q_t	QRS	QRI	QRB	Q_t	QRS	QRI	QRB
Solimões	0	1113	270	514	1897	33 506	8129	15 464	57 100	0.587	0.142	0.271
+ Içа	90	1115	224	512	1851	38 792	7803	17 805	64 400	0.602	0.121	0.276
+ Jutai	372	1132	171	515	1818	41 729	6305	18 966	67 000	0.623	0.094	0.283
+ Jur + Jap	628	1033	105	470	1607	54 624	5538	24 838	85 000	0.643	0.065	0.292
+ Jur + Jap	808	1033	105	470	1607	54 624	5538	24 838	85 000	0.643	0.065	0.292
+ Purus	1026	937	24	430	1392	60 623	1579	27 798	90 000	0.674	0.018	0.309
+ Negro	1553	995	−318	421	1098	86 126	−27 521	36 395	95 000	0.907	−0.290	0.383
+ Madeira	1744	518	3	386	907	67 479	344	50 277	118 100	0.571	0.003	0.426
∑ Rios	2000	518	3	386	907	67 479	344	50 277	118 100	0.571	0.003	0.426

		Cruise 4										
		mm yr^{-1}				m^3 s^{-1}				QK/Q_t		
Station	km	QRS	QRI	QRB	Q_t	QRS	QRI	QRB	Q_t	QRS	QRI	QRB
SAI	90	895	265	493	1653	31 191	9226	17 197	57 614	0.541	0.160	0.298
Xib	231	972	323	517	1812	34 340	11 414	18 260	64 014	0.536	0.178	0.285
Tup	372	868	434	515	1816	32 444	16 228	19 242	67 914	0.478	0.239	0.283
Jut	628	895	298	476	1669	48 238	16 027	25 638	89 903	0.537	0.178	0.285
Ita	808	786	403	480	1669	43 818	22 462	26 796	93 076	0.471	0.241	0.288

Ano	923	834	354	482	1669	47 284	20 054	27 325	94 663	0.499	0.212	0.289
Man	1026	725	369	439	1532	50 049	25 478	30 298	105 825	0.473	0.241	0.286
SJA	1553	582	306	354	1242	53 464	28 165	32 495	114 125	0.468	0.247	0.285
Pau	1744	520	351	310	1182	71 579	48 275	42 671	162 525	0.440	0.297	0.263
Óbi	2000	463	392	279	1134	68 036	57 700	41 064	166 800	0.408	0.346	0.246

		mm yr^{-1}				m^3 s^{-1}				QK/Q_t		
Station	km	QRS	QRI	QRB	Q_t	QRS	QRI	QRB	Q_t	QRS	QRI	QRB
Solimões	0	934	279	528	1741	28 112	8392	15 896	52 400	0.536	0.160	0.303
+ Içа	90	940	222	528	1690	32 696	7730	18 375	58 800	0.556	0.131	0.312
+ Jutai	372	939	236	526	1701	34 617	8711	19 372	62 700	0.552	0.139	0.309
+ Jur + Jap	628	831	151	479	1462	43 941	8003	25 356	77 300	0.568	0.104	0.328
+ Jur + Jap	808	831	151	479	1462	43 941	8003	25 356	77 300	0.568	0.104	0.328
+ Purus	1026	777	201	438	1416	50 272	13 029	28 299	91 600	0.549	0.142	0.309
+ Negro	1553	832	−106	428	1154	71 986	−9134	37 049	99 900	0.721	−0.091	0.371
+ Madeira	1744	637	119	382	1138	83 003	15 506	49 790	148 300	0.560	0.105	0.336
$\sum$ Rios	2000	637	119	382	1138	83 003	15 506	49 790	148 300	0.560	0.105	0.336

Cruise 5

		mm yr^{-1}				m^3 s^{-1}				QK/Q_t		
Station	km	QRS	QRI	QRB	Q_t	QRS	QRI	QRB	Q_t	QRS	QRI	QRB
SAI	90	342	389	397	1128	11 913	13 562	13 849	39 325	0.303	0.345	0.352
Xib	231	334	603	434	1371	11 786	21 307	15 332	48 425	0.243	0.440	0.317
Tup	372	355	644	409	1407	13 260	24 086	15 279	52 625	0.252	0.458	0.290
Jut	628	360	987	459	1806	19 417	53 178	24 708	97 304	0.200	0.547	0.254
Ita	808	480	865	462	1806	26 744	48 232	25 762	100 738	0.265	0.479	0.256
Ano	923	468	883	455	1806	26 529	50 109	25 817	102 455	0.259	0.489	0.252
Man	1026	440	838	435	1712	30 377	57 863	30 059	118 299	0.257	0.489	0.254
SJA	1553	465	785	388	1638	42 701	72 169	35 628	150 499	0.284	0.480	0.237
Pau	1744	359	579	335	1274	49 425	79 642	46 132	175 199	0.282	0.455	0.263
Óbi	2000	359	495	352	1206	52 855	72 740	51 706	177 300	0.298	0.410	0.292

Table A1. (*Continued*)

Station	km	mm yr^{-1}				m^3 s^{-1}				QK/Q_t		
		QRS	QRI	QRB	Q_t	QRS	QRI	QRB	Q_t	QRS	QRI	QRB
Station	km	mm yr^{-1}				m^3 s^{-1}				QK/Q_t		
		QRS	QRI	QRB	Q_t	QRS	QRI	QRB	Q_t	QRS	QRI	QRB
Solimões	0	370	512	406	1289	11 151	15 419	12 230	38 800	0.287	0.397	0.315
+ Içа	90	353	624	400	1377	12 277	21 720	13 903	47 900	0.256	0.453	0.290
+ Jutai	372	345	666	403	1414	12 698	24 550	14 852	52 100	0.244	0.471	0.285
+ Jur + Jap	628	302	745	360	1407	15 977	39 405	19 018	74 400	0.215	0.530	0.256
+ Jur + Jap	808	302	745	360	1407	15 977	39 405	19 018	74 400	0.215	0.530	0.256
+ Purus	1026	263	785	334	1382	17 030	50 776	21 594	89 400	0.190	0.568	0.242
+ Negro	1553	248	843	315	1405	21 428	72 936	27 235	121 600	0.176	0.600	0.224
+ Madeira	1744	198	606	319	1123	25 775	79 006	41 519	146 300	0.176	0.540	0.284
$\sum$ Rios	2000	198	606	319	1123	25 775	79 006	41 519	146 300	0.176	0.540	0.284

Cruise 6

Station	km	mm yr^{-1}				m^3 s^{-1}				QK/Q_t		
		QRS	QRI	QRB	Q_t	QRS	QRI	QRB	Q_t	QRS	QRI	QRB
SAI	90	117	439	275	831	4067	15 297	9591	28 954	0.140	0.528	0.331
Xib	231	221	404	359	984	7818	14 265	12 671	34 754	0.225	0.410	0.365
Tup	372	239	332	396	967	8927	12 419	14 808	36 154	0.247	0.344	0.410
Jut	628	280	496	287	1063	15 065	26 734	15 449	57 248	0.263	0.467	0.270
Ita	808	320	404	339	1063	17 839	22 549	18 880	59 268	0.301	0.380	0.319
Ano	923	370	334	359	1063	20 959	18 929	20 390	60 278	0.348	0.314	0.338
Man	1026	281	221	341	844	19 440	15 280	23 578	58 298	0.333	0.262	0.404
SJA	1553	219	275	275	769	20 128	25 316	25 254	70 698	0.285	0.358	0.357
Pau	1744	83	172	309	564	11 362	23 658	42 478	77 498	0.147	0.305	0.548
Óbi	2000	86	165	373	624	12 633	24 233	54 834	91 700	0.138	0.264	0.598

Station	km	mm yr^{-1}				m^3 s^{-1}				QK/Q_t		
		QRS	QRI	QRB	Q_t	QRS	QRI	QRB	Q_t	QRS	QRI	QRB
Solimões	0	151	438	295	884	4538	13 180	8882	26 600	0.171	0.495	0.334
+ Içа	90	155	489	288	931	5381	17 015	10 004	32 400	0.166	0.525	0.309
+ Jutai	372	164	465	288	917	6027	17 145	10 628	33 800	0.178	0.507	0.314
+ Jur + Jap	628	145	526	264	934	7663	27 798	13 939	49 400	0.155	0.563	0.282
+ Jur + Jap	808	145	526	264	934	7663	27 798	13 939	49 400	0.155	0.563	0.282
+ Purus	1026	153	400	254	807	9873	25 879	16 448	52 200	0.189	0.496	0.315
+ Negro	1553	167	325	254	746	14 474	28 123	22 004	64 600	0.224	0.435	0.341
+ Madeira	1744	92	223	233	548	12 027	29 016	30 357	71 400	0.168	0.406	0.425
$\sum$ Rios	2000	92	223	233	548	12 027	29 016	30 357	71 400	0.168	0.406	0.425

Cruise 7

Station	km	mm yr^{-1}				m^3 s^{-1}				QK/Q_t		
		QRS	QRI	QRB	Q_t	QRS	QRI	QRB	Q_t	QRS	QRI	QRB
SAI	90	1032	123	459	1614	35 972	4286	15 997	56 255	0.639	0.076	0.284
Xib	231	1203	66	529	1799	42 506	2345	18 704	63 555	0.669	0.037	0.294
Tup	372	1158	133	510	1801	43 302	4975	19 077	67 355	0.643	0.074	0.283
Jut	628	888	308	426	1622	47 811	16 566	22 974	87 350	0.547	0.190	0.263
Ita	808	839	306	476	1622	46 801	17 076	26 556	90 433	0.518	0.189	0.294
Ano	923	794	403	425	1622	45 019	22 853	24 102	91 974	0.489	0.248	0.262
Man	1026	764	231	455	1450	52 800	15 953	31 425	100 178	0.527	0.159	0.314
SJA	1553	697	281	417	1395	64 081	25 820	38 277	128 178	0.500	0.201	0.299
Pau	1744	742	97	400	1238	102 012	13 324	54 942	170 278	0.599	0.078	0.323
Óbi	2000	678	102	423	1204	99 736	15 065	62 199	177 000	0.563	0.085	0.351

Station	km	mm yr^{-1}				m^3 s^{-1}				QK/Qt		
		QRS	QRI	QRB	Q_t	QRS	QRI	QRB	Q_t	QRS	QRI	QRB
Solimões	0	1070	138	503	1711	32 205	4167	15 128	51 500	0.625	0.081	0.294
+ Içа	90	1056	120	513	1690	36 755	4187	17 858	58 800	0.625	0.071	0.304
+ Jutai	372	1056	129	513	1699	38 926	4767	18 907	62 600	0.622	0.076	0.302
+ Jur + Jap	628	954	82	487	1524	50 467	4356	25 778	80 600	0.626	0.054	0.320
+ Jur + Jap	808	954	82	487	1524	50 467	4356	25 778	80 600	0.626	0.054	0.320

Table A1. (*Continued*)

Station	km	mm yr^{-1}				m^3 s^{-1}				*QK*/*Qt*		
		*Q*RS	*Q*RI	*Q*RB	Q_t	*Q*RS	*Q*RI	*Q*RB	Q_t	*Q*RS	*Q*RI	QRB
+ Purus	1026	897	54	460	1412	58 026	3494	29 780	91 300	0.636	0.038	0.326
+ Negro	1553	889	24	466	1379	76 903	2099	40 299	119 300	0.645	0.018	0.338
+ Madeira	1744	714	87	438	1239	92 995	11 341	57 064	161 400	0.576	0.070	0.354
∑ Rios	2000	714	87	438	1239	92 995	11 341	57 064	161 400	0.576	0.070	0.354

Cruise 8

Station	km	mm yr^{-1}				m^3 s^{-1}				*QK*/Q_t		
		*Q*RS	*Q*RI	*Q*RB	Q_t	*Q*RS	*Q*RI	*Q*RB	Q_t	*Q*RS	*Q*RI	*Q*RB
SAI	90	307	723	434	1465	10 696	25 217	15 141	51 053	0.209	0.494	0.297
Xib	231	340	898	445	1683	12 011	31 713	15 729	59 453	0.202	0.533	0.265
Tup	372	275	991	412	1678	10 300	37 048	15 405	62 753	0.164	0.590	0.245
Jut	628	264	1220	397	1881	14 196	65 734	21 374	101 305	0.140	0.649	0.211
Ita	808	372	1086	423	1881	20 741	60 550	23 589	104 880	0.198	0.577	0.225
Ano	923	338	1127	415	1881	19 166	63 950	23 552	106 668	0.180	0.600	0.221
Man	1026	360	987	490	1837	24 897	68 171	33 834	126 902	0.196	0.537	0.267
SJA	1553	404	1052	428	1885	37 162	96 691	39 349	173 202	0.215	0.558	0.227
Pau	1744	286	722	392	1400	39 335	99 253	53 914	192 502	0.204	0.516	0.280
Óbi	2000	319	640	421	1381	46 937	94 151	61 912	203 000	0.231	0.464	0.305

Station	km	mm yr^{-1}				m^3 s^{-1}				*QK*/Q_t		
		*Q*RS	*Q*RI	*Q*RB	Q_t	*Q*RS	*Q*RI	*Q*RB	Q_t	*Q*RS	*Q*RI	*Q*RB
Solimões	0	304	827	464	1594	9160	24 886	13 954	48 000	0.191	0.518	0.291
+ Içа	90	306	856	458	1621	10 659	29 788	15 953	56 400	0.189	0.528	0.283
+ Jutai	372	310	852	458	1620	11 411	31 410	16 878	59 700	0.191	0.526	0.283
+ Jur + Jap	628	287	828	420	1535	15 196	43 781	22 223	81 200	0.187	0.539	0.274
+ Jur + Jap	808	287	828	420	1535	15 196	43 781	22 223	81 200	0.187	0.539	0.274
+ Purus	1026	242	861	402	1506	15 665	55 703	26 031	97 400	0.161	0.572	0.267
+ Negro	1553	207	1030	423	1661	17 945	89 139	36 616	143 700	0.125	0.620	0.255
+ Madeira	1744	162	692	397	1251	21 043	90 210	51 747	163 000	0.129	0.553	0.317
∑ Rios	2000	162	692	397	1251	21 043	90 210	51 747	163 000	0.129	0.553	0.317

Ave

Station	km	mm yr^{-1}				m^3 s^{-1}				QK/Q_t		
		QRS	QRI	QRB	Q_t	QRS	QRI	QRB	Q_t	QRS	QRI	QRB
SAI	90	511	486	396	1392	17 789	16 928	13 811	48 537	0.367	0.349	0.285
Xib	231	575	575	431	1581	20 328	20 307	15 215	55 849	0.364	0.364	0.272
Tup	372	578	579	428	1585	21 625	21 659	15 990	59 274	0.365	0.365	0.270
Jut	628	550	653	426	1629	29 641	35 166	22 963	87 770	0.338	0.401	0.262
Ita	808	572	619	438	1629	31 913	34 550	24 404	90 868	0.351	0.380	0.269
Ano	923	572	620	437	1629	32 433	35 189	24 794	92 416	0.351	0.381	0.268
Man	1026	513	593	399	1505	35 427	40 964	27 597	103 987	0.341	0.394	0.265
SJA	1553	460	646	341	1446	42 266	59 353	31 306	132 925	0.318	0.447	0.236
Pau	1744	358	490	317	1165	49 209	67 371	43 608	160 187	0.307	0.421	0.272
Óbi	2000	345	437	341	1122	50 661	64 234	50 105	165 000	0.307	0.389	0.304

Station	km	mm yr^{-1}				m^3 s^{-1}				QK/Q_t		
		QRS	QRI	QRB	Q_t	QRS	QRI	QRB	Q_t	QRS	QRI	QRB
Solimões	0	567	568	426	1560	17 067	17 093	12 816	46 975	0.363	0.364	0.273
+ Içá	90	568	568	424	1560	19 760	19 771	14 756	54 288	0.364	0.364	0.272
+ Jutai	372	570	571	425	1566	21 005	21 040	15 668	57 713	0.364	0.365	0.271
+ jur + Jap	628	513	561	391	1464	27 127	29 649	20 675	77 450	0.350	0.383	0.267
+ jur + Jap	808	513	561	391	1464	27 127	29 649	20 675	77 450	0.350	0.383	0.267
+ Purus	1026	471	543	366	1381	30 488	35 139	23 686	89 313	0.341	0.393	0.265
+ Negro	1553	466	543	358	1366	40 319	46 986	30 945	118 250	0.341	0.397	0.262
+ Madeira	1744	344	433	340	1117	44 814	56 421	44 277	145 513	0.308	0.388	0.304
$\sum$ Rios	2000	344	433	340	1117	44 814	56 421	44 277	145 513	0.308	0.388	0.304

Table A2. Results of model M1. Calibration of linear coefficient (a = slope; b = x intersect) between the concentrations in the inflow (in) and in the outflow (out). View of correlation coefficient r^2 and determination of mean bias for the 10 sampling stations located along the Amazon main stem.

i / j			Cations (μmol L^{-1})				μeq L^{-1}		Anions (μmol L^{-1})					
		pH	Na^+	K^+	Ca^{2+}	Mg^{2+}	S^+	S^-	HCO_3^-	Cl^-	NO_3^-	DOC^-	SO_4^{2-}	HPO_4^{2-}
SAI	a	1.37	0.97	1.16	0.95	0.92	0.89	0.89	1.08	0.68	1.06	0.58	0.78	0.29
	b	−2.81	−5	−8	−48	−5	−37	−37	−211	27	−2.5	7.2	4.2	0.6
	r^2	0.73	0.92	0.95	0.82	0.58	0.75	0.75	0.82	0.94	0.91	0.53	0.72	0.13
	In	7.34	202	32	457	80	1308	1308	992	155	13.4	19.0	63.2	0.90
	Out	7.23	191	29	389	69	1137	1137	866	133	11.6	18.2	52.9	0.86
	Bias	−0.11	−11	−3	−68	−10	−171	−171	−126	−21	−1.7	−0.8	−10.3	−0.04
Xib	a	0.49	1.13	1.10	0.90	1.03	0.87	0.87	0.86	0.64	0.90	0.65	0.71	0.67
	b	3.66	−24	−3	21	−4	111	111	91	45	1.7	5.7	11.9	0.3
	r^2	0.37	0.79	0.64	0.97	0.90	0.96	0.96	0.93	0.88	0.92	0.88	0.76	0.54
	In	7.27	181	29	400	71	1152	1152	872	136	12.6	19.1	55.8	0.84
	Out	7.26	179	29	380	69	1107	1107	838	132	13.1	17.9	51.9	0.86
	Bias	−0.02	−2	0	−20	−2	−46	−46	−34	−4	0.5	−1.2	−3.9	0.02
Tup	a	0.87	1.24	0.91	0.78	0.86	0.72	0.72	0.61	0.67	1.17	0.81	0.49	0.47
	b	0.90	−40	4	68	8	271	271	291	39	−1.1	3.0	28.6	0.5
	r^2	0.78	0.66	0.73	0.89	0.74	0.80	0.80	0.58	0.90	0.80	0.96	0.34	0.22
	In	7.20	173	28	380	67	1096	1096	825	128	11.9	19.6	54.7	0.81
	Out	7.19	173	29	362	65	1057	1057	788	125	12.9	18.7	55.6	0.88
	Bias	−0.01	1	1	−18	−2	−39	−39	−38	−3	1.0	−0.9	0.9	0.07
Jut	a	1.21	0.26	1.33	0.74	1.47	0.90	0.90	0.61	0.03	0.84	1.20	0.51	0.76
	b	−1.65	106	−12	12	−43	−106	−105	161	87	2.0	−4.0	14.3	0.1
	r^2	0.81	0.17	0.87	0.89	0.79	0.88	0.88	0.63	0.00	0.54	0.94	0.36	0.45
	In	7.18	170	29	373	67	1078	1078	817	122	11.9	20.0	52.7	0.81
	Out	7.05	151	26	283	55	852	852	650	90	12.0	19.5	39.3	0.72
	Bias	−0.13	−19	−3	−90	−12	−226	−226	−167	−32	0.0	−0.5	−13.5	−0.09
Ita	a	1.12	0.75	1.36	0.75	1.06	0.77	0.77	0.85	0.55	1.51	1.08	0.17	0.90
	b	−0.91	35	−8	48	−4	147	147	36	32	−5.7	−1.9	45.7	0.1
	r^2	0.83	0.38	0.66	0.92	0.92	0.87	0.87	0.89	0.37	0.84	0.93	0.04	0.47
	In	7.09	145	25	305	56	894	894	674	101	11.1	19.6	43.2	0.70
	Out	7.00	143	26	272	55	823	823	602	87	10.9	19.1	51.2	0.74
	Bias	−0.09	−2	1	−33	−1	−70	−70	−72	−13	−0.2	−0.5	8.0	0.04

Ano	*a*	1.23	0.66	1.20	0.76	1.20	0.76	0.76	0.71	0.54	1.54	1.01	0.37	0.60
	b	−1.75	49	−5	39	−12	142	143	132	32	−5.7	−1.2	31.1	0.4
	r^2	0.85	0.24	0.84	0.95	0.87	0.87	0.87	0.85	0.37	0.74	0.82	0.11	0.23
	In	7.09	145	25	305	56	894	894	674	101	11.1	19.6	43.2	0.70
	Out	6.99	144	25	268	54	813	813	603	86	11.2	18.5	46.3	0.79
	Bias	−0.10	−1	0	−38	−2	−80	−80	−71	−15	0.1	−1.0	3.1	0.09
Man	*a*	1.12	1.53	2.30	0.75	1.19	0.86	0.86	0.65	0.95	1.66	0.89	0.37	1.14
	b	−0.92	−72	−29	40	−10	58	58	159	−6	−6.7	2.5	28.7	0.0
	r^2	0.82	0.83	0.80	0.87	0.85	0.80	0.80	0.62	0.54	0.94	0.71	0.10	0.34
	In	6.98	135	25	276	52	817	817	619	89	10.5	20.3	38.7	0.7
	Out	6.91	133	28	241	50	743	743	552	78	10.5	20.5	40.0	0.8
	Bias	−0.07	−2	2	−36	−2	−75	−75	−67	−11	0.0	0.2	1.3	0.07
SJA	*a*	1.01	1.14	1.16	0.79	1.16	0.87	0.87	0.93	1.04	1.46	0.83	−0.11	1.26
	b	−0.12	−13	−3	29	−7	47	49	14	−9	−3.3	3.1	31.0	−0.1
	r^2	0.85	0.89	0.82	0.96	0.86	0.97	0.97	0.79	0.87	0.91	0.80	0.02	0.39
	In	6.87	110	22	211	41	639	638	469	72	8.6	26.4	30.8	0.57
	Out	6.78	111	22	189	40	591	591	438	65	9.0	25.2	26.3	0.63
	Bias	−0.09	1	0	−22	−1	−47	−47	−31	−7	0.4	−1.2	−4.5	0.07
Pau	*a*	1.14	1.51	1.13	0.78	1.14	0.88	0.88	0.82	1.09	1.32	0.69	0.13	1.22
	b	−1.05	−53	−2	27	−6	43	45	61	−11	−1.7	5.0	27.5	−0.1
	r^2	0.83	0.82	0.94	0.95	0.98	0.92	0.92	0.77	0.91	0.95	0.76	0.01	0.74
	In	6.87	107	25	196	46	619	618	453	65	9.0	24.7	33.0	0.55
	Out	6.80	106	25	176	46	575	575	423	60	10.0	22.0	29.6	0.60
	Bias	−0.07	0	1	−20	0	−44	−43	−30	−5	1.0	−2.7	−3.4	0.05
Óbi	*a*	1.17	1.18	1.86	0.84	1.22	0.90	0.90	0.86	0.80	1.49	0.63	0.85	0.59
	b	−1.23	−16	−19	15	−9	30	32	49	6	−2.4	6.1	0.7	0.4
	r^2	0.84	0.62	0.80	0.93	0.93	0.91	0.91	0.95	0.86	0.88	0.68	0.57	0.11
	In	6.87	107	25	196	46	619	618	453	65	9.0	24.7	33.0	0.6
	Out	6.75	109	26	176	46	580	580	433	58	11.0	21.4	27.3	0.7
	Bias	−0.13	2	1	−20	0	−39	−38	−19	−6	1.9	−3.3	−5.8	0.17

i / *j*		mg L^{-1}	μmoI L^{-1}				mg L^{-1}					$\delta^{18}O$
		DOC	DIC	CO_2	O_2	SiO_2	FSS	CSS	TSS	POCF	POCC	H_2O
SAI	*a*	0.58	1.19	1.70	0.58	0.83	0.92	0.58	0.83	0.98	0.38	0.98
	b	1.34	−310	−53	69	22	−30	25	2	−0.45	0.39	0.02
	r^2	0.53	0.93	0.92	0.61	0.95	0.99	0.97	0.98	0.95	0.28	1.00
	In	3.56	1098	105	181	148	349	107	456	3.76	0.82	−6.85
	Out	3.41	984	118	174	145	292	86	379	3.20	0.72	−6.67
	Bias	−0.14	−114	12	−7	−3	−57	−21	−78	−0.56	−0.11	0.18

Table A2. (*Continued*)

j \ *i*		mg L^{-1}	μmol L^{-1}				mg L^{-1}					$\delta^{18}O$
		DOC	DIC	CO_2	O_2	SiO_2	FSS	CSS	TSS	POCF	POCC	H_2O
Xib	*a*	0.65	0.85	0.67	0.85	0.96	1.05	0.23	0.91	1.04	0.05	0.95
	b	1.07	115	37	20	4	−28	62	17	−0.36	0.65	−0.26
	r^2	0.88	0.95	0.73	0.86	0.99	0.98	0.20	0.83	0.98	0.00	0.99
	In	3.57	981	109	181	143	312	95	406	3.43	0.74	−6.69
	Out	3.35	946	108	173	142	298	82	381	3.23	0.70	−6.58
	Bias	−0.22	−34	−1	−8	0	−13	−12	−26	−0.21	−0.04	0.11
Tup	*a*	0.81	0.73	0.93	0.70	1.04	0.97	0.55	1.01	0.92	0.25	0.98
	b	0.55	226	9	43	−5	4	35	−8	0.29	0.48	−0.02
	r^2	0.96	0.71	0.93	0.69	0.97	0.98	0.47	0.90	0.90	0.07	0.99
	In	3.67	946	121	175	142	294	89	383	3.28	0.70	−6.61
	Out	3.49	906	118	165	144	288	83	372	3.27	0.65	−6.45
	Bias	−0.17	−40	−2	−10	2	−6	−6	−12	−0.01	−0.04	0.16
Jut	*a*	1.20	0.71	1.13	0.84	0.85	102	0.42	0.94	1.05	0.39	0.94
	b	−0.75	128	−1	16	18	−56	37	−37	−0.59	0.39	−0.04
	r^2	0.94	0.69	0.85	0.76	0.92	0.94	0.51	0.87	0.91	0.04	0.99
	In	3.75	943	126	172	144	287	85	372	3.18	0.67	−6.52
	Out	3.65	786	136	161	143	222	69	291	2.64	0.62	−6.10
	Bias	−0.09	−157	10	−11	−1	−65	−16	−81	−0.54	−0.05	0.42
Ita	*a*	1.08	0.87	1.15	0.86	0.97	0.93	0.44	0.84	1.21	0.38	0.92
	b	−0.35	55	−5	2	5	6	32	33	−0.70	0.40	−0.28
	r^2	0.93	0.86	0.83	0.60	0.83	0.90	0.68	0.86	0.94	0.06	0.98
	In	3.66	802	128	176	135	238	68	306	2.83	0.64	−6.33
	Out	3.57	742	140	153	137	219	61	279	2.64	0.62	−6.05
	Bias	−0.08	−60	12	−23	2	−20	−7	−27	−0.19	−0.02	0.29
Ano	*a*	1.01	0.73	1.28	0.83	1.07	0.94	0.37	0.87	0.95	0.25	0.89
	b	−0.22	174	−16	10	−8	3	38	25	−0.06	0.38	−0.46
	r^2	0.82	0.84	0.87	0.60	0.88	0.84	0.39	0.78	0.76	0.03	0.96
	In	3.66	802	128	176	135	238	68	306	2.83	0.64	−6.33
	Out	3.47	747	144	155	137	217	61	278	2.53	0.52	−6.03
	Bias	−0.19	−55	16	−21	2	−22	−7	−29	−0.30	−0.11	0.31

Man	*a*	0.89	0.67	1.16	0.86	0.81	0.97	0.30	0.86	0.99	0.36	0.92
	b	0.46	206	−12	9	30	−7	32	18	−0.33	0.25	−0.28
	r^2	0.71	0.71	0.85	0.63	0.63	0.93	0.58	0.88	0.87	0.19	0.98
	In	3.79	771	152	165	137	216	60	276	2.59	0.56	−6.22
	Out	3.83	712	159	150	141	190	48	238	2.13	0.43	−5.98
	Bias	0.04	−59	8	−15	4	−26	−12	−38	−0.46	−0.13	0.24
SJA	*a*	0.83	0.96	1.42	0.84	1.00	0.64	−0.17	0.41	0.74	0.20	0.95
	b	0.59	24	−40	20	2	48	35	98	0.25	0.27	−0.19
	r^2	0.80	0.75	0.87	0.91	0.89	0.95	0.09	0.85	0.86	0.19	0.97
	In	4.93	614	146	160	119	165	45	210	2.06	0.43	−5.88
	Out	4.71	607	169	153	122	149	32	181	1.75	0.35	−5.75
	Bias	−0.22	−7	23	−7	3	−15	−13	−29	−0.31	−0.08	0.14
Pau	*a*	0.69	0.68	1.13	0.88	0.98	0.65	−0.05	0.52	0.56	−0.09	0.99
	b	0.94	180	−4	12	4	62	32	95	0.86	0.36	0.07
	r^2	0.76	0.65	0.68	0.88	0.86	0.85	0.01	0.73	0.51	0.02	0.99
	In	4.62	591	138	162	127	213	49	262	2.22	0.45	−5.91
	Out	4.11	583	160	153	125	199	33	232	2.15	0.35	−5.74
	Bias	−0.51	−8	22	−9	−2	−14	−16	−30	−0.08	−0.10	0.17
Óbi	*a*	0.63	0.68	121	0.92	0.39	0.52	−0.05	0.40	0.32	0.22	1.00
	b	1.13	200	−4	1	81	81	32	117	1.55	0.20	0.21
	r^2	0.68	0.78	0.60	0.86	0.28	0.74	0.01	0.58	0.26	0.16	0.99
	In	4.62	591	138	162	127	213	49	262	2.22	0.45	−5.91
	Out	4.01	593	160	151	129	193	33	226	2.32	0.32	−5.63
	Bias	−0.61	2	22	−10	3	−19	−17	−36	0.10	−0.13	0.28

	i	δ^{13}C(‰)			C/N			Carbon cycle (μmol L^{-1})						
j		DIC	POCF	POCC	POCF	POCC	DOC	DIC	POCF	POCC	PONF	PONC	DOC	DON
SAI	*a*	1.02	0.68	0.78	0.96	1.48	0.41	1.19	0.98	0.38	0.46	0.91	0.58	0.86
	b	−0.13	−8.74	−6.12	5.6	8.1	18.4	−310	−37	32	3.4	−1.1	112	2.7
	r^2	0.96	0.49	0.67	0.11	0.07	0.10	0.93	0.95	0.28	0.80	0.54	0.53	0.51
	In	−12.55	−26.69	−27.44	11.2	21.9	31.8	1098	313	68	28.0	3.1	296	9.3
	Out	−12.94	−26.93	−27.35	16.7	48.3	29.8	984	267	60	16.0	1.2	284	9.5
	Bias	−0.39	−0.24	0.09	5.5	26.4	−2.0	−114.0	−46	−9	−12.0	−1.9	−12	0.2
Xib	*a*	0.98	0.87	0.87	0.26	1.66	0.51	0.85	1.04	0.05	0.87	0.06	0.65	0.67
	b	−0.64	−3.62	−3.67	8.1	−15.4	11.1	114.5	−30	54	1.7	2.5	89	4.5
	r^2	0.91	0.85	0.76	0.35	0.67	0.31	0.95	0.98	0.00	0.97	0.00	0.88	0.48
	In	−12.78	−26.78	−27.49	11.1	22.0	30.9	980.8	286	62	25.8	2.8	297	9.6
	Out	−13.11	−26.96	−27.55	10.9	20.3	26.7	946.3	269	58	24.7	2.9	279	10.4
	Bias	−0.34	−0.18	−0.06	−0.2	−1.7	−4.2	−34.5	−17	−3	−1.2	0.1	−18	0.8

Table A2. (*Continued*)

i / *j*		$\delta^{13}C(‰)$			C/N			Carbon cycle (μmol L^{-1})						
		DIC	POCF	POCC	POCF	POCC	DOC	DIC	POCF	POCC	PONF	PONC	DOC	DON
Tup	*a*	1.00	0.60	0.81	0.55	1.75	0.89	0.73	0.92	0.25	0.82	0.49	0.81	0.93
	b	−0.23	−11.03	−5.42	4.8	−16.2	−0.3	225.8	24	40	4.9	1.2	46	2.4
	r^2	0.99	0.57	0.79	0.55	0.67	0.52	0.71	0.90	0.07	0.91	0.19	0.96	0.53
	In	−13.04	−26.81	−27.50	11.0	22.0	30.0	946.0	273	58	24.8	2.6	306	10.2
	Out	−13.24	−26.98	−27.65	10.6	22.3	26.4	906.1	272	55	25.7	2.5	291	11.0
	Bias	−0.20	−0.18	−0.15	−0.4	0.3	−3.6	−40.0	−1	−4	0.9	−0.2	−14	0.9
Jut	*a*	1.11	1.06	1.07	0.67	0.75	0.08	0.71	1.05	0.39	0.95	0.28	1.20	0.26
	b	0.91	1.19	1.78	3.2	5.9	24.0	127.9	−50	32	−1.6	1.6	−62	10.2
	r^2	0.92	0.60	0.78	0.41	0.18	0.01	0.69	0.91	0.04	0.91	0.05	0.94	0.03
	In	−13.29	−26.84	−27.52	10.9	22.0	29.8	942.6	265	56	24.3	2.5	312	10.5
	Out	−13.86	−27.22	−27.82	10.3	23.0	24.9	785.7	220	51	21.5	2.2	304	12.2
	Bias	−0.57	−0.38	−0.30	−0.7	1.0	−5.0	−156.9	−45	−4	−2.8	−0.3	−8	1.8
Ita	*a*	1.24	1.16	0.68	0.22	0.05	0.06	0.87	1.21	0.38	0.74	0.30	1.08	0.03
	b	2.49	4.04	−8.97	8.3	22.8	28.3	55.2	−58	34	4.8	1.5	−29	12.5
	r^2	0.86	0.78	0.56	0.01	0.00	0.00	0.86	0.94	0.06	0.76	0.06	0.93	0.00
	In	−13.63	−26.93	−27.58	10.8	24.1	29.5	801.7	236	53	21.7	2.2	305	10.4
	Out	−14.38	−27.22	−27.87	10.8	24.3	22.8	741.8	220	51	20.4	2.1	298	13.1
	Bias	−0.75	−0.30	−0.29	0.0	0.2	−6.7	−59.9	−15	−2	−1.4	−0.1	−7	2.7
Ano	*a*	1.33	1.27	0.69	0.18	−0.04	0.91	0.73	0.95	0.25	0.77	0.40	1.01	1.42
	b	3.68	7.02	−8.46	8.7	24.1	8.9	174.1	−5	32	3.5	1.0	−18	−3.9
	r^2	0.84	0.66	0.56	0.09	0.00	0.07	0.84	0.76	0.03	0.79	0.11	0.82	0.70
	In	−13.63	−26.93	−27.58	10.8	24.1	29.5	801.7	236	53	21.7	2.2	305	10.4
	Out	−14.45	−27.25	−27.70	10.5	23.0	30.3	746.6	210	44	20.1	1.9	289	9.5
	Bias	−0.81	−0.33	−0.12	−0.4	−1.1	0.8	−55.1	−25	−9	−1.6	−0.3	−16	−0.8
Man	*a*	1.23	1.18	0.78	0.43	−0.39	1.04	0.67	0.99	0.36	0.90	0.41	0.89	1.40
	b	2.55	4.38	−6.12	5.7	32.4	2.2	206.4	−28	21	−0.4	0.9	38	−3.5
	r^2	0.93	0.72	0.72	0.47	0.25	0.19	0.71	0.87	0.19	0.89	0.22	0.71	0.71
	In	−14.17	−27.02	−27.63	10.7	24.4	28.4	770.6	215	47	20.2	1.9	316	11.1
	Out	−15.02	−27.44	−27.72	10.3	23.3	29.1	711.7	178	36	17.3	1.6	319	11.0
	Bias	−0.85	−0.42	−0.09	−0.4	−1.1	0.7	−58.9	−38	−11	−2.9	−0.4	3	−0.1

SJA	*a*	1.22	1.04	0.52	−0.47	−0.19	1.35	0.96	0.74	0.20	0.59	−0.19	0.83	0.76
	b	2.81	0.66	−13.38	15.1	29.4	0.9	23.9	21	22	5.3	1.5	49	2.0
	r^2	0.96	0.95	0.25	0.04	0.01	0.04	0.75	0.86	0.19	0.77	0.21	0.80	0.34
	In	−14.74	−27.07	−27.67	10.6	24.4	29.8	614.4	172	36	16.2	1.5	411	13.8
	Out	−15.20	−27.47	−27.80	9.9	23.5	31.5	607.3	146	29	14.7	1.2	392	12.4
	Bias	−0.46	−0.40	−0.13	−0.7	−0.9	1.8	−7.1	−26	−7	−1.5	−0.2	−18	−1.3
Pau	*a*	1.22	1.04	0.09	0.71	−0.06	2.50	0.68	0.56	−0.09	0.71	−0.24	0.69	1.32
	b	2.48	0.96	−25.20	3.0	23.7	−29.8	179.5	72	30	4.4	1.6	78	−7.2
	r^2	0.93	0.70	0.05	0.91	0.00	0.39	0.65	0.51	0.02	0.71	0.13	0.76	0.91
	In	−14.86	−27.02	−27.48	9.5	22.3	29.0	590.7	185	37	19.5	1.7	385	13.3
	Out	−15.66	−27.21	−27.70	9.7	21.2	32.5	582.6	179	29	18.4	1.4	343	10.6
	Bias	−0.81	−0.20	−0.23	0.2	−1.1	3.5	−8.1	−6	−8	−1.1	−0.3	−42	−2.7
Óbi	*a*	1.31	0.92	−0.09	0.62	−0.92	1.73	0.68	0.32	0.22	0.43	0.05	0.63	1.10
	b	3.77	−2.17	−30.64	3.9	41.1	−15.1	199.8	130	17	10.5	1.2	95	−2.8
	r^2	0.89	0.40	0.04	0.47	0.58	0.24	0.78	0.26	0.16	0.57	0.01	0.68	0.75
	In	−14.86	−27.02	−27.48	9.5	22.3	29.0	590.7	185	37	19.5	1.7	385	13.3
	Out	−15.82	−27.32	−28.01	10.1	19.8	27.9	593.1	194	26	19.2	1.3	334	12.0
	Bias	−0.96	−0.30	−0.53	0.6	−2.6	−1.1	2.4	8	−11	−0.3	−0.3	−51	−1.3

i / *j*		Silicates (μmol L^{-1})			Carbonates (μmol L^{-1})		Carbon cycle (μmol L^{-1})				
		NaSil	CaSil	MgSil	$CaCO_3$	Dolomite	$CO_{2\ CARB}$	$CO_{2\ SIL}$	$CO_{2\ TOT}$	FR	Re
SAI	*a*	1.67	1.67	1.67	1.14	1.48	1.24	1.53	1.08	2.12	0.37
	b	−19.1	−7.6	−6.1	−91	−45	−181	−50	−210	−0.51	1.51
	r^2	0.53	0.53	0.53	0.86	0.70	0.83	0.46	0.82	0.75	0.25
	In	47.2	18.9	15.1	311	64	439	147	1026	0.428	2.09
	Out	58.0	23.2	18.6	263	51	364	170	898	0.405	2.30
	Bias	10.8	4.3	3.4	−48	−14	−76	23	−129	−0.023	0.21
Xib	*a*	1.14	1.14	1.14	0.93	1.26	1.03	0.67	0.86	1.60	0.09
	b	−2.6	−1.0	−0.8	5	−17	−29	56	98	−0.26	1.91
	r^2	0.24	0.24	0.24	0.93	0.75	0.94	0.10	0.94	0.65	0.05
	In	44.8	17.9	14.3	270	56	383	139	905	0.423	2.03
	Out	46.2	18.5	14.8	256	54	364	142	871	0.418	2.08
	Bias	1.4	0.6	0.5	−14	−2	−19	4	−34	−0.005	0.05

Table A2. (*Continued*)

i / *j*		Silicates (μmol L^{-1})			Carbonates (μmol L^{-1})		Carbon cycle (μmol L^{-1})				
		NaSil	CaSil	MgSil	$CaCO_3$	Dolomite	$CO_{2\ CARB}$	$CO_{2\ SIL}$	$CO_{2\ TOT}$	FR	Re
Tup	*a*	1.25	1.25	1.25	0.73	1.24	0.85	0.69	0.61	1.76	0.20
	b	−4.7	−1.9	−1.5	52	−16	32	60	302	−0.33	1.68
	r^2	0.13	0.13	0.13	0.56	0.72	0.62	0.04	0.58	0.41	0.04
	In	44.1	17.6	14.1	255	53	361	136	858	0.421	2.00
	Out	47.8	19.1	15.3	238	50	337	146	821	0.411	2.10
	Bias	3.7	1.5	1.2	−17	−3	−23	10	−37	−0.010	0.10
Jut	*a*	1.42	1.42	1.42	0.51	1.73	0.74	1.39	0.62	1.84	0.71
	b	−7.7	−3.1	−2.5	59	−52	−3	−28	160	−0.39	0.83
	r^2	0.29	0.29	0.29	0.57	0.78	0.64	0.26	0.67	0.53	0.39
	In	47.4	19.0	15.2	249	52	352	144	849	0.415	2.07
	Out	60.6	24.2	19.4	184	35	254	174	683	0.373	2.31
	Bias	13.2	5.3	4.2	−65	−16	−98	29	−167	−0.042	0.24
Ita	*a*	2.14	2.14	2.14	0.89	1.38	1.02	1.85	0.85	2.41	0.51
	b	−38.6	−15.5	−12.4	−16	−20	−52	−82	39	−0.60	1.23
	r^2	0.47	0.47	0.47	0.83	0.96	0.90	0.36	0.90	0.85	0.20
	In	44.0	17.6	14.1	203	42	286	133	705	0.406	2.01
	Out	55.2	22.1	17.7	162	37	236	161	633	0.373	2.28
	Bias	11.2	4.5	3.6	−41	−5	−50	28	−72	−0.033	0.27
Ano	*a*	2.07	2.07	2.07	0.71	1.70	0.98	1.51	0.71	2.77	0.23
	b	−32.2	−12.9	−10.3	21	−34	−42	−32	142	−0.75	1.81
	r^2	0.27	0.27	0.27	0.66	0.95	0.84	0.17	0.86	0.80	0.03
	In	44.0	17.6	14.1	203	42	286	133	705	0.406	2.01
	Out	57.8	23.1	18.5	163	36	234	166	634	0.369	2.31
	Bias	13.7	5.5	4.4	−40	−6	−52	33	−71	−0.037	0.30
Man	*a*	2.59	2.59	2.59	0.56	1.33	0.79	2.42	0.66	1.76	0.58
	b	−63.6	−25.5	−20.4	45	−16	13	−169	166	−0.33	1.09
	r^2	0.65	0.65	0.65	0.49	0.87	0.77	0.60	0.63	0.76	0.22
	In	46.1	18.4	14.7	182	37	256	138	650	0.394	2.04
	Out	55.1	22.1	17.6	146	33	211	162	585	0.361	2.27
	Bias	9.1	3.6	2.9	−36	−4	−45	24	−65	−0.033	0.23

SJA	*a*	1.36	1.36	1.36	0.80	1.39	1.00	1.07	0.92	1.84	0.34
	b	−5.8	−2.3	−1.9	15	−14	−18	14	27	−0.35	1.51
	r^2	0.50	0.50	0.50	0.60	0.79	0.81	0.44	0.79	0.90	0.19
	In	38.5	15.4	12.3	136	28	193	116	501	0.384	1.97
	Out	45.9	18.3	14.7	119	25	170	134	473	0.358	2.17
	Bias	7.4	3.0	2.4	−17	−3	−23	18	−28	−0.026	0.20
Pau	*a*	1.91	1.91	1.91	0.63	1.35	0.94	1.15	0.81	1.58	0.06
	b	−31.5	−12.6	−10.1	26	−14	−8	0	73	−0.24	2.12
	r^2	0.26	0.26	0.26	0.51	0.80	0.72	0.13	0.76	0.40	0.00
	In	42.0	16.8	13.4	113	33	179	127	484	0.369	2.06
	Out	46.7	18.7	14.9	96	31	158	139	456	0.347	2.23
	Bias	4.7	1.9	1.5	−17	−2	−20	12	−29	−0.022	0.18
Óbi	*a*	1.18	1.18	1.18	0.74	1.57	1.06	0.69	0.87	1.65	0.21
	b	3.1	1.2	1.0	15	−22	−30	70	54	−0.27	1.85
	r^2	0.08	0.08	0.08	0.93	0.74	0.88	0.04	0.94	0.39	0.02
	In	42.0	16.8	13.4	113	33	179	127	484	0.369	2.06
	Out	50.7	20.3	16.2	98	30	158	150	466	0.339	2.28
	Bias	8.8	3.5	2.8	−15	−3	−20	23	−18	−0.030	0.23

Table A3. Results of model M3. Chemical composition (C)K of hydrological reservoirs (indexed k) RS, RI, and RB, established by chemical tracing for all parameters (indexed i) for the 10 sampling stations (index j) located along the Amazon main stem and the seven virtual stations whose chemical composition is calculated by adding the successive inputs of major tributaries. View of R-squared value (r^2) and mean value (Ave) for each parameter. Notice that $QRS/Q_t\,(ij) \times (Cij)RS + QRI/Q_t\,(ij) \times (Cij)RI + QRB/Q_t + (Cij)RB = (Cij)Ave$.

j \ i		mm yr^{-1}		Cations (μmol L^{-1})					μeq L^{-1}		Anions (μmol L^{-1})					
		QK	pH	NH_4^+	Na^+	K^+	Ca^{2+}	Mg^{2+}	S^+	S^-	HCO_3^-	Cl^-	NO_3^-	DOC^-	SO_4^{2-}	HPO_4^{2-}
VG	RS	567	7.23	−0.54	35	51	720	96	1716	1716	1504	11	5.4	36	80	0.10
	RI	568	7.14	−0.29	70	44	497	74	1255	1255	1216	53	−0.3	32	−25	0.65
	RB	426	7.75	2.35	600	−10	55	65	834	834	13	482	42.2	−20	158	2.29
	Ave	1560	7.34	0.34	202	32	457	80	1308	1308	992	155	13.4	19	63	0.90
	r^2		0.18	0.32	1.00	0.79	0.62	0.54	0.57	0.57	0.60	0.95	0.79	0.74	0.51	0.54
SAI	RS	511	7.34	—	30	49	674	103	1632	1632	1485	58	3.7	27	28	0.88
	RI	486	7.32	—	60	44	536	84	1341	1341	1296	65	−3.1	27	−24	1.23
	RB	396	6.99	—	560	−17	−157	8	248	248	−459	315	39.9	−4	180	0.37
	Ave	1392	7.23	—	191	29	389	69	1137	1137	866	133	11.6	18	53	0.86
	r^2		0.02	—	1.00	0.73	0.55	0.66	0.46	0.46	0.68	0.67	0.70	0.43	0.24	0.33
Xib	RS	575	7.40	—	31	54	644	95	1563	1563	1276	74	10.3	26	88	0.53
	RI	575	7.26	—	63	50	441	66	1127	1127	997	82	4.1	23	10	0.84
	RB	431	7.05	—	530	−30	−54	38	470	470	41	277	29.0	1	59	1.33
	Ave	1581	7.26	—	179	29	380	69	1107	1107	838	132	13.1	18	52	0.86
	r^2		0.20	—	1.00	0.66	0.71	0.81	0.68	0.68	0.57	0.84	0.65	0.33	0.54	0.24
Tup	RS	578	6.95	—	30	40	517	75	1252	1252	1041	82	11.5	26	45	0.89
	RI	579	6.91		60	36	385	55	976	976	814	88	0.3	23	24	1.03
	RB	428	7.90	—	520	6	123	65	904	904	409	236	31.9	3	112	0.66
	Ave	1585	7.19	—	173	29	362	65	1057	1057	788	125	12.9	19	56	0.88
	r^2		0.37	—	1.00	0.27	0.38	0.44	0.31	0.31	0.41	0.68	0.86	0.27	0.09	0.06
Jut	RS	550	6.67	—	28	52	579	110	1458	1458	1135	162	4.5	54	52	0.13
	RI	653	6.67	—	59	37	335	61	887	887	799	99	0.4	39	−25	0.49
	RB	426	8.12	—	450	−24	−180	−26	15	15	−204	−16	39.3	−54	121	1.83
	Ave	1629	7.05	—	151	26	283	55	852	852	650	90	12.0	20	39	0.72
	r^2		0.17	—	1.00	0.18	0.77	0.70	0.80	0.80	0.47	0.76	0.60	0.38	0.93	0.08
Ita	RS	572	6.97	—	24	62	764	123	1860	1860	1676	127	−5.5	60	3	−0.88
	RI	619	6.60	—	49	31	321	54	829	829	765	71	−6.2	35	−18	0.08
	RB	438	7.62	—	430	−27	−439	−33	−540	−540	−1034	60	56.7	−57	212	3.81
	Ave	1629	7.00	—	143	26	272	55	823	823	602	87	10.9	19	51	0.74
	r^2		0.47	—	1.00	0.28	0.80	0.74	0.81	0.81	0.77	0.62	0.93	0.83	0.62	0.81

Ano	RS	572	7.17	—	24	53	700	130	1736	1736	1371	138	0.4	43	91	0.57
	RI	620	6.57	—	49	33	313	53	815	815	736	76	−5.3	32	−13	0.78
	RB	437	7.35	—	435	−23	−362	−43	−397	−397	−591	33	48.7	−32	72	1.10
	Ave	1629	6.99	—	144	25	268	54	813	813	603	86	11.2	19	46	0.79
	r^2		0.59	—	1.00	0.35	0.86	0.86	0.87	0.87	0.80	0.69	0.89	0.69	0.58	0.03
Man	RS	513	6.78	—	30	70	442	77	1137	1137	843	83	10.3	36	81	0.54
	RI	593	6.27	—	35	25	185	31	492	492	442	31	−1.6	30	−5	0.57
	RB	399	8.01	—	410	−23	64	46	608	608	343	140	28.9	−14	53	1.36
	Ave	1505	6.91	—	133	28	241	50	743	743	552	78	10.5	21	40	0.77
	r^2		0.80	—	1.00	0.57	0.79	0.88	0.85	0.85	0.65	0.94	0.80	0.58	0.52	0.06
SJA	RS	460	6.70	—	18	65	420	116	1156	1156	937	61	3.1	40	58	−0.84
	RI	646	6.28	—	37	22	84	18	262	262	172	17	−1.7	36	18	0.35
	RB	341	7.84	—	377	−34	77	−22	454	454	268	162	37.3	−16	−2	3.17
	Ave	1446	6.78	—	111	22	189	40	591	591	438	65	9.0	25	26	0.63
	r^2		0.73	—	1.00	0.73	0.81	0.91	0.87	0.87	0.76	0.91	0.84	0.82	0.08	0.59
Pau	RS	358	6.66	—	28	39	250	69	706	706	584	52	10.0	26	17	0.02
	RI	490	6.34	—	33	21	102	21	302	302	232	17	0.6	28	12	0.41
	RB	317	7.66	—	308	17	205	57	848	848	535	134	24.6	8	71	1.56
	Ave	1165	6.80	—	106	25	176	46	575	575	423	60	10.0	22	30	0.60
	r^2		0.60	—	1.00	0.31	0.55	0.71	0.68	0.68	0.59	0.85	0.80	0.49	0.25	0.90
Obi	RS	345	6.59	0.02	28	44	239	67	686	686	524	66	10.8	22	31	0.51
	RI	433	6.20	0.72	33	18	113	24	327	327	274	19	−2.3	26	5	0.65
	RB	345	7.58	1.31	285	19	190	54	790	790	543	100	27.7	13	51	1.05
	Ave	1122	6.75	0.69	109	26	176	46	580	580	433	58	11.0	21	27	0.73
	r^2		0.53	0.64	1.00	0.16	0.21	0.30	0.32	0.32	0.25	0.70	0.72	0.21	0.17	0.07

	i	mm yr^{-1}	mg L^{-1}	μmol L^{-1}				mg L^{-1}						δ^{18}O
j		Q_K	DOC	DIC	CO_2	O_2	SiO_2	FSS	CSS	TSS	POCF	POCC	POC	H_2O
VG	RS	567	6.7	1681	176	153	10	750	439	1189	7.5	1.7	9.2	−12.4
	RI	568	5.9	1393	176	190	76	210	354	564	2.8	1.5	4.3	−12.9
	RB	426	−3.8	−72	−83	206	429	0	−662	−663	0.0	−1.3	−1.3	8.7
	Ave	1560	3.6	1098	105	181	148	349	107	456	3.8	0.8	4.6	−6.8
	r^2		0.74	0.49	0.18	0.08	0.97	1.00	0.97	1.00	0.98	0.56	0.95	0.76

Table A3. (*Continued*)

i / *j*		mm yr^{-1}	mg L^{-1}	μmol L^{-1}				mg L^{-1}						$\delta^{18}O$
		Q_K	DOC	DIC	CO_2	O_2	SiO_2	FSS	CSS	TSS	POCF	POCC	POC	H_2O
SAI	RS	511	5.0	1610	128	133	39	635	264	899	6.0	1.5	7.5	−11.4
	RI	486	5.1	1417	123	186	85	170	238	409	1.6	1.4	3.0	−12.5
	RB	396	−0.8	−354	98	211	353	0	−328	−330	1.6	−1.1	0.5	6.5
	Ave	1392	3.4	984	118	174	145	292	86	379	3.2	0.7	3.9	−6.7
	r^2		0.43	0.43	0.00	0.32	0.93	1.00	0.93	0.99	0.97	0.91	0.97	0.64
Xib	RS	575	4.8	1401	126	149	43	650	145	795	6.7	1.1	7.8	−12.0
	RI	575	4.2	1128	131	179	90	170	61	231	2.5	0.3	2.8	−12.9
	RB	431	0.2	96	55	196	344	0	27	27	−0.4	0.7	0.3	9.1
	Ave	1581	3.3	946	108	173	142	298	82	381	3.2	0.7	3.9	−6.6
	r^2		0.33	0.45	0.03	0.10	0.92	1.00	0.58	0.98	0.97	0.96	0.98	0.89
Tup	RS	578	4.9	1238	196	123	58	625	224	849	5.6	0.9	6.5	−11.3
	RI	579	4.3	999	183	148	106	165	70	235	1.7	0.3	1.9	−12.0
	RB	428	0.5	332	−74	246	310	0	−89	−89	2.2	0.8	3.1	7.6
	Ave	1585	3.5	906	118	165	144	288	83	372	3.3	0.7	3.9	−6.4
	r^2		0.27	0.34	0.22	0.16	0.78	1.00	0.80	0.98	0.95	0.72	0.95	0.90
Jut	RS	550	10.1	1427	291	16	1	575	148	723	6.4	0.6	7.0	−12.9
	RI	653	7.2	1063	262	71	91	70	53	123	1.7	−0.4	1.3	−11.1
	RB	426	−10.2	−466	−258	487	406	0	−9	−9	−0.7	2.1	1.5	10.4
	Ave	1629	3.7	786	136	161	143	222	69	291	2.6	0.6	3.3	−6.1
	r^2		0.38	0.28	0.16	0.26	0.75	1.00	0.45	0.97	0.90	0.83	0.96	0.30
Ita	RS	572	11.2	1972	297	64	19	590	259	849	9.1	1.1	10.2	−16.4
	RI	619	6.6	1043	277	103	108	30	91	121	2.0	−0.3	1.7	−11.2
	RB	438	−10.7	−1294	−259	339	332	0	−241	−240	−4.8	1.3	−3.5	14.8
	Ave	1629	3.6	742	140	153	137	219	61	279	2.6	0.6	3.3	−6.0
	r^2		0.83	0.62	0.36	0.15	0.73	1.00	0.71	0.99	0.90	0.83	0.94	0.61
Ano	RS	572	8.0	1593	224	98	57	590	195	784	5.5	1.3	6.8	−11.5
	RI	620	6.0	1029	290	108	118	25	49	74	0.8	−0.2	0.7	−10.0
	RB	437	−6.0	−761	−170	295	267	0	−97	−96	1.0	0.5	1.5	6.6
	Ave	1629	3.5	747	144	155	137	217	61	278	2.5	0.5	3.1	−6.0
	r^2		0.69	0.68	0.50	0.19	0.49	1.00	0.78	0.99	0.93	0.84	0.96	0.47

Man	RS	513	6.8	1058	216	102	92	540	112	652	5.0	0.9	5.9	−10.9
	RI	593	5.6	766	317	106	123	15	39	54	0.7	0.2	0.8	−9.2
	RB	399	−2.7	186	−148	275	230	0	−22	−22	0.6	0.2	0.8	5.1
	Ave	1505	3.8	712	159	150	141	190	48	238	2.1	0.4	2.6	−6.0
	r^2		0.58	0.28	0.64	0.20	0.43	1.00	0.64	0.99	0.90	0.73	0.89	0.59
SJA	RS	460	7.4	1219	280	104	62	442	22	466	5.1	0.6	5.6	−11.3
	RI	646	6.8	418	248	123	102	20	66	84	0.7	0.3	0.9	−7.9
	RB	341	−3.0	141	−130	277	240	0	−20	−20	−0.7	0.2	−0.5	5.8
	Ave	1446	4.7	607	169	153	122	149	32	181	1.8	0.4	2.1	−5.7
	r^2		0.82	0.57	0.29	0.26	0.60	1.00	0.66	0.97	0.77	0.27	0.80	0.60
Pau	RS	358	4.9	820	237	116	123	620	58	679	5.8	0.6	6.3	−7.8
	RI	490	5.3	466	236	116	107	20	51	70	1.2	0.5	1.7	−7.3
	RB	317	1.5	494	−44	250	154	0	−24	−23	−0.4	−0.2	−0.6	−0.9
	Ave	1165	4.1	583	160	153	125	199	33	232	2.1	0.3	2.5	−5.7
	r^2		0.49	0.59	0.50	0.48	0.44	1.00	0.40	0.99	0.94	0.55	0.93	0.46
Obi	RS	345	4.3	731	207	117	116	610	65	676	5.3	0.8	6.1	−7.3
	RI	433	5.0	561	283	91	128	15	60	74	2.1	0.4	2.5	−7.8
	RB	345	2.5	495	−41	261	145	0	−34	−33	−0.3	−0.3	−0.6	−1.3
	Ave	1122	4.0	593	160	151	129	193	33	226	2.3	0.3	2.6	−5.6
	r^2		0.21	0.15	0.54	0.63	0.17	1.00	0.54	0.99	0.85	0.83	0.90	0.43

i / j		mm yr^{-1}	δ^{13}C (‰)			C/N			Carbon cycle (μmol L^{-1})						
		QK	DIC	POCF	POCC	POCF	POCC	DOC	DIC	POCF	POCC	PONF	PONC	DOC	DON
VG	RS	567	−12.6	−25.4	−25.2	10.9	13.9	19.1	1681	625	146	56.4	7.9	555	24.0
	RI	568	−14.9	−26.2	−25.2	13.5	16.7	−1.9	1393	235	126	15.3	6.8	495	29.2
	RB	426	−9.4	−29.0	−33.5	8.4	39.6	93.8	−72	3	−110	7.2	−8.2	−313	−36.7
	Ave	1560	−12.5	−26.7	−27.4	11.2	21.9	31.8	1098	313	68	28.0	3.1	296	9.3
	r^2		0.67	0.50	0.45	0.33	0.35	0.38	0.49	0.98	0.56	0.91	0.82	0.74	0.80
SAI	RS	511	−12.7	−26.1	−25.0	14.8	33.6	29.9	1610	499	123	32.4	4.1	419	16.6
	RI	486	−14.8	−27.1	−24.4	8.9	−6.0	3.1	1417	133	118	17.2	5.3	427	23.6
	RB	396	−11.0	−27.8	−34.0	28.8	133.9	62.4	−354	132	−94	−6.6	−7.4	−64	−16.8
	Ave	1392	−12.9	−26.9	−27.4	16.7	48.3	29.8	984	267	60	16.0	1.2	284	9.5
	r^2		0.44	0.61	0.76	0.26	0.59	0.19	0.43	0.97	0.91	0.68	0.87	0.43	0.33

Table A3. (*Continued*)

i / *j*		mm yr^{-1}	δ^{13}C (‰)			C/N			Carbon cycle (μmol L^{-1})						
		QK	DIC	POCF	POCC	POCF	POCC	DOC	DIC	POCF	POCC	PONF	PONC	DOC	DON
Xib	RS	575	−12.8	−25.8	−25.4	11.4	17.6	−3.7	1401	556	91	49.7	4.5	402	23.7
	RI	575	−15.4	−26.6	−26.2	11.2	23.6	14.0	1128	205	27	18.1	0.9	353	19.9
	RB	431	−10.5	−28.9	−32.3	9.9	19.6	84.4	96	−30	57	0.0	3.4	16	−19.8
	Ave	1581	−13.1	−27.0	−27.6	10.9	20.3	26.7	946	269	58	24.7	2.9	279	10.4
	r^2		0.83	0.46	0.32	0.02	0.10	0.24	0.45	0.97	0.96	0.93	0.85	0.33	0.42
Tup	RS	578	−13.0	−26.5	−26.4	11.9	9.5	25.7	1238	470	75	41.0	4.8	409	13.5
	RI	579	−15.6	−27.2	−26.6	11.6	20.7	17.3	999	138	23	10.9	1.4	357	20.8
	RB	428	−10.3	−27.4	−30.7	7.4	41.6	39.6	332	187	68	25.1	0.8	43	−5.5
	Ave	1585	−13.2	−27.0	−27.7	10.6	22.3	26.4	906	272	55	25.7	2.5	291	11.0
	r^2		0.72	0.28	0.20	0.12	0.31	0.04	0.34	0.95	0.72	0.82	0.73	0.27	0.28
Jut	RS	550	−15.9	−25.8	−23.2	12.4	18.8	45.5	1427	530	52	51.8	2.7	841	4.0
	RI	653	−17.4	−27.2	−25.7	11.9	12.1	3.7	1063	139	−31	13.0	−0.1	604	19.9
	RB	426	−5.8	−29.1	−37.0	4.9	45.1	30.8	−466	−56	178	−4.8	5.2	−847	11.1
	Ave	1629	−13.9	−27.2	−27.8	10.3	23.0	24.9	786	220	51	21.5	2.2	304	12.2
	r^2		0.70	0.23	0.22	0.05	0.39	0.77	0.28	0.90	0.83	0.87	0.67	0.38	0.50
Ita	RS	572	−11.6	−23.1	−26.5	34.4	37.1	66.1	1972	759	89	29.9	2.6	933	0.1
	RI	619	−17.1	−26.7	−26.2	17.5	17.2	−6.9	1043	163	−24	4.3	−0.1	549	23.7
	RB	438	−14.2	−33.4	−32.0	−29.4	17.8	8.2	−1294	−404	109	30.5	4.6	−889	15.1
	Ave	1629	−14.4	−27.2	−27.9	10.8	24.3	22.8	742	220	51	20.4	2.1	298	13.1
	r^2		0.72	0.68	0.36	0.70	0.29	0.55	0.62	0.90	0.83	0.86	0.76	0.83	0.45
Ano	RS	572	−9.8	−23.2	−26.2	12.2	19.9	27.2	1593	461	108	40.4	4.8	664	27.2
	RI	620	−16.9	−26.9	−26.4	10.1	14.0	−40.0	1029	69	−15	7.8	0.3	500	28.8
	RB	437	−16.9	−33.1	−31.5	8.7	39.9	134.0	−761	84	42	11.0	0.5	−501	−40.9
	Ave	1629	−14.4	−27.3	−27.7	10.5	23.0	30.3	747	210	44	20.1	1.9	289	9.5
	r^2		0.82	0.72	0.21	0.30	0.71	0.63	0.68	0.93	0.84	0.85	0.83	0.69	0.89
Man	RS	513	−13.2	−24.7	−27.6	11.3	28.7	28.3	1058	418	76	38.7	2.9	567	17.8
	RI	593	−18.8	−27.8	−27.1	10.6	22.5	36.2	766	56	14	5.1	0.6	470	19.1
	RB	399	−11.7	−30.3	−28.7	8.4	17.8	19.6	186	49	18	8.1	1.2	−222	−9.8
	Ave	1505	−15.0	−27.4	−27.7	10.3	23.3	29.1	712	178	36	17.3	1.6	319	11.0
	r^2		0.91	0.77	0.09	0.07	0.15	0.02	0.28	0.90	0.73	0.85	0.73	0.58	0.20

SJA	RS	460	−12.2	−25.7	−30.4	8.7	42.3	23.4	1219	424	46	42.7	0.9	620	28.3
	RI	646	−19.1	−27.9	−26.4	7.9	16.6	54.0	418	56	23	8.6	1.4	569	18.1
	RB	341	−11.9	−29.0	−27.1	15.3	11.1	0.0	141	−59	19	−11.3	1.5	−249	−19.7
	Ave	1446	−15.2	−27.5	−27.8	9.9	23.5	31.5	607	146	29	14.7	1.2	392	12.4
	r^2		0.88	0.41	0.65	0.14	0.40	0.10	0.57	0.77	0.27	0.76	0.06	0.82	0.20
Pau	RS	358	−14.6	−25.7	−28.5	7.5	28.8	22.9	820	480	48	55.2	2.1	404	8.5
	RI	490	−19.5	−27.8	−26.9	11.4	22.0	−10.1	466	98	44	6.2	2.0	438	25.1
	RB	317	−10.9	−28.0	−28.0	9.8	11.6	109.0	494	−36	−15	−4.4	−0.5	125	−9.5
	Ave	1165	−15.7	−27.2	−27.7	9.7	21.2	32.5	583	179	29	18.4	1.4	343	10.6
	r^2		0.80	0.60	0.68	0.59	0.11	0.81	0.59	0.94	0.55	0.91	0.30	0.49	0.67
Obi	RS	345	−14.6	−27.4	−28.3	10.7	21.6	5.6	731	443	66	45.3	3.2	357	12.5
	RI	433	−20.6	−28.5	−27.4	12.9	16.7	−9.7	561	171	34	11.9	1.9	416	26.8
	RB	345	−11.1	−25.8	−28.5	5.9	21.9	97.5	495	−27	−23	2.3	−1.2	208	−7.2
	Ave	1122	−15.8	−27.3	−28.0	10.1	19.8	27.9	593	194	26	19.2	1.3	334	12.0
	r^2		0.60	0.43	0.19	0.58	0.10	0.63	0.15	0.85	0.83	0.76	0.81	0.21	0.53

i / *j*		mm yr^{-1}	Silicates (μmol L^{-1})			Carbonates (μmol L^{-1})		Carbon cycle (μmol L^{-1})				
		QK	NaSil	CaSil	MgSil	$CaCO_3$	Dolomite	CO_{2CARB}	$CO_{2\ SIL}$	$CO_{2\ TOT}$	FR	Re
VG	RS	567	24	10	8	541	88	718	109	1546	0.49	3.92
	RI	568	17	7	6	445	68	581	87	1249	0.47	2.76
	RB	426	118	47	38	−175	27	−121	278	37	0.29	−1.25
	Ave	1560	47	19	15	311	64	439	147	1026	0.43	2.09
	r^2		0.52	0.52	0.52	0.61	0.45	0.59	0.38	0.61	0.48	0.83
SAI	RS	511	−28	−11	−9	544	112	768	−18	1517	0.58	2.36
	RI	486	−5	−2	−1	475	85	646	32	1323	0.52	2.28
	RB	396	245	98	78	−361	−71	−503	582	−422	0.04	2.23
	Ave	1392	58	23	19	263	51	364	170	898	0.41	2.30
	r^2		0.70	0.70	0.70	0.72	0.80	0.78	0.62	0.67	0.79	0.00
Xib	RS	575	−42	−17	−14	465	109	683	−50	1313	0.59	1.96
	RI	575	−19	−8	−6	367	72	512	3	1025	0.52	1.77
	RB	431	252	101	81	−172	−43	−258	586	74	0.06	2.66
	Ave	1581	46	18	15	256	54	364	142	871	0.42	2.08
	r^2		0.91	0.91	0.91	0.55	0.85	0.69	0.92	0.58	0.83	0.26

Table A3. (*Continued*)

i / *j*		mm yr^{-1}	Silicates (μmol L^{-1})			Carbonates (μmol L^{-1})		Carbon cycle (μmol L^{-1})				
		QK	NaSil	CaSil	MgSil	$CaCO_3$	Dolomite	CO_{2CARB}	$CO_{2\ SIL}$	$CO_{2\ TOT}$	FR	Re
Tup	RS	578	−52	−21	−17	400	92	584	−86	1080	0.60	1.71
	RI	579	−28	−11	−9	307	64	435	−31	839	0.54	1.32
	RB	428	284	114	91	−74	−27	−128	700	446	−0.02	3.70
	Ave	1585	48	19	15	238	50	337	146	821	0.41	2.10
	r^2		0.91	0.91	0.91	0.52	0.64	0.61	0.88	0.43	0.82	0.23
Jut	RS	550	−135	−54	−43	429	153	734	−279	1193	0.83	0.96
	RI	653	−42	−17	−13	303	74	451	−65	839	0.59	1.35
	RB	426	470	188	151	−314	−176	−666	1125	−214	−0.55	5.53
	Ave	1629	61	24	19	184	35	254	174	683	0.37	2.31
	r^2		0.89	0.89	0.89	0.55	0.82	0.76	0.81	0.51	0.88	0.18
Ita	RS	572	−104	−42	−33	648	156	959	−192	1729	0.95	1.09
	RI	619	−22	−9	−7	287	60	408	−22	794	0.56	1.23
	RB	438	372	149	119	−650	−151	−952	881	−1026	−0.65	5.33
	Ave	1629	55	22	18	162	37	236	161	633	0.37	2.28
	r^2		0.83	0.83	0.83	0.77	0.72	0.80	0.75	0.78	0.78	0.49
Ano	RS	572	−115	−46	−37	487	167	820	−229	1415	0.91	0.34
	RI	620	−27	−11	−9	274	62	398	−33	764	0.57	1.06
	RB	437	404	162	129	−420	−173	−764	964	−571	−0.62	6.66
	Ave	1629	58	23	18	163	36	234	166	634	0.37	2.31
	r^2		0.92	0.92	0.92	0.74	0.90	0.87	0.88	0.82	0.86	0.61
Man	RS	513	−53	−21	−17	288	94	476	−59	891	0.64	1.68
	RI	593	4	2	1	159	30	219	35	471	0.45	1.36
	RB	399	270	108	86	−57	−41	−140	636	361	−0.13	4.36
	Ave	1505	55	22	18	146	33	211	162	585	0.36	2.27
	r^2		0.95	0.95	0.95	0.41	0.85	0.69	0.94	0.67	0.85	0.81
SJA	RS	460	−42	−17	−14	249	130	509	−38	978	0.67	1.89
	RI	646	20	8	6	46	12	69	70	207	0.35	1.73
	RB	341	215	86	69	84	−91	−97	489	296	−0.04	3.40
	Ave	1446	46	18	15	119	25	170	134	473	0.36	2.17
	r^2		0.83	0.83	0.83	0.55	0.86	0.71	0.83	0.77	0.53	0.63

Pau	RS	358	−25	−10	−8	166	77	319	−21	619	0.56	1.45
	RI	490	16	7	5	68	16	100	61	261	0.37	1.73
	RB	317	174	70	56	62	2	66	440	571	0.07	3.89
	Ave	1165	47	19	15	96	31	158	139	456	0.35	2.23
	r^2		0.90	0.90	0.90	0.41	0.63	0.56	0.94	0.61	0.75	0.90
Obi	RS	345	−38	−15	−12	144	78	302	−48	558	0.57	1.64
	RI	433	14	6	5	84	19	122	53	298	0.38	1.48
	RB	345	185	74	59	70	−4	60	469	585	0.06	3.94
	Ave	1122	51	20	16	98	30	158	150	466	0.34	2.28
	r^2		0.91	0.91	0.91	0.17	0.38	0.31	0.97	0.27	0.72	0.86

i / *j*		mm yr^{-1}		Cations (μmol L^{-1})					μeq L^{-1}		Anions (μmol L^{-1})					
		QK	pH	NH_4^+	Na^+	K^+	Ca^{2+}	Mg^{2+}	S^+	S^-	HCO_3^-	Cl^-	NO_3^-	DOC^-	SO_4^{2-}	HPO_4^{2-}
Solimões	RS	567	7.23	−0.54	35	51	720	96	1716	1716	1504	11	5.4	36	80	0.10
	RI	568	7.14	−0.29	70	44	497	74	1255	1255	1216	53	−0.3	32	−25	0.65
	RB	426	7.75	2.35	600	−10	55	65	834	834	13	482	42.2	−20	158	2.29
	Ave	1560	7.34	0.34	202	32	457	80	1308	1308	992	155	13.4	19	63	0.90
	r^2		0.18	0.32	1.00	0.79	0.62	0.54	0.57	0.57	0.60	0.95	0.79	0.74	0.51	0.54
+ Iça	RS	568	7.29	−0.42	31	58	743	99	1770	1770	1635	11	2.9	42	39	0.19
	RI	568	7.15	−0.38	63	45	478	72	1206	1206	1210	47	−0.6	34	−44	0.75
	RB	424	7.40	2.66	539	−30	−162	31	253	253	−603	421	43.2	−31	212	1.83
	Ave	1560	7.27	0.43	181	29	400	71	1152	1152	872	136	12.6	19	56	0.84
	r^2		0.13	0.40	1.00	0.86	0.69	0.67	0.67	0.67	0.77	0.92	0.74	0.74	0.59	0.49
+ Jutai	RS	570	7.12	−0.41	30	54	713	94	1698	1698	1540	10	2.4	42	52	0.19
	RI	571	7.08	−0.38	60	43	466	69	1172	1172	1149	43	−1.0	34	−28	0.72
	RB	425	7.47	2.73	516	−26	−183	29	188	188	−568	403	42.1	−30	171	1.76
	Ave	1566	7.20	0.45	173	28	380	67	1096	1096	825	128	11.9	20	55	0.81
	r^2		0.04	0.46	1.00	0.82	0.72	0.69	0.71	0.71	0.84	0.93	0.78	0.74	0.56	0.49
+ Juruá	RS	490	7.04	−0.33	28	53	681	93	1627	1627	1438	9	3.7	43	67	0.16
	RI	530	7.04	−0.40	59	42	471	70	1183	1183	1128	41	−1.6	35	−12	0.67
	RB	385	7.55	2.66	502	−20	−156	30	235	234	−403	379	41.0	−30	124	1.81
	Ave	1405	7.18	0.46	170	29	373	67	1078	1078	817	122	11.9	20	53	0.81
	r^2		0.04	0.50	1.00	0.80	0.74	0.68	0.71	0.71	0.86	0.95	0.78	0.72	0.48	0.46

Table A3. (*Continued*)

i / *j*		mm yr^{-1}		Cations (μmol L^{-1})					μeq L^{-1}		Anions (μmol L^{-1})					
		QK	pH	NH_4^+	Na^+	K^+	Ca^{2+}	Mg^{2+}	S^+	S^-	HCO_3^-	Cl^-	NO_3^-	DOC^-	SO_4^{2-}	HPO_4^{2-}
+ Japura	RS	513	7.35	−0.61	24	55	623	88	1499	1499	1458	3	2.9	45	−5	0.49
	RI	561	7.03	−0.27	49	36	327	53	843	843	865	28	2.1	32	−43	0.76
	RB	391	6.83	3.14	441	−29	−141	18	172	172	−628	333	34.7	−30	231	0.89
	Ave	1464	7.09	0.52	145	25	305	56	894	894	674	101	11.1	20	43	0.70
	r^2		0.27	0.53	1.00	0.84	0.70	0.77	0.73	0.73	0.77	0.93	0.55	0.53	0.66	0.28
+ Purus	RS	471	6.80	−0.26	22	50	562	76	1347	1347	1214	9	3.1	48	36	0.43
	RI	543	6.59	−0.15	44	34	304	47	779	779	738	25	1.3	34	−11	0.70
	RB	366	7.79	2.67	414	−19	−133	29	193	192	−324	286	33.8	−35	115	1.05
	Ave	1381	6.98	0.56	135	25	276	52	817	817	619	89	10.5	20	39	0.70
	r^2		0.35	0.38	1.00	0.78	0.81	0.81	0.83	0.83	0.85	0.96	0.64	0.63	0.58	0.22
+ Negro	RS	466	6.77	−0.44	18	42	382	53	933	935	818	0	5.0	49	31	0.44
	RI	543	6.52	0.04	37	25	166	27	455	454	391	17	2.6	41	1	0.47
	RB	358	7.55	2.84	342	−8	54	44	535	532	132	248	22.3	−24	76	0.88
	Ave	1366	6.87	0.61	110	22	211	41	639	638	469	72	8.6	26	31	0.57
	r^2		0.70	0.56	1.00	0.77	0.88	0.93	0.91	0.91	0.90	0.98	0.79	0.62	0.62	0.06
+ Madiera	RS	344	6.59	0.95	28	41	302	57	789	790	628	3	3.9	41	57	0.07
	RI	433	6.36	0.47	33	22	120	25	351	350	284	10	0.4	39	8	0.30
	RB	340	7.81	0.77	280	11	185	62	788	787	490	196	25.2	−10	41	1.36
	Ave	1117	6.87	0.71	107	25	196	46	619	618	453	65	9.0	25	33	0.55
	r^2		0.73	0.18	1.00	0.69	0.80	0.90	0.85	0.85	0.75	0.98	0.82	0.76	0.83	0.46

i / *j*		mm yr^{-1}	mg L^{-1}	μmol L^{-1}				mg L^{-1}						$\delta^{18}O$
		QK	DOC	DIC	CO_2	O_2	SiO_2	FSS	CSS	TSS	POCF	POCC	POC	H_2O
Solimões	RS	567	6.7	1681	176	153	10	750	439	1189	7.5	1.7	9.2	−12.4
	RI	568	5.9	1393	176	190	76	210	354	564	2.8	1.5	4.3	−12.9
	RB	426	−3.8	−72	−83	206	429	0	−662	−663	0.0	−1.3	−1.3	8.7
	Ave	1560	3.6	1098	105	181	148	349	107	456	3.8	0.8	4.6	−6.8
	r^2		0.74	0.49	0.18	0.08	0.97	1.00	0.97	1.00	0.98	0.56	0.95	0.76
+ Içá	RS	568	7.8	1822	187	174	8	673	482	1154	6.9	1.8	8.7	−14.8
	RI	568	6.4	1384	174	199	77	184	347	531	2.5	1.4	4.0	−13.8
	RB	424	−5.9	−685	−82	167	411	0	−761	−762	0.0	−1.7	−1.7	13.7
	Ave	1560	3.6	981	109	181	143	312	95	406	3.4	0.7	4.2	−6.7
	r^2		0.74	0.66	0.12	0.07	0.97	1.00	0.96	0.99	0.97	0.55	0.95	0.75

+ Jutai	RS	570	7.8	1762	222	148	12	635	440	1076	6.6	1.7	8.3	−14.7
	RI	571	6.4	1339	190	174	80	173	314	488	2.4	1.3	3.8	−13.7
	RB	425	−5.6	−676	−108	214	398	0	−684	−685	−0.1	−1.5	−1.5	13.8
	Ave	1566	3.7	946	121	175	142	294	89	383	3.3	0.7	4.0	−6.6
	r^2		0.74	0.70	0.12	0.05	0.98	1.00	0.93	0.99	0.97	0.53	0.95	0.77
+ Juruá	RS	490	8.0	1671	233	131	24	646	394	1041	6.6	1.5	8.1	−13.8
	RI	530	6.6	1327	199	156	84	164	296	460	2.4	1.3	3.6	−13.7
	RB	385	−5.6	−513	−109	246	379	0	−600	−602	0.0	−1.2	−1.2	12.6
	Ave	1405	3.7	943	126	172	144	287	85	372	3.2	0.7	3.8	−6.5
	r^2		0.72	0.71	0.14	0.05	0.97	1.00	0.90	0.99	0.97	0.50	0.94	0.78
+ Japura	RS	513	8.3	1640	182	198	35	537	426	961	5.7	2.2	7.9	−17.2
	RI	561	5.9	1037	171	202	91	132	236	367	2.2	1.3	3.6	−13.5
	RB	391	−5.7	−636	−7	109	328	0	−642	−638	−0.1	−2.5	−2.5	18.2
	Ave	1464	3.7	802	128	176	135	238	68	306	2.8	0.6	3.5	−6.3
	r^2		0.53	0.62	0.03	0.06	0.95	1.00	0.84	0.98	0.96	0.61	0.92	0.67
+ Purus	RS	471	8.9	1523	309	125	51	501	318	819	5.2	1.8	7.0	−15.1
	RI	543	6.4	1021	284	133	101	114	170	284	2.0	1.1	3.0	−12.3
	RB	366	−6.6	−570	−248	262	301	0	−437	−435	0.1	−1.8	−1.6	14.2
	Ave	1381	3.8	771	152	165	137	216	60	276	2.6	0.6	3.1	−6.2
	r^2		0.63	0.72	0.25	0.05	0.88	1.00	0.73	0.98	0.97	0.61	0.94	0.66
+ Negro	RS	466	9.1	1075	258	134	53	383	202	583	4.3	1.2	5.4	−12.8
	RI	543	7.6	616	225	132	85	86	82	168	1.5	0.5	2.1	−9.5
	RB	358	−4.6	12	−120	239	258	0	−215	−213	0.0	−0.7	−0.7	8.5
	Ave	1366	4.9	614	146	160	119	165	45	210	2.1	0.4	2.5	−5.9
	r^2		0.62	0.87	0.41	0.16	0.76	1.00	0.71	0.98	0.98	0.68	0.96	0.61
+ Madiera	RS	344	7.7	877	248	76	95	665	192	857	5.5	1.4	7.0	−10.3
	RI	433	7.3	522	234	105	101	20	48	68	1.0	0.5	1.5	−8.4
	RB	340	−2.0	389	−95	320	191	0	−94	−93	0.5	−0.6	−0.1	1.7
	Ave	1117	4.6	591	138	162	127	213	49	262	2.2	0.4	2.7	−5.9
	r^2		0.76	0.67	0.59	0.39	0.55	1.00	0.81	0.99	0.95	0.72	0.94	0.41

i / j		mm yr^{-1}	δ^{13}C (‰)			C/N			Carbon cycle (μmol L^{-1})						
		QK	DIC	POCF	POCC	POCF	POCC	DOC	DIC	POCF	POCC	PONF	PONC	DOC	DON
Solimões	RS	567	−12.6	−25.4	−25.2	10.9	13.9	19.1	1681	625	146	56.4	7.9	555	24.0
	RI	568	−14.9	−26.2	−25.2	13.5	16.7	−1.9	1393	235	126	15.3	6.8	495	29.2
	RB	426	−9.4	−29.0	−33.5	8.4	39.6	93.8	−72	3	−110	7.2	−8.2	−313	−36.7
	Ave	1560	−12.5	−26.7	−27.4	11.2	21.9	31.8	1098	313	68	28.0	3.1	296	9.3
	r^2		0.67	0.50	0.45	0.33	0.35	0.38	0.49	0.98	0.56	0.91	0.82	0.74	0.80

Table A3. (*Continued*)

i / *j*		mm yr^{-1}	δ^{13}C (‰)			C/N			Carbon cycle (μmol L^{-1})						
		QK	DIC	POCF	POCC	POCF	POCC	DOC	DIC	POCF	POCC	PONF	PONC	DOC	DON
+ Içа	RS	568	−13.0	−25.1	−23.9	11.3	11.7	18.6	1822	576	153	50.4	8.5	648	26.8
	RI	568	−15.1	−26.2	−24.8	13.4	16.2	2.2	1384	211	120	13.5	6.5	534	28.6
	RB	424	−9.4	−29.9	−36.0	7.6	43.4	85.9	−685	−1	−138	9.4	−9.9	−490	−38.7
	Ave	1560	−12.8	−26.8	−27.5	11.1	22.0	30.9	981	286	62	25.8	2.8	297	9.6
	r^2		0.63	0.54	0.55	0.26	0.33	0.28	0.66	0.97	0.55	0.90	0.81	0.74	0.66
+ Jutai	RS	570	−13.7	−25.2	−24.0	11.2	11.5	22.7	1762	551	140	48.8	7.9	654	25.7
	RI	571	−15.5	−26.3	−24.9	13.1	16.0	8.1	1339	204	110	13.7	6.0	535	27.4
	RB	425	−8.9	−29.6	−35.7	8.0	44.0	69.1	−676	−5	−122	7.6	−8.9	−470	−33.7
	Ave	1566	−13.0	−26.8	−27.5	11.0	22.0	30.0	946	273	58	24.8	2.6	306	10.2
	r^2		0.56	0.51	0.52	0.25	0.35	0.25	0.70	0.97	0.53	0.90	0.81	0.74	0.62
+ Juruá	RS	490	−14.1	−25.2	−24.3	11.0	11.8	27.9	1671	546	126	49.1	7.1	668	23.8
	RI	530	−15.8	−26.3	−24.9	13.2	15.9	11.1	1327	197	105	12.9	5.8	551	27.4
	RB	385	−8.8	−29.7	−35.2	7.6	43.5	58.1	−513	1	−103	8.3	−7.8	−469	−29.9
	Ave	1405	−13.3	−26.8	−27.5	10.9	22.0	29.8	943	265	56	24.3	2.5	312	10.5
	r^2		0.43	0.47	0.49	0.28	0.36	0.24	0.71	0.97	0.50	0.89	0.78	0.72	0.59
+ Japura	RS	513	−13.4	−25.2	−23.3	11.2	30.3	33.3	1640	473	187	42.0	7.3	695	20.8
	RI	561	−15.3	−26.4	−24.9	12.3	26.9	18.0	1037	186	112	13.9	4.3	492	20.2
	RB	391	−11.5	−29.9	−37.0	8.3	12.2	40.9	−636	−5	−207	6.4	−7.5	−475	−17.6
	Ave	1464	−13.6	−26.9	−27.6	10.8	24.1	29.5	802	236	53	21.7	2.2	305	10.4
	r^2		0.44	0.36	0.43	0.22	0.05	0.31	0.62	0.96	0.61	0.89	0.62	0.53	0.30
+ Purus	RS	471	−15.6	−25.5	−24.8	11.1	29.8	43.2	1523	434	151	39.0	5.9	740	20.3
	RI	543	−17.3	−26.8	−26.0	12.2	26.8	23.5	1021	163	88	12.3	3.4	532	21.1
	RB	366	−7.7	−29.3	−33.8	7.8	14.1	16.7	−570	12	−148	7.7	−5.4	−550	−15.5
	Ave	1381	−14.2	−27.0	−27.6	10.7	24.4	28.4	771	215	47	20.2	1.9	316	11.1
	r^2		0.56	0.37	0.23	0.24	0.04	0.39	0.72	0.97	0.61	0.90	0.64	0.63	0.35
+ Negro	RS	466	−15.7	−26.0	−25.5	11.1	31.9	39.9	1075	356	97	32.6	3.7	758	20.1
	RI	543	−17.3	−27.1	−26.9	11.4	28.1	28.3	616	129	45	11.1	1.6	633	21.6
	RB	358	−9.6	−28.4	−31.6	8.8	9.1	18.8	12	−2	−58	2.6	−1.7	−380	−6.3
	Ave	1366	−14.7	−27.1	−27.7	10.6	24.4	29.8	614	172	36	16.2	1.5	411	13.8
	r^2		0.80	0.44	0.12	0.17	0.11	0.36	0.87	0.98	0.68	0.93	0.69	0.62	0.49
+ Madiera	RS	344	−17.0	−26.4	−25.8	7.2	22.7	41.1	877	461	119	53.6	5.4	642	15.6
	RI	433	−18.4	−27.4	−27.0	10.5	26.2	24.5	522	79	42	7.0	1.6	611	22.9
	RB	340	−8.2	−27.2	−29.9	10.7	17.2	22.3	389	41	−52	0.8	−2.1	−163	−1.3
	Ave	1117	−14.9	−27.0	−27.5	9.5	22.3	29.0	591	185	37	19.5	1.7	385	13.3
	r^2		0.77	0.49	0.10	0.35	0.37	0.42	0.67	0.95	0.72	0.97	0.73	0.76	0.47

i / *j*			mm yr^{-1}	Silicates (μmol L^{-1})			Carbonates (μmol L^{-1})		Carbon cycle (μmol L^{-1})			
		QK	NaSil	CaSil	MgSil	$CaCO_3$	Dolomite	$CO_{2\ CARB}$	$CO_{2\ SIL}$	$CO_{2\ TOT}$	FR	Re
Solimões	RS	567	24	10	8	541	88	718	109	1546	0.49	3.92
	RI	568	17	7	6	445	68	581	87	1249	0.47	2.76
	RB	426	118	47	38	−175	27	−121	278	37	0.29	−1.25
	Ave	1560	47	19	15	311	64	439	147	1026	0.43	2.09
	r^2		0.52	0.52	0.52	0.61	0.45	0.59	0.38	0.61	0.48	0.83
+ Içа	RS	568	20	13	8	602	93	788	105	1680	0.51	4.15
	RI	568	16	10	6	448	67	581	83	1245	0.48	2.73
	RB	424	117	77	47	−412	−6	−425	257	−591	0.23	−1.76
	Ave	1560	45	29	18	270	56	383	139	905	0.42	2.03
	r^2		0.50	0.50	0.50	0.76	0.56	0.73	0.39	0.78	0.50	0.87
+ Jutai	RS	570	20	13	8	565	88	742	102	1585	0.51	4.02
	RI	571	17	11	7	424	63	550	85	1185	0.48	2.66
	RB	425	113	73	45	−388	−8	−404	250	−556	0.22	−1.60
	Ave	1566	44	28	18	255	53	361	136	858	0.42	2.00
	r^2		0.52	0.52	0.52	0.85	0.61	0.81	0.39	0.84	0.58	0.84
+ Juruá	RS	490	20	12	8	520	86	692	101	1485	0.51	3.69
	RI	530	18	11	7	411	64	539	85	1163	0.48	2.57
	RB	385	123	75	49	−317	−10	−337	281	−392	0.21	−0.69
	Ave	1405	47	29	19	249	52	352	144	849	0.41	2.07
	r^2		0.64	0.64	0.64	0.88	0.65	0.84	0.48	0.87	0.67	0.83
+ Japura	RS	513	21	12	8	537	82	701	106	1507	0.54	3.76
	RI	561	21	12	8	315	46	407	87	901	0.46	2.34
	RB	391	107	62	43	−397	−17	−431	233	−625	0.15	−0.76
	Ave	1464	44	25	18	203	42	286	133	705	0.41	2.01
	r^2		0.63	0.63	0.63	0.74	0.66	0.72	0.65	0.77	0.50	0.90
+ Purus	RS	471	13	7	5	449	72	593	80	1265	0.55	3.05
	RI	543	20	11	8	265	41	346	82	774	0.46	2.07
	RB	366	128	71	51	−287	−12	−311	295	−325	0.10	0.68
	Ave	1381	46	25	18	182	37	256	138	650	0.39	2.04
	r^2		0.81	0.81	0.81	0.86	0.76	0.83	0.74	0.85	0.71	0.72
+ Negro	RS	466	18	10	7	297	48	392	85	868	0.50	3.01
	RI	543	19	11	8	136	21	179	72	430	0.41	2.01
	RB	358	94	54	38	−73	13	−46	223	132	0.19	0.56
	Ave	1366	38	22	15	136	28	193	116	501	0.38	1.97
	r^2		0.87	0.87	0.87	0.87	0.89	0.88	0.87	0.90	0.61	0.80
+ Madiera	RS	344	25	15	10	185	49	284	101	669	0.45	2.54
	RI	433	23	14	9	85	17	120	78	319	0.37	1.86
	RB	340	84	49	33	75	35	146	215	508	0.28	1.81
	Ave	1117	42	25	17	113	33	179	127	484	0.37	2.06
	r^2		0.89	0.89	0.89	0.57	0.86	0.69	0.88	0.74	0.44	0.53

Table A4. Results of model M4. Values of K_{BIO} defining the chemical response to the river to the variations of the hydrobiological index I_{BIO}. $K_{BIO} > 0$ determines rise of concentrations or rise of values when river photosynthesis prevails and conversely $K_{BIO} < 0$ reveals rise of concentrations or values when the organic matter decay predominates. Values established for the 10 sampling stations located along the Amazon main stem. Chemical composition of the aquifers RB* extrapolated for $I_{BIO} = 0$. View of R-squared value (r2) and mean value (Ave) for each parameter. Notice that $QRS/Q_t\,(ij) \times (Cij)RS + QR/Q_t(ij) \times (Cij)RI + QRB/Q_t\,(ij) \times \{(Cij)RB^* + K_{BIO}(ij) \times I_{BIO}(j)\} = (C)Ave$.

i			Cations (μmol L^{-1})					μeq L^{-1}		Anions (μmol L^{-1})					
j		pH	NH_4^+	Na^+	K^+	Ca^{2+}	Mg^{2+}	S^+	S^-	HCO_3	Cl^-	NO_3^-	DOC^-	SO_4^{2-}	HPO_4^{2-}
VG	RB*	7.21	1.25	600	−8	341	95	1465	1465	585	500	35.6	−19	179	2.5
	K_{BIO}	0.0046	0.01	0.00	−0.02	−2.38	−0.25	−5.27	−5.27	−4.76	−0.15	0.06	−0.01	−0.20	−0.002
	r^2	0.70	0.58	1.00	0.79	0.89	0.85	0.90	0.90	0.98	0.96	0.86	0.74	0.51	0.56
SAI	RB*	6.73	0.00	560	−14	−111	13	351	351	−334	312	38.2	−2	168	0.3
	K_{BIO}	0.0058	0.00	0.00	−0.05	−1.02	−0.12	−2.34	−2.34	−2.79	0.05	0.05	−0.05	0.19	0.001
	r^2	0.90	0.00	1.00	0.82	0.68	0.80	0.63	0.63	0.92	0.67	0.82	0.60	0.26	0.35
Xib	RB*	6.67	0.00	570	−30	114	55	878	878	481	316	23.7	4	25	1.2
	K_{BIO}	0.0047	0.00	0.00	−0.09	−2.64	−0.24	−5.85	−5.85	−6.66	−0.29	0.10	−0.07	0.53	0.002
	r^2	0.55	0.00	1.00	0.68	0.88	0.91	0.89	0.89	0.96	0.90	0.81	0.41	0.58	0.26
Tup	RB*	7.14	0.00	530	−10	393	84	1472	1472	1053	288	34.8	3	47	−0.2
	K_{BIO}	0.0050	0.00	0.00	0.10	−1.76	−0.12	−3.65	−3.65	−4.16	−0.31	−0.01	−0.01	0.41	0.006
	r^2	0.79	0.00	1.00	0.40	0.60	0.51	0.53	0.53	0.86	0.82	0.86	0.27	0.14	0.28
Jut	RB*	6.36	0.00	450	−5	−53	17	374	374	345	−55	16.6	−55	61	−0.1
	K_{BIO}	0.0077	0.00	0.00	−0.08	−0.55	−0.19	−1.55	−1.55	−2.37	0.17	0.10	0.00	0.26	0.008
	r^2	0.80	0.00	1.00	0.24	0.81	0.80	0.85	0.85	0.75	0.81	0.86	0.38	0.97	0.63
Ita	RB*	6.28	0.00	450	−27	−390	−20	−397	−397	−688	24	51.3	−67	138	3.4
	K_{BIO}	0.0065	0.00	0.00	−0.01	−0.41	−0.08	−0.98	−0.98	−2.02	0.16	0.04	0.02	0.40	0.003
	r^2	0.83	0.00	1.00	0.29	0.81	0.75	0.83	0.83	0.85	0.67	0.96	0.84	0.71	0.89
Ano	RB*	6.27	0.00	450	−28	−342	−32	−324	−324	−438	4	39.1	−33	52	−0.2
	K_{BIO}	0.0065	0.00	0.00	0.02	−0.26	−0.09	−0.68	−0.68	−1.18	0.16	0.07	−0.01	0.13	0.008
	r^2	0.85	0.00	1.00	0.36	0.87	0.88	0.87	0.87	0.84	0.73	0.95	0.69	0.59	0.63
Man	RB*	7.33	0.00	410	−45	86	46	629	629	665	124	19.3	−2	−89	0.3
	K_{BIO}	0.0041	0.00	0.00	0.13	−0.13	0.00	−0.13	−0.13	−1.91	0.10	0.06	−0.07	0.84	0.01
	r^2	0.91	0.00	1.00	0.64	0.79	0.88	0.85	0.85	0.83	0.96	0.86	0.69	0.86	0.33
SJA	RB*	7.11	0.00	375	−46	46	−18	387	387	439	135	24.6	−11	−103	2.4
	K_{BIO}	0.0049	0.00	0.00	0.08	0.21	−0.03	0.44	0.44	−1.16	0.18	0.09	−0.03	0.67	0.01
	r^2	0.87	0.00	1.00	0.80	0.82	0.91	0.88	0.88	0.78	0.94	0.96	0.83	0.56	0.74

Pau	RB*	6.58	0.00	285	−13	40	21	393	393	344	88	12.2	19	−36	1.2
	K_{BIO}	0.0067	0.00	0.00	0.21	1.07	0.23	2.80	2.80	1.13	0.25	0.07	−0.06	0.70	0.002
	r^2	0.84	0.00	1.00	0.72	0.77	0.83	0.84	0.84	0.63	0.90	0.90	0.58	0.85	0.94
Obi	RB*	6.10	2.20	318	−49	−128	−33	−50	−50	10	65	6.4	32	−83	0.5
	K_{BIO}	0.0111	−0.01	0.00	0.44	2.13	0.59	5.87	5.87	3.69	0.30	0.17	−0.13	0.92	0.004
	r^2	0.86	0.79	1.00	0.47	0.59	0.64	0.66	0.66	0.51	0.78	0.91	0.42	0.69	0.12
Ave	RB*	6.66	0.22	440	−27	−35	13	371	371	188	130	26.6	−11	18	0.9
	K_{BIO}	0.0061	0.000	0.00	0.066	−0.52	−0.028	−1.03	−1.03	−2.02	0.055	0.072	−0.037	0.44	0.004
	r^2	0.82	0.08	1.00	0.54	0.76	0.79	0.78	0.78	0.79	0.82	0.89	0.57	0.62	0.52

i		mg L^{-1}	μmol L^{-1}				mg L^{-1}					
j		DOC	DIC	CO_2	O_2	SiO_2	FSS	CSS	TSS	POCF	POCC	POC
VIG	RB*	−3.5	716	132	24	418	0	−719	−719	0.3	−1.8	−1.5
	K_{BIO}	0.00	−6.56	−1.79	1.53	0.09	0.00	0.46	0.46	−0.002	0.004	0.002
	r^2	0.74	0.96	0.80	0.66	0.98	1.00	0.99	1.00	0.98	0.63	0.95
SAI	RB*	−0.4	−125	209	188	345	0	−331	−331	1.8	−1.1	0.7
	K_{BIO}	−0.01	−5.20	−2.41	0.56	0.20	0.00	0.03	0.03	−0.005	−0.001	−0.006
	r^2	0.60	0.96	0.96	0.70	0.99	1.00	0.94	0.99	0.98	0.96	0.99
Xib	RB*	0.8	696	215	60	356	0	−53	−53	0.1	0.7	0.8
	K_{BIO}	−0.01	−8.80	−2.15	1.78	0.11	0.00	1.03	1.03	−0.008	0.001	−0.007
	r^2	0.41	0.97	0.76	0.75	0.93	1.00	0.74	0.99	0.98	0.96	0.99
Tup	RB*	0.6	1317	263	79	385	0	−171	−171	3.5	0.7	4.2
	K_{BIO}	0.00	−6.37	−2.20	1.09	−0.44	0.00	0.51	0.51	−0.008	0.001	−0.007
	r^2	0.27	0.94	0.89	0.70	0.89	1.00	0.83	0.99	0.96	0.72	0.96
Jut	RB*	−10.3	706	361	218	417	0	−116	−116	1.0	0.8	1.9
	K_{BIO}	0.00	−5.06	−2.69	1.18	−0.04	0.00	0.46	0.46	−0.007	0.006	−0.002
	r^2	0.38	0.92	0.95	0.84	0.76	1.00	0.53	0.98	0.91	0.90	0.96
Ita	RB*	−12.6	−445	242	66	382	0	−234	−234	−5.5	0.3	−5.2
	K_{BIO}	0.00	−4.50	−2.48	1.34	−0.18	0.00	−0.11	−0.11	0.002	0.005	0.007
	r^2	0.84	0.91	0.95	0.81	0.79	1.00	0.71	0.99	0.90	0.88	0.94
Ano	RB*	−6.2	−203	235	95	334	0	−85	−85	0.6	0.6	1.2
	K_{BIO}	0.00	−3.67	−2.49	1.22	−0.36	0.00	−0.09	−0.09	0.002	0.000	0.002
	r^2	0.69	0.92	0.94	0.71	0.68	1.00	0.78	0.99	0.93	0.84	0.96

Table A4. (*Continued*)

i		mg L^{-1}	μmol L^{-1}				mg L^{-1}					
j		DOC	DIC	CO_2	O_2	SiO_2	FSS	CSS	TSS	POCF	POCC	POC
Man	RB*	−0.3	833	168	77	278	0	−17	−17	0.5	0.0	0.5
	K_{BIO}	−0.01	−3.81	−1.90	1.18	−0.29	0.00	−0.02	−0.02	0.001	0.001	0.002
	r^2	0.69	0.89	0.93	0.74	0.66	1.00	0.64	0.99	0.90	0.76	0.89
SJA	RB*	−2.1	695	256	131	283	0	32	32	0.4	0.1	0.5
	K_{BIO}	−0.01	−3.71	−2.55	0.98	−0.29	0.00	−0.34	−0.34	−0.007	0.001	−0.006
	r^2	0.83	0.80	0.91	0.80	0.79	1.00	0.80	0.98	0.81	0.31	0.83
Pau	RB*	3.6	590	246	147	167	0	60	60	−0.1	0.2	0.1
	K_{BIO}	−0.01	−0.68	−1.81	0.62	−0.11	0.00	−0.52	−0.52	−0.001	−0.002	−0.003
	r^2	0.58	0.62	0.89	0.66	0.47	1.00	0.77	1.00	0.94	0.66	0.93
Obi	RB*	6.0	342	332	159	103	0	55	56	−0.9	0.1	−0.8
	K_{BIO}	−0.02	0.99	−2.70	0.79	0.29	0.00	−0.65	−0.65	0.002	−0.003	−0.001
	r^2	0.42	0.18	0.89	0.77	0.42	1.00	0.80	0.99	0.86	0.91	0.90
Ave	RB*	−2.1	441	253	122	305	0	−86	−86	0.1	0.2	0.4
	K_{BIO}	−0.01	−4.31	−2.29	1.12	−0.09	0.00	0.07	0.07	−0.003	0.001	−0.002
	r^2	0.57	0.81	0.91	0.75	0.74	1.00	0.75	0.99	0.92	0.79	0.93

i		$\delta^{13}C$			$\delta^{18}O$	C/N			Carbon cycle (μmol L δ^{-1})						
j		DIC	POCF	POCC	H_2O	POCF	POCC	DOC	DIC	POCF	POCC	PONF	PONC	DOC	DON
VG	RB*	−12.3	−29.7	−33.0	8.7	6.8	31.1	98.7	716	24	−151	12.3	−8.8	−295	−32.2
	K_{BIO}	0.024	0.005	−0.005	−0.001	0.015	0.076	0.083	−6.56	−0.18	0.34	−0.042	0.005	−0.15	−0.04
	r^2	0.91	0.57	0.47	0.76	0.36	0.58	0.39	0.96	0.98	0.63	0.92	0.83	0.74	0.82
SAI	RB*	−12.0	−27.8	−33.7	6.0	28.0	103.7	57.5	−125	151	−89	−4.9	−9.8	−32	−14.2
	K_{BIO}	0.022	−0.002	−0.010	0.009	0.008	0.247	0.302	−5.20	−0.42	−0.12	−0.043	−0.016	−0.72	−0.09
	r^2	0.93	0.65	0.90	0.67	0.26	0.80	0.35	0.96	0.98	0.96	0.73	0.98	0.60	0.52
Xib	RB*	−11.8	−29.4	−32.2	11.4	6.8	−0.1	53.9	696	9	56	9.9	4.7	69	−15.0
	K_{BIO}	0.024	0.003	−0.008	−0.004	0.040	0.267	0.528	−8.80	−0.63	0.07	−0.136	−0.015	−1.04	−0.12
	r^2	0.93	0.47	0.33	0.89	0.61	0.41	0.44	0.97	0.98	0.96	0.96	0.88	0.41	0.53
Tub	RB*	−13.8	−27.7	−31.8	10.2	1.8	33.8	−0.4	1317	291	57	47.9	0.6	50	5.4
	K_{BIO}	0.023	0.001	0.006	−0.014	0.037	0.062	0.285	−6.37	−0.64	0.08	−0.148	0.001	−0.09	−0.08
	r^2	0.90	0.29	0.22	0.92	0.49	0.34	0.13	0.94	0.96	0.72	0.91	0.73	0.27	0.33

Jut	RB*	−12.7	−34.4	−41.5	9.9	0.8	34.6	19.3	706	86	70	16.4	0.3	−857	14.4
	K_{BIO}	0.030	0.023	0.019	0.002	0.019	0.042	0.057	−5.06	−0.61	0.47	−0.091	0.021	0.06	−0.01
	r^2	0.98	0.76	0.36	0.30	0.12	0.41	0.78	0.92	0.91	0.90	0.90	0.80	0.38	0.50
Ita	RB*	−21.7	−37.0	−37.4	17.5	−41.7	−17.5	−4.3	−445	−461	29	43.7	4.1	−1046	28.5
	K_{BIO}	0.036	0.015	0.024	−0.006	0.045	0.163	0.075	−4.50	0.13	0.41	−0.054	0.004	0.37	−0.06
	r^2	0.92	0.90	0.71	0.62	0.80	0.46	0.55	0.91	0.90	0.88	0.88	0.77	0.84	0.47
Ano	RB*	−23.1	−36.9	−34.0	9.5	5.4	35.6	209.5	−203	53	50	14.1	0.9	−519	−58.7
	K_{BIO}	0.036	0.020	0.013	−0.013	0.020	0.030	−0.254	−3.67	0.19	−0.03	−0.018	−0.003	−0.12	0.05
	r^2	0.98	1.00	0.31	0.49	0.56	0.73	0.64	0.92	0.93	0.84	0.85	0.83	0.69	0.91
Man	RB*	−15.4	−32.0	−30.4	6.7	4.3	7.3	−32.6	833	41	−2	14.4	1.3	−23	4.7
	K_{BIO}	0.022	0.009	0.010	−0.009	0.025	0.060	0.328	−3.81	0.05	0.12	−0.038	0.000	−1.17	−0.09
	r^2	0.98	0.86	0.16	0.61	0.63	0.36	0.12	0.89	0.90	0.76	0.86	0.73	0.69	0.27
SIA	RB*	−16.8	−31.7	−27.8	8.0	16.0	−16.6	−81.3	695	32	8	−1.6	2.7	−174	−8.8
	K_{BIO}	0.031	0.018	0.005	−0.015	−0.006	0.188	0.548	−3.71	−0.61	0.07	−0.065	−0.008	−0.46	−0.07
	r^2	0.99	0.95	0.67	0.65	0.14	0.73	0.16	0.80	0.81	0.31	0.82	0.46	0.83	0.25
Pau	RB*	−17.1	−30.1	−27.5	0.0	10.8	−19.4	92.3	590	−12	18	0.1	2.8	298	2.1
	K_{BIO}	0.037	0.014	−0.003	−0.010	−0.004	0.221	0.265	−0.68	−0.10	−0.19	−0.026	−0.021	−1.00	−0.06
	r^2	0.96	0.87	0.70	0.48	0.59	0.56	0.85	0.62	0.94	0.66	0.92	0.70	0.58	0.69
Obi	RB*	−22.1	−30.0	−26.0	−3.3	9.2	10.1	15.1	342	−75	5	−3.2	1.0	502	31.6
	K_{BIO}	0.080	0.030	−0.017	0.019	−0.026	0.083	0.820	0.99	0.14	−0.23	0.028	−0.017	−2.08	−0.28
	r^2	0.93	0.91	0.49	0.47	0.66	0.24	0.86	0.18	0.86	0.91	0.76	0.98	0.42	0.88
Ave	RB*	−16.6	−31.7	−32.2	7.6	4.2	17.1	32.9	441	12	20	13.7	0.9	−173	−1.0
	K_{BIO}	0.033	0.012	0.003	−0.004	0.016	0.131	0.276	−4.31	−0.24	0.09	−0.058	−0.004	−0.58	−0.08
	r^2	0.95	0.77	0.48	0.61	0.49	0.50	0.49	0.81	0.92	0.79	0.86	0.79	0.57	0.54

	i		μmol L^{-1}								$m.Ma^{-1}$	$TC.km^{-2}.a^{-1}$
	j		NaSil	$CaCO_3$	Dolomite	CO_2 CARB	CO_2 SIL	CO_2 TOT	FR	Re	VCh	FCO_2
VG		RB*	100	59	63	185	235	605	0.36	−1.4	−8.2	−31.24
		K_{BIO}	0.15	−1.95	−0.30	−2.54	0.36	−4.73	−0.001	0.001	−0.056	−0.062
		r^2	0.59	0.95	0.83	0.97	0.46	0.98	0.80	0.83	0.73	0.98
SAI		RB*	248	−311	−66	−444	590	−297	0.06	2.4	−5.9	−23.88
		K_{BIO}	−0.05	−1.09	−0.11	−1.30	−0.18	−2.78	0.000	−0.004	−0.012	−0.036
		r^2	0.70	0.91	0.84	0.93	0.63	0.92	0.83	0.14	0.64	0.95
Xib		RB*	254	13	−26	−39	590	511	0.12	2.5	−3.1	−15.62
		K_{BIO}	0.29	−2.94	−0.34	−3.62	0.61	−6.62	−0.001	0.003	−0.087	−0.098
		r^2	0.94	0.93	0.94	0.98	0.95	0.96	0.98	0.31	0.72	0.97

Table A4. (*Continued*)

i		μmol L^{-1}								m.Ma^{-1}	TC.$km^{-2}.a^{-1}$
j		NaSil	$CaCO_3$	Dolomite	CO_2 CARB	CO_2 SIL	CO_2 TOT	FR	Re	VCh	FCO_2
Tup	RB*	242	243	6	255	580	1091	0.14	1.4	2.9	−7.09
	K_{BIO}	0.31	−2.07	−0.22	−2.51	0.86	−4.17	−0.001	0.014	−0.069	−0.032
	r^2	0.95	0.96	0.73	0.94	0.93	0.87	0.95	0.53	0.80	0.81
Jut	RB*	505	−171	−144	−460	1227	306	−0.52	6.5	41.2	8.52
	K_{BIO}	−0.17	−0.61	−0.13	−0.88	−0.49	−2.24	0.000	−0.005	-0.133	−0.076
	r^2	0.91	0.68	0.85	0.85	0.85	0.75	0.88	0.24	0.82	0.66
Ita	RB*	426	−541	−157	−855	1013	−697	−0.63	5.7	17.0	−10.17
	K_{BIO}	−0.16	−0.72	−0.02	−0.77	−0.41	−1.94	0.000	−0.001	−0.129	−0.060
	r^2	0.85	0.83	0.72	0.83	0.77	0.85	0.79	0.49	0.97	0.92
Ano	RB*	446	−398	−174	−746	1060	−433	−0.65	6.4	21.0	−3.49
	K_{BIO}	−0.16	−0.29	−0.04	−0.37	−0.36	−1.10	0.000	0.001	−0.143	−0.051
	r^2	0.93	0.76	0.90	0.87	0.90	0.85	0.86	0.61	0.96	0.83
Man	RB*	286	106	−45	15	654	683	−0.06	4.0	15.1	5.65
	K_{BIO}	−0.10	−0.96	0.03	−0.91	−0.10	−1.91	0.000	0.002	−0.118	−0.054
	r^2	0.96	0.75	0.85	0.82	0.94	0.84	0.88	0.82	0.96	0.80
SJA	RB*	240	148	−95	−42	541	458	−0.04	3.3	5.4	0.38
	K_{BIO}	−0.18	−0.43	0.03	−0.37	−0.36	−1.09	0.000	0.000	−0.105	−0.044
	r^2	0.88	0.58	0.86	0.72	0.87	0.79	0.53	0.63	0.94	0.77
Pau	RB*	197	39	−42	−45	467	377	−0.02	3.7	7.0	3.15
	K_{BIO}	−0.25	0.16	0.31	0.77	−0.40	1.15	0.001	0.000	−0.062	−0.020
	r^2	0.94	0.42	0.79	0.63	0.95	0.65	0.80	0.90	0.91	0.75
Obi	RB*	253	−33	−114	−260	567	47	−0.17	4.4	11.3	4.66
	K_{BIO}	−0.30	0.65	0.68	2.02	−0.29	3.74	0.001	−0.001	−0.091	−0.024
	r^2	0.93	0.30	0.66	0.55	0.97	0.53	0.78	0.86	0.89	0.47
Ave	RB*	310	−91	−86	−262	729	205	−0.18	4.0	11.2	−3.79
	K_{BIO}	−0.06	−0.93	−0.01	−0.95	−0.07	−1.97	0.000	0.001	−0.091	−0.051
	r^2	0.90	0.71	0.81	0.81	0.88	0.80	0.83	0.55	0.86	0.79

Table A5. Results of model M5, combining chemical tracing (implying variable contribution of hydrological reservoirs) and variable regional contribution (M1 × M3). Values of linear coefficients $\alpha(ij)$, $\beta(ij)$, $\gamma(ij)$, and $\delta(ij)$ are adjusted for each chemical parameter (indexed *i*) and each sampling station (noted *j*) is located on the Amazon River main stem, in reference to the following equation (see text): $\Delta C(ijk) = \alpha(ij) \times \Delta(QRS/Q_t), (jk) + \beta(ij) \times \Delta(QRI/Q_t), (jk) + \gamma(ij) \times \Delta Q_t(I\text{-}O), (jk) + \delta(ij)$ View of R-squared value (r^2) is after reconstitution of water composition.

r^2	Cations (μmol L^{-1})					μeq L^{-1}		Anions (μmol L^{-1})					
Station	NH_4^+	Na^+	K^+	Ca^{2+}	Mg^{2+}	S^+	S^-	HCO_3^-	Cl^-	NO_3^-	DOC^-	SO_4^{2-}	HPO_4^{2-}
SAI	—	1.00	0.94	0.86	0.74	0.80	0.80	0.84	0.98	0.93	0.70	0.82	0.27
Xib	—	0.93	0.97	1.00	0.99	1.00	1.00	0.96	0.64	0.94	0.86	0.93	0.94
Tup	—	1.00	0.93	0.91	0.97	0.90	0.90	0.67	1.00	0.88	0.98	0.71	0.41
Jut	—	0.99	0.87	0.94	0.88	0.95	0.95	0.98	1.00	0.98	0.95	0.87	0.88
Ita	—	1.00	0.81	0.95	0.96	0.95	0.95	0.98	1.00	0.89	0.94	0.78	0.56
Ano	—	1.00	0.83	0.98	0.97	0.98	0.98	0.94	1.00	0.87	0.88	0.82	0.65
Man	—	1.00	0.77	0.94	0.93	0.94	0.94	0.94	0.99	0.93	0.78	0.93	0.83
SJA	—	1.00	0.91	0.98	0.91	0.99	0.99	0.93	1.00	0.90	0.95	0.01	0.47
Pau	—	1.00	0.96	0.97	0.99	0.98	0.98	0.93	1.00	0.97	0.83	0.28	0.97
Obi	0.01	1.00	0.83	0.94	0.96	0.95	0.95	0.98	1.00	0.97	0.71	0.83	0.15
Ave	0.01	0.99	0.88	0.95	0.93	0.94	0.94	0.91	0.96	0.93	0.86	0.70	0.61

r^2		mg L^{-1}	μmol L^{-1}				mg L^{-1}						$\delta^{18}O$
Station	pH	DOC	DIC	CO_2	O_2	SiO_2	FSS	CSS	TSS	POCF	POCC	POC	H_2O
SAI	0.79	0.73	0.91	0.96	0.74	0.95	1.00	0.94	0.99	0.99	0.59	0.98	1.00
Xib	0.78	0.87	0.95	0.72	0.92	0.99	0.98	0.23	0.89	0.99	0.82	0.96	0.99
Tup	0.91	0.98	0.79	0.98	0.77	0.97	1.00	0.43	0.95	0.96	0.08	0.93	0.99
Jut	0.98	0.97	0.98	0.97	0.93	1.00	0.98	0.40	0.91	0.93	0.14	0.88	0.98
Ita	0.84	0.98	0.95	0.85	0.76	0.91	0.96	0.53	0.97	0.92	0.52	0.94	0.99
Ano	0.85	0.93	0.98	0.88	0.74	0.90	0.91	0.55	0.87	0.88	0.45	0.84	0.98
Man	0.93	0.84	0.97	0.94	0.64	0.65	0.99	0.49	0.99	0.96	0.81	0.97	0.98
SJA	0.93	0.96	0.91	0.95	0.97	0.92	0.98	0.31	0.90	0.87	0.03	0.88	0.98
Pau	0.94	0.85	0.79	0.82	0.94	0.91	0.92	0.31	0.86	0.94	0.17	0.91	0.99
Obi	0.93	0.74	0.85	0.81	0.91	0.44	0.95	0.81	0.92	0.90	0.69	0.96	1.00
Ave	0.89	0.88	0.91	0.89	0.83	0.86	0.97	0.50	0.93	0.93	0.43	0.92	0.99

r^2	$\delta^{13}C$			C/N			Carbon cycle (μmol L^{-1})						
Station	DIC	POCF	POCC	POCF	POCC	DOC	DIC	POCF	POCC	PONF	PONC	DOC	DON
SAI	0.98	0.75	0.75	0.57	0.50	0.83	0.91	0.99	0.59	0.80	0.66	0.73	0.90

Table A5. (*Continued*)

r^2	$\delta^{13}C$			C/N			Carbon cycle (μmol L^{-1})						
Station	DIC	POCF	POCC	POCF	POCC	DOC	DIC	POCF	POCC	PONF	PONC	DOC	DON
Xib	0.97	0.92	0.82	0.42	0.95	0.83	0.95	0.99	0.82	0.99	0.85	0.86	0.88
Tup	1.00	0.67	0.87	0.57	0.77	0.85	0.79	0.96	0.08	0.95	0.29	0.98	0.68
Jut	0.84	0.14	0.46	0.01	0.00	0.11	0.50	0.87	0.01	0.92	0.01	0.66	0.05
Ita	0.96	0.93	0.77	0.68	0.08	0.80	0.95	0.92	0.52	0.97	0.52	0.98	0.35
Ano	0.94	0.91	0.60	0.51	0.29	0.86	0.98	0.88	0.45	0.97	0.43	0.93	0.83
Man	0.98	0.93	0.82	0.56	0.00	0.65	0.97	0.96	0.81	0.98	0.70	0.84	0.80
SJA	0.98	0.96	0.82	0.30	0.40	0.48	0.91	0.87	0.03	0.88	0.33	0.96	0.54
Pau	0.97	0.84	0.63	0.91	0.75	0.81	0.79	0.94	0.17	0.96	0.39	0.85	0.87
Obi	0.91	0.86	0.18	0.81	0.30	0.74	0.85	0.90	0.69	0.88	0.80	0.74	0.83
Ave	0.95	0.79	0.67	0.53	0.41	0.70	0.86	0.93	0.42	0.93	0.50	0.85	0.67

r^2	Silicates (μmol L^{-1})				Carbonates (μmol L^{-1})		Carbon cycle (μmol L^{-1})				
Station	NaSil	KSil	CaSil	MgSil	$CaCO_3$	Dolomite	CO_2 CARB	CO_2 SIL	CO_2 TOT	FR	Re
SAI	0.96	0.94	0.96	0.96	0.89	0.85	0.87	0.96	0.84	0.91	0.75
Xib	0.94	0.97	0.94	0.94	0.96	0.97	0.97	0.94	0.96	0.96	0.38
Tup	1.00	0.93	1.00	1.00	0.71	0.99	0.84	1.00	0.67	0.99	0.97
Jut	0.98	0.87	0.98	0.98	0.99	0.90	0.98	0.98	0.98	0.99	0.86
Ita	0.99	0.81	0.99	0.99	0.97	0.95	0.98	1.00	0.99	0.97	0.99
Ano	1.00	0.83	1.00	1.00	0.93	0.96	0.96	1.00	0.93	0.97	0.99
Man	1.00	0.77	1.00	1.00	0.92	0.92	0.95	0.99	0.94	0.98	0.92
SJA	0.94	0.91	0.94	0.94	0.77	0.86	0.95	0.94	0.93	0.96	0.91
Pau	0.99	0.96	0.99	0.99	0.85	0.99	0.95	0.99	0.92	1.00	0.92
Obi	1.00	0.83	1.00	1.00	0.99	0.98	0.99	0.99	0.98	1.00	0.84
Ave	0.98	0.88	0.98	0.98	0.90	0.94	0.94	0.98	0.92	0.97	0.85

γ (ij)	Cations (μmol L^{-1})					μeq L^{-1}		Anions (μmol L^{-1})					
Station	NH_4^+	Na^+	K^+	Ca^{2+}	Mg^{2+}	S^+	S^-	HCO_3^-	Cl^-	NO_3^-	DOC^-	SO_4^{2-}	HPO_4^{2-}
SAI	—	−0.03	−0.29	−0.42	−0.70	−0.38	−0.38	−0.36	−0.26	−0.22	0.17	0.64	−0.30
Xib	—	−0.01	−0.05	0.01	−0.15	0.00	0.00	0.42	−0.90	−0.83	0.17	−1.65	−0.17
Tup	—	−0.03	−0.41	0.29	0.80	0.31	0.31	0.81	−0.89	0.81	0.18	−4.60	−1.93

Jut	—	0.00	0.43	0.28	0.19	0.26	0.26	0.62	−0.69	−1.36	−0.21	−1.35	−0.82
Ita	—	0.00	0.31	0.14	0.09	0.14	0.14	0.43	−0.66	−0.26	−0.01	−1.80	0.43
Ano	—	0.02	0.10	0.16	0.14	0.15	0.15	0.28	−0.63	−0.70	0.29	−0.24	−1.13
Man	—	0.02	−0.71	0.17	0.10	0.12	0.12	0.62	−0.70	−0.02	0.31	−4.87	−1.45
SJA	—	0.25	0.33	0.47	0.70	0.46	0.46	1.07	−0.66	−0.02	0.38	−4.10	0.16
Pau	—	−0.02	0.14	0.64	0.34	0.46	0.47	0.99	−0.70	0.26	−0.17	−1.66	1.33
Obi	−1.79	−0.27	0.28	0.15	0.11	0.13	0.14	−0.04	−0.69	0.05	0.18	2.42	1.41
Ave	−1.79	−0.01	0.01	0.19	0.16	0.16	0.17	0.48	−0.68	−0.23	0.13	−1.72	−0.25

γ (ij)		mg L^{-1}	μmol L^{-1}				mg L^{-1}						δ^{18}O
Station	pH	DOC	DIC	CO_2	O_2	SiO_2	FSS	CSS	TSS	POCF	POCC	POC	H_2O
SAI	−0.08	−0.18	−0.15	1.21	0.02	−0.28	−0.04	1.43	0.34	0.73	0.03	0.53	0.05
Xib	0.03	0.25	0.39	0.19	0.02	−0.04	−0.10	2.74	0.76	−0.31	0.32	−0.14	−0.22
Tup	0.03	0.29	0.77	0.42	0.29	0.00	0.11	0.51	0.48	0.80	−0.55	0.51	0.17
Jut	0.02	−0.31	0.58	0.30	−0.25	0.25	−0.44	0.81	−0.22	−0.25	−1.86	−0.47	−0.05
Ita	0.01	−0.12	0.45	0.35	−0.51	0.14	0.35	3.28	0.86	0.08	0.28	0.21	−0.15
Ano	−0.01	0.21	0.37	0.50	−0.43	0.09	−0.08	2.19	0.41	−0.24	−0.02	−0.14	−0.19
Man	0.06	0.25	0.48	−0.28	−0.18	−0.06	0.00	2.52	0.57	−0.37	0.31	−0.20	−0.08
SJA	0.08	0.32	0.86	−0.06	−0.18	0.14	1.09	5.07	1.91	−0.09	1.10	0.19	−0.17
Pau	0.13	−0.14	0.54	−1.14	−0.42	−0.13	1.30	0.48	1.31	0.22	−0.53	0.08	−0.08
Obi	0.10	0.20	−0.42	−1.77	0.29	−0.55	0.92	2.57	1.45	−0.69	0.59	−0.34	−0.04
Ave	0.04	0.08	0.39	−0.03	−0.13	−0.04	0.31	2.16	0.79	−0.01	−0.03	0.02	−0.08

γ (ij)	δ^{13}C			C/N			Carbon cycle (μmol L^{-1})						
Station	DIC	POCF	POCC	POCF	POCC	DOC	DIC	POCF	POCC	PONF	PONC	DOC	DON
SAI	−0.04	0.07	0.09	2.00	1.81	−8.1	−0.15	0.73	0.03	−0.49	−0.99	−0.18	7.69
Xib	−0.09	−0.01	0.13	0.11	−0.51	0.92	0.39	−0.31	0.32	−0.41	1.38	0.17	−0.58
Tup	−0.07	−0.02	0.11	0.24	0.44	0.95	0.77	0.80	−0.55	0.60	−0.46	0.29	−0.39
Jut	0.04	−0.04	−0.05	0.36	0.22	1.90	−0.58	0.25	1.86	−0.07	1.54	0.31	−3.58
Ita	−0.17	−0.02	0.00	−0.85	−0.24	−2.19	0.45	0.08	0.28	0.91	0.89	−0.12	4.63
Ano	−0.21	−0.05	0.03	−0.20	0.05	−0.06	0.37	−0.24	−0.02	−0.02	0.11	0.21	−0.03
Man	0.00	0.00	0.05	−0.07	−0.49	0.53	0.48	−0.37	0.31	−0.32	0.79	0.25	0.13
SJA	−0.02	0.00	0.05	−0.68	−0.34	4.48	0.86	−0.09	1.10	0.92	1.92	0.32	−0.31

Table A5. (*Continued*)

γ (*ij*)	δ^{13}C			C/N			Carbon cycle (μmol L^{-1})						
Station	DIC	POCF	POCC	POCF	POCC	DOC	DIC	POCF	POCC	PONF	PONC	DOC	DON
Pau	−0.11	0.01	0.09	−0.14	0.39	−0.31	0.54	0.22	−0.53	0.37	−0.69	−0.14	−0.27
Obi	−0.14	0.09	0.15	−0.39	0.28	1.98	−0.42	−0.69	0.59	−0.37	0.87	0.20	−0.69
Ave	−0.08	0.00	0.07	0.04	0.16	0.01	0.27	0.04	0.34	0.11	0.54	0.13	0.66

γ (*ij*)	Silicates (μmol L^{-1})				Carbonates (μmol L^{-1})		Carbon cycle (μmol L^{-1})				
Station	NaSil	KSil	CaSil	MgSil	$CaCO_3$	Dolomite	CO_2 CARB	CO_2 SIL	CO_2 TOT	FR	Re
SAI	1.33	−0.29	1.33	1.33	−0.31	−1.24	−0.58	1.06	−0.35	−0.26	1.11
Xib	2.41	−0.05	2.41	2.41	0.47	−0.97	0.04	1.91	0.41	−0.38	1.49
Tup	2.28	−0.41	2.28	2.28	0.56	0.18	0.46	1.78	0.80	−0.32	1.08
Jut	1.54	0.43	1.54	1.54	0.54	−0.63	0.21	1.40	0.56	−0.26	0.83
Ita	1.48	0.31	1.48	1.48	0.38	−0.54	0.13	1.24	0.41	−0.28	0.72
Ano	1.47	0.10	1.47	1.47	0.07	−0.58	−0.10	1.21	0.26	−0.38	0.66
Man	1.40	−0.71	1.40	1.40	0.78	−0.46	0.43	0.98	0.60	−0.15	0.72
SJA	1.76	0.33	1.76	1.76	0.99	0.16	0.79	1.43	1.03	−0.21	1.15
Pau	1.06	0.14	1.06	1.06	1.30	−0.08	0.81	0.90	0.94	−0.09	0.60
Obi	0.67	0.28	0.67	0.67	−0.53	−0.41	−0.48	0.76	−0.02	−0.44	0.66
Ave	1.54	0.01	1.54	1.54	0.43	−0.46	0.17	1.27	0.46	−0.28	0.90

$\Delta QRS/Q_t$	Cations (μmol L^{-1})					μeq L^{-1}		Anions (μmol L^{-1})					
Station	NH_4^+	Na^+	K^+	Ca^{2+}	Mg^{2+}	S^+	S^-	HCO_3^-	Cl^-	NO_3^-	DOC^-	SO_4^{2-}	HPO_4^{2-}
SAI	—	−2.32	0.91	0.03	0.83	−0.37	−0.37	0.30	2.01	0.18	4.86	−9.86	7.08
Xib	—	−2.60	2.64	−0.13	0.65	−0.42	−0.42	−0.14	0.03	0.03	−1.01	−1.63	2.42
Tup	—	−2.60	−2.77	−1.06	−0.14	−1.28	−1.28	0.07	0.02	4.12	−0.38	−21.76	0.23
Jut	—	−2.93	4.26	1.54	−1.26	0.21	0.21	0.47	−0.39	3.57	0.24	−0.84	6.21
Ita	—	−2.71	−2.83	−0.75	−1.24	−1.25	−1.25	−1.27	−0.09	−2.40	0.68	−0.20	−3.17
Ano	—	−2.88	−0.64	−1.17	−2.77	−1.67	−1.67	0.27	−0.19	−0.36	−0.07	−19.23	3.42
Man	—	−3.69	1.03	−1.70	−2.38	−2.17	−2.17	−3.60	0.47	4.54	−0.18	17.67	3.31
SJA	—	−3.68	2.27	−1.71	0.03	−1.77	−1.75	−1.52	−0.33	−3.37	−3.17	6.42	−2.35
Pau	—	−2.31	−0.47	−0.75	−0.59	−1.13	−1.12	−1.21	0.07	−1.57	0.26	−2.30	−3.01
Obi	−1.51	−1.83	−0.28	−0.22	−0.29	−0.61	−0.59	−0.08	0.03	−2.49	−0.39	−4.99	0.88
Ave	−1.51	−2.75	−0.44	−0.59	−0.72	−1.04	−1.04	−0.67	0.16	−0.68	−0.89	−3.67	1.50

ΔQRS/Q_t		mg L^{-1}	μmol L^{-1}				mg L^{-1}						$\delta^{18}O$
Station	pH	DOC	DIC	CO_2	O_2	SiO_2	FSS	CSS	TSS	POCF	POCC	POC	H_2O
SAI	−0.13	−3.37	0.13	1.92	3.26	−0.08	2.89	−6.16	1.23	0.79	6.53	2.23	−0.01
Xib	−0.12	−0.09	0.10	0.92	0.69	−0.26	2.85	−10.47	1.10	2.52	9.78	3.98	0.88
Tup	−0.26	−0.23	0.60	4.44	−1.09	0.17	1.54	−2.95	1.42	2.63	−2.82	1.40	0.72
Jut	0.39	0.72	−0.26	−5.53	1.83	−0.58	2.98	9.46	4.39	−0.51	7.38	1.07	0.17
Ita	−0.05	0.94	−0.98	−0.35	1.57	−0.67	−2.71	−7.99	−3.70	−2.63	−13.01	−4.55	0.79
Ano	0.03	0.03	0.24	−0.12	1.46	−0.24	−1.32	−4.66	−2.41	−1.27	−12.07	−3.06	1.48
Man	−0.61	0.01	−1.67	5.95	0.23	−0.34	−3.39	−16.36	−6.65	−2.61	−10.73	−4.45	0.22
SJA	0.02	−2.90	−1.49	−2.65	1.83	−0.59	−2.69	−9.65	−3.77	−0.92	−4.12	−1.71	−0.15
Pau	−0.26	0.16	−0.21	3.19	0.37	0.35	3.61	11.29	4.40	5.26	9.94	5.84	−0.14
Obi	−0.10	−0.43	0.39	1.69	−0.20	0.24	5.58	12.32	6.65	5.30	7.00	5.45	−0.24
Ave	−0.11	−0.51	−0.32	0.95	0.99	−0.20	0.94	−2.52	0.27	0.86	−0.21	0.62	0.37

ΔQRS/Q_t	$\delta^{13}C$			C/N			Carbon cycle (μmol L^{-1})						
Station	DIC	POCF	POCC	POCF	POCC	DOC	DIC	POCF	POCC	PONF	PONC	DOC	DON
SAI	0.20	0.01	−0.09	8.72	19.10	−2.1	0.13	0.79	6.53	−2.89	0.57	−3.37	−1.41
Xib	0.43	−0.06	0.32	0.88	−1.57	−10.56	0.10	2.52	9.78	1.91	11.45	−1.01	13.27
Tup	−0.23	−0.14	0.36	0.52	−5.17	6.62	0.60	2.63	−2.82	2.10	4.09	−0.23	−9.86
Jut	−0.42	0.34	0.15	0.91	−0.18	−1.98	0.26	0.51	−7.38	−0.32	−9.59	−0.72	8.50
Ita	−0.10	−0.03	0.42	0.87	−2.54	−11.33	−0.98	−2.63	−13.01	−3.35	−9.68	0.94	−3.19
Ano	0.12	0.09	0.14	−1.01	−4.07	−29.45	0.24	−1.27	−12.07	−0.60	−6.95	0.03	9.66
Man	−0.93	−0.21	−0.06	−1.00	−0.31	7.38	−1.67	−2.61	−10.73	−1.78	−11.67	0.01	−3.64
SJA	−0.15	−0.01	0.09	−0.21	−1.42	−6.49	−1.49	−0.92	−4.12	−0.99	4.27	−2.90	2.56
Pau	0.03	0.07	0.24	0.22	−0.77	−10.37	−0.21	5.26	9.94	4.96	11.59	0.16	3.54
Obi	−0.17	−0.10	0.37	1.06	−1.24	−7.87	0.39	5.30	7.00	4.32	9.51	−0.43	3.10
Ave	−0.12	−0.01	0.19	1.10	0.18	−6.62	−0.26	0.96	−1.69	0.34	−0.50	−0.75	2.25

ΔQRS/Q_t	Silicates (μmol L^{-1})				Carbonates (μmol L^{-1})		Carbon cycle (μmol L^{-1})				
Station	NaSil	KSil	CaSil	MgSil	$CaCO_3$	Dolomite	CO_2CARB	CO_2SIL	CO_2 TOT	FR	Re
SAI	−17.46	0.91	−17.46	−17.46	1.83	6.67	3.19	−14.10	0.22	3.40	−10.30
Xib	−10.32	2.64	−10.32	−10.32	0.55	4.17	1.65	−8.02	−0.14	1.83	−6.11

Table A5. (*Continued*)

$\Delta QRS/Q_t$	Silicates (μmol L^{-1})				Carbonates (μmol L^{-1})		Carbon cycle (μmol L^{-1})				
Station	NaSil	KSil	CaSil	MgSil	$CaCO_3$	Dolomite	CO_2CARB	CO_2SIL	CO_2 TOT	FR	Re
Tup	−10.41	−2.77	−10.41	−10.41	1.80	2.78	2.17	−9.16	0.14	2.07	−7.12
Jut	−8.13	4.26	−8.13	−8.13	3.19	1.34	2.48	−7.21	0.57	1.85	−3.65
Ita	−7.68	−2.83	−7.68	−7.68	−0.18	1.21	0.21	−6.60	−1.24	1.49	−2.22
Ano	−7.52	−0.64	−7.52	−7.52	3.39	−0.32	2.20	−6.09	0.25	2.26	−1.31
Man	−12.08	1.03	−12.08	−12.08	−2.47	1.82	−1.32	−9.63	−3.52	2.18	−5.99
SJA	−9.38	2.27	−9.38	−9.38	−1.39	4.88	0.39	−7.27	−1.60	1.92	−4.67
Pau	−7.04	−0.47	−7.04	−7.04	0.05	2.65	1.00	−6.13	−1.17	2.07	−3.20
Obi	−5.76	−0.28	−5.76	−5.76	1.44	2.35	1.79	−5.03	−0.16	1.90	−2.31
Ave	−9.58	−0.44	−9.58	−9.58	0.82	2.76	1.38	−7.92	−0.66	2.10	4.69

$\Delta QRI/Q_t$	Cations (μmol L^{-1})					μeq L^{-1}		Anions (μmol L^{-1})					
Station	NH_4^+	Na^+	K^+	Ca^{2+}	Mg^{2+}	S^+	S^-	HCO_3^-	Cl^-	NO_3^-	DOC^-	SO_4^{2-}	HPO_4^{2-}
SAI	—	−2.18	0.35	0.74	1.18	0.27	0.27	0.68	1.52	1.86	−479	−7.28	6.83
Xib	—	−2.38	2.13	0.05	0.51	−0.31	−0.31	−0.10	0.03	0.12	−1.45	−0.80	1.56
Tup	—	−2.40	−2.26	−0.80	−0.14	−1.07	−1.07	0.06	0.01	1.65	−0.54	−15.55	0.82
Jut	—	−2.75	−2.44	0.22	−0.73	−0.51	−0.51	−0.12	−0.30	1.47	−0.21	−4.14	3.82
Ita	—	−2.53	−2.50	−0.79	−0.93	−1.20	−1.20	−0.76	−0.11	−2.07	0.51	−4.62	−2.38
Ano	—	−2.65	−0.37	−1.01	−1.78	−1.40	−1.40	0.16	−0.16	−0.94	−0.04	−15.84	2.36
Man	—	−3.14	0.81	−1.62	−1.83	−1.96	−1.96	−2.59	0.32	−3.43	−0.15	8.44	2.11
SJA	—	−3.26	2.29	−1.52	0.57	−1.49	−1.48	−0.87	−0.28	−2.85	−2.87	2.80	−2.33
Pau	—	−2.20	−0.06	−0.42	−0.07	−0.76	−0.76	−0.41	0.07	−1.27	−0.17	−3.58	−1.38
Obi	−2.75	−1.95	0.56	−0.17	0.13	−0.44	−0.44	−0.28	−0.01	−1.73	−0.36	−2.29	1.90
Ave	−2.75	−2.55	−0.15	−0.53	−0.31	−0.89	−0.89	−0.42	0.11	−0.72	−1.01	−4.29	1.33

$\Delta QRI/Q_t$		mgL^{-1}	μmol L^{-1}				mg L^{-1}						$\delta^{18}O$
Station	pH	DOC	DIC	CO_2	O_2	SiO_2	FSS	CSS	TSS	POCF	POCC	POC	H_2O
SAI	0.23	−2.02	−0.39	−4.49	3.24	0.58	0.77	−4.75	−0.23	−2.63	2.08	−1.52	−0.38
Xib	0.08	−0.83	−0.23	−2.51	−0.13	0.01	0.72	−14.00	−1.50	1.01	3.22	1.44	0.54
Tup	−0.14	−0.46	0.34	2.42	−0.73	0.09	0.23	−3.90	−0.12	0.48	−3.03	−0.24	0.25
Jut	0.18	0.07	−0.42	−2.93	1.01	−0.70	1.02	4.57	1.86	−0.68	3.48	0.24	0.12
Ita	−0.02	0.70	−0.60	−0.38	1.13	−0.55	−2.81	−5.76	−3.35	−1.90	−10.45	−3.41	0.57
Ano	0.02	0.01	0.15	−0.08	0.99	−0.15	−1.91	−3.42	−2.49	−1.69	−8.83	−2.84	1.00

Man	−0.41	0.01	−1.28	3.87	0.29	−0.20	−3.27	−13.34	−5.68	−2.56	−8.98	−3.96	0.00
SJA	0.06	−2.63	−1.02	−2.51	1.59	−0.51	−2.77	−9.79	−3.79	−1.04	−4.00	−1.73	−0.19
Pau	−0.06	−0.18	−0.15	0.69	−0.06	0.11	1.29	2.46	1.35	2.22	3.16	2.31	−0.13
Obi	−0.01	−0.35	−0.26	−0.20	−0.01	−0.18	2.18	5.56	2.82	1.40	3.39	1.75	−0.18
Ave	−0.01	−0.57	−0.39	−0.61	0.73	−0.15	−0.46	−4.24	−1.11	−0.54	−2.00	−0.80	−0.04

$\Delta QRI/Q_t$	$\delta^{13}C$			C/N			Carbon cycle (μmol L^{-1})						
Station	DIC	POCF	POCC	POCF	POCC	DOC	DIC	POCF	POCC	PONF	PONC	DOC	DON
SAI	0.39	−0.30	−0.45	0.42	16.71	11.2	−0.39	−2.63	2.08	−1.64	−1.64	−2.02	−17.26
Xib	0.08	−0.10	0.25	−0.39	0.67	−9.20	−0.23	1.01	3.22	1.49	2.30	−1.45	10.82
Tup	−0.09	−0.11	0.21	0.31	−2.34	1.47	0.34	0.48	−3.03	0.17	0.41	−0.46	−2.41
Jut	−0.34	0.18	0.16	0.73	0.03	−1.19	0.42	0.68	−3.48	0.05	−5.25	−0.07	7.98
Ita	−0.01	0.02	0.30	1.50	−1.53	−9.67	−0.60	−1.90	−10.45	−3.37	−7.83	0.70	−2.66
Ano	0.16	0.11	0.12	−0.59	−3.14	−21.62	0.15	−1.69	−8.83	−1.32	−482	0.01	7.69
Man	−0.58	−0.10	−0.03	−0.68	−0.77	4.43	−1.28	−2.56	−8.98	−1.98	−8.96	0.01	−1.44
SJA	−0.04	−0.01	−0.01	0.01	−0.44	−6.80	−1.02	−1.04	−400	−1.29	−452	−2.63	3.23
Pau	0.11	0.10	0.06	−0.07	1.84	−8.58	−0.15	2.22	3.16	2.24	2.90	−0.18	2.43
Obi	−0.12	−0.03	0.21	0.57	0.10	−4.36	−0.26	1.40	3.39	0.88	4.28	−0.35	1.64
Ave	−0.04	−0.02	0.08	0.18	1.11	−4.43	−0.30	−0.40	−2.69	−0.48	−2.31	−0.65	1.00

$\Delta QRI/Q_t$	Silicates (μmol L^{-1})				Carbonates (μmol L^{-1})		Carbon cycle (μmol L^{-1})				
Station	NaSil	KSil	CaSil	MgSil	$CaCO_3$	Dolomite	$CO_{2\ CARB}$	$CO_{2\ SIL}$	$CO_{2\ TOT}$	FR	Re
SAI	−15.47	0.35	−15.47	−15.47	1.83	5.82	2.93	−12.43	0.65	2.62	−8.59
Xib	−9.77	2.13	−9.77	−9.77	0.62	3.68	1.58	−7.68	−0.12	1.73	−6.29
Tup	−9.76	−2.26	−9.76	−9.76	1.67	2.76	2.05	−8.53	0.08	1.99	−6.71
Jut	−7.82	−2.44	−7.82	−7.82	1.65	2.28	1.73	−6.74	−0.05	1.69	−3.30
Ita	−7.24	−2.50	−7.24	−7.24	0.51	1.66	0.83	−6.28	−0.76	1.68	−2.67
Ano	−7.27	−0.37	−7.27	−7.27	2.55	0.95	2.03	−5.95	0.13	2.14	−2.11
Man	−10.07	0.81	−10.07	−10.07	−1.36	1.96	−0.46	−8.13	−2.54	2.08	−5.04
SJA	−8.34	2.29	−8.34	−8.34	−0.79	5.21	0.94	−6.47	−0.99	1.87	−4.14
Pau	−6.58	−0.06	−6.58	−6.58	0.86	3.05	1.67	−5.62	−0.45	2.05	−2.85
Obi	−5.64	0.56	−5.64	−5.64	0.50	2.69	1.33	−4.62	−0.33	1.63	−1.96
Ave	−8.80	−0.15	−8.80	−8.80	0.80	3.01	1.46	−7.24	−0.44	1.95	−4.37

Table A5. (*Continued*)

$\delta(ij)$	Cations (μmol L^{-1})					μeq L^{-1}		Anions (μmol L^{-1})					
Station	NH_4^+	Na^+	K^+	Ca^{2+}	Mg^{2+}	S^+	S^-	HCO_3^-	Cl^-	NO_3^-	DOC^-	SO_4^{2-}	HPO_4^{2-}
$\delta(ij)$	Cations (μmol L^{-1})					μeq L^{-1}		Anions (μmol L^{-1})					
Station	NH_4^+	Na^+	K^+	Ca^{2+}	Mg^{2+}	S^+	S^-	HCO_3^-	Cl^-	NO_3^-	DOC^-	SO_4^{2-}	HPO_4^{2-}
SAI	—	−0.08	−0.09	−0.13	−0.10	−0.12	−0.12	−0.11	−0.12	−0.11	−0.07	−0.24	0.03
Xib	—	−0.01	0.01	−0.04	−0.02	−0.04	−0.04	−0.05	0.00	0.07	−0.05	0.02	0.03
Tup	—	0.01	0.06	−0.04	−0.05	−0.03	−0.03	−0.06	0.00	0.03	−0.04	0.32	0.14
Jut	—	0.06	−0.01	−0.09	−0.03	−0.06	−0.06	−0.10	0.00	0.28	0.03	0.23	0.12
Ita	—	−0.02	−0.02	−0.12	−0.02	−0.09	−0.09	−0.17	−0.01	0.03	−0.02	0.66	0.00
Ano	—	−0.01	−0.03	−0.13	−0.04	−0.10	−0.10	−0.14	−0.01	0.15	−0.11	0.30	0.36
Man	—	−0.02	0.23	−0.14	−0.02	−0.09	−0.09	−0.18	0.01	0.02	−0.04	0.95	0.36
SJA	—	0.05	−0.08	−0.10	−0.13	−0.08	−0.08	−0.17	0.00	0.12	−0.03	0.64	0.21
Pau	—	0.06	0.03	−0.13	−0.03	−0.08	−0.08	−0.13	0.00	0.12	−0.07	0.30	0.01
Obi	0.33	0.03	0.04	−0.11	−0.01	−0.08	−0.08	−0.04	0.00	0.18	−0.14	−0.43	0.14
Ave	0.33	0.01	0.01	−0.10	−0.04	−0.08	−0.08	−0.12	−0.01	0.09	−0.05	0.27	0.14

δ (ij)		mg L^{-1}		μmol L^{-1}						mg L^{-1}			$\delta^{18}O$
Station	pH	DOC	DIC	CO_2	O_2	SiO_2	FSS	CSS	TSS	POCF	POCC	POC	H_2O
SAI	−0.01	−0.05	−0.11	0.05	0.00	−0.01	−0.17	−0.17	−0.18	−0.22	−0.07	−0.19	0.01
Xib	0.00	−0.07	−0.04	0.03	−0.05	0.00	−0.05	0.01	−0.07	−0.06	0.00	−0.06	0.01
Tup	0.00	−0.06	−0.05	−0.01	−0.06	0.01	−0.02	0.06	−0.04	−0.02	0.01	−0.02	0.01
Jut	−0.01	0.04	−0.08	0.07	−0.05	0.02	0.00	0.12	0.01	−0.02	0.32	0.02	0.03
Ita	−0.01	−0.01	−0.14	0.04	−0.03	−0.02	−0.12	−0.46	−0.19	−0.07	0.04	−0.08	0.06
Ano	−0.01	−0.10	−0.12	0.04	−0.03	−0.01	−0.05	−0.29	−0.12	−0.04	−0.04	−0.06	0.07
Man	−0.02	−0.04	−0.13	0.09	−0.05	0.04	−0.09	−0.39	−0.18	−0.10	−0.20	−0.13	0.04
SJA	−0.02	−0.03	−0.10	0.18	−0.04	0.01	−0.07	−0.37	−0.16	−0.10	−0.12	−0.11	0.04
Pau	−0.02	−0.08	−0.06	0.19	−0.01	0.02	−0.09	−0.03	−0.11	−0.05	−0.04	−0.06	0.04
Obi	−0.03	−0.15	0.07	0.43	−0.12	0.12	−0.01	−0.22	−0.09	0.29	−0.19	0.18	0.04
Ave	−0.01	−0.05	−0.08	0.11	−0.04	0.02	−0.07	−0.17	−0.11	−0.04	−0.03	−0.05	−0.02

δ (ij)	$\delta^{13}C$			C/N			Carbon cycle (μmol L^{-1})						
Station	DIC	POCF	POCC	POCF	POCC	DOC	DIC	POCF	POCC	PONF	PONC	DOC	DON
SAI	−0.03	−0.02	−0.01	0.37	0.94	0.4	−0.11	−0.22	−0.07	−0.40	−0.44	−0.05	−0.29
Xib	−0.03	−0.01	0.00	−0.02	−0.01	−0.20	−0.04	−0.06	0.00	−0.04	0.01	−0.05	0.27

Tup	−0.01	0.00	−0.01	−0.03	0.03	−0.20	−0.05	−0.02	0.01	0.01	−0.02	−0.06	0.24
Jut	−0.01	−0.01	0.00	−0.03	0.01	−0.15	0.08	0.02	−0.32	0.05	−0.29	−0.04	0.13
Ita	−0.02	−0.01	0.00	0.16	0.08	0.41	−0.14	−0.07	0.04	−0.20	−0.10	−0.01	−0.50
Ano	−0.01	0.00	0.00	0.03	−0.03	0.27	−0.12	−0.04	−0.04	−0.07	−0.08	−0.10	0.00
Man	−0.05	−0.01	−0.01	−0.02	0.03	−0.07	−0.13	−0.10	−0.20	−0.09	−0.23	−0.04	0.09
SJA	−0.02	−0.01	0.00	0.02	0.06	−0.02	−0.10	−0.10	−0.12	−0.12	−0.17	−0.03	−0.13
Pau	−0.03	−0.01	−0.01	0.03	−0.09	0.71	−0.06	−0.05	−0.04	−0.08	0.08	−0.08	−0.34
Obi	−0.02	−0.02	−0.03	0.09	−0.15	−0.17	0.07	0.29	−0.19	0.21	−0.05	−0.15	−0.02
Ave	−0.02	−0.01	−0.01	0.06	0.09	0.10	−0.06	−0.04	−0.09	−0.07	−0.13	−0.06	−0.06

δ (*ij*)	Silicates (umol L^{-1})				Carbonates (umol L^{-1})		Carbon cycle (umol L^{-1})				
Station	NaSil	KSil	CaSil	MgSil	$CaCO_3$	Dolomite	$CO_{2\ CARB}$	$CO_{2\ SIL}$	$CO_{2\ TOT}$	FR	Re
SAI	0.03	−0.09	0.03	0.03	−0.14	−0.13	−0.14	0.01	−0.11	−0.03	0.00
Xib	−0.04	0.01	−0.04	−0.04	−0.06	−0.01	−0.05	−0.02	−0.04	0.00	0.01
Tup	0.05	0.06	0.05	0.05	−0.07	−0.08	−0.07	0.05	−0.05	−0.02	0.05
Jut	0.20	−0.01	0.20	0.20	−0.15	−0.08	−0.13	0.15	−0.09	−0.05	0.05
Ita	−0.04	−0.02	−0.04	−0.04	−0.25	−0.01	−0.18	−0.03	−0.16	−0.03	−0.01
Ano	−0.01	−0.03	−0.01	−0.01	−0.20	−0.02	−0.15	−0.01	−0.14	−0.02	0.00
Man	−0.06	0.23	−0.06	−0.06	−0.30	−0.02	−0.22	0.00	−0.17	−0.05	−0.01
SJA	0.14	−0.08	0.14	0.14	−0.21	−0.29	−0.24	0.12	−0.15	−0.09	0.06
Pau	0.19	0.03	0.19	0.19	−0.28	−0.13	−0.23	0.17	−0.12	−0.11	0.08
Obi	0.04	0.04	0.04	0.04	−0.06	0.00	−0.04	0.02	−0.04	0.00	−0.05
Ave	0.05	0.01	0.05	0.05	−0.17	−0.08	−0.15	0.05	−0.11	−0.04	0.02

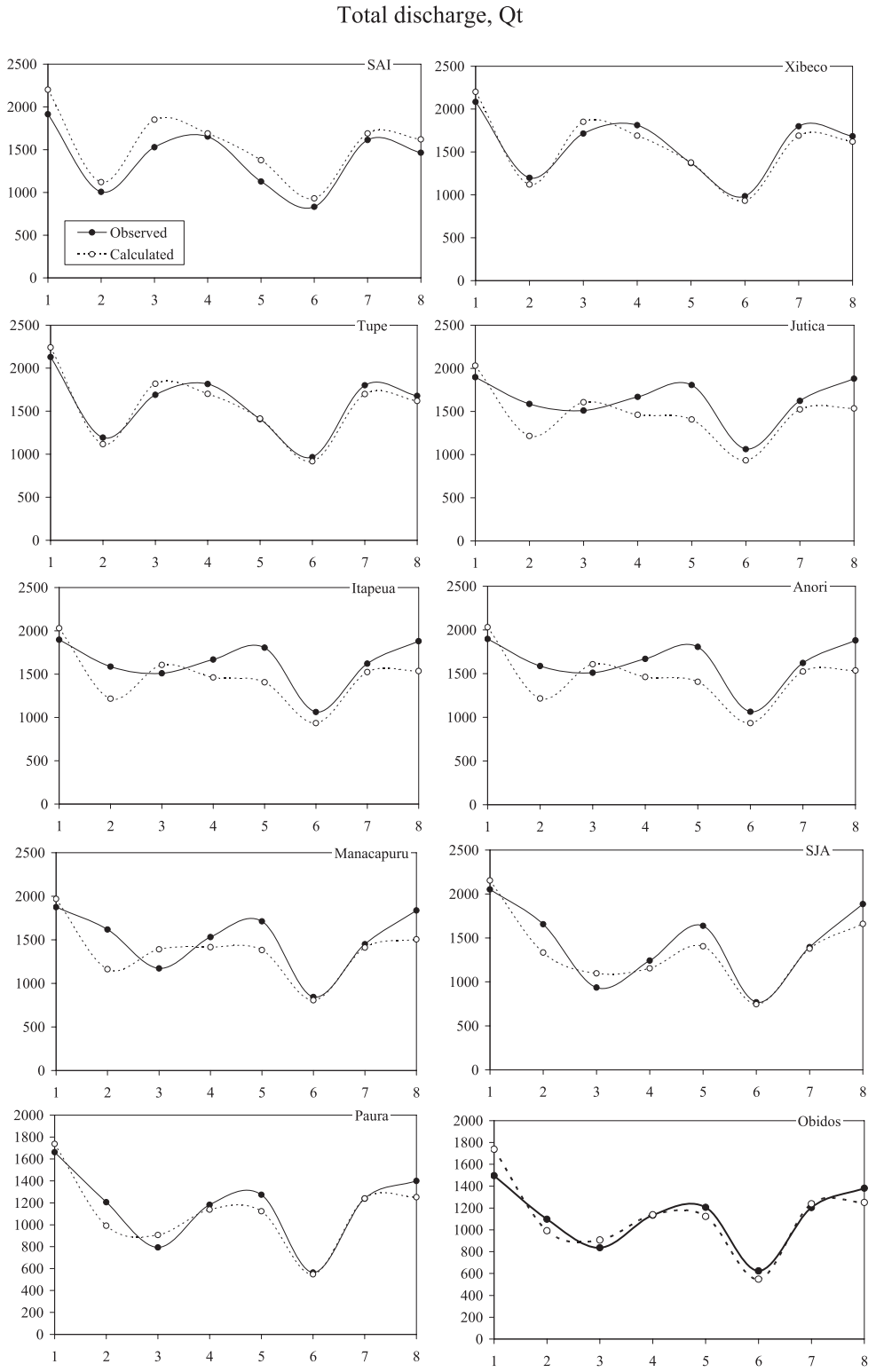

Figure A1. Comparison between the fluctuations of discharge of the Amazon River (10 stations) and the theoretical compositional fluctuations (9 virtual stations) estimated by cumulating the inputs and inflows: total discharge; Q_t; and river flow components superficial runoff QRS, interflow QRI, and baseflow QRB (all data given in mm yr^{-1}).

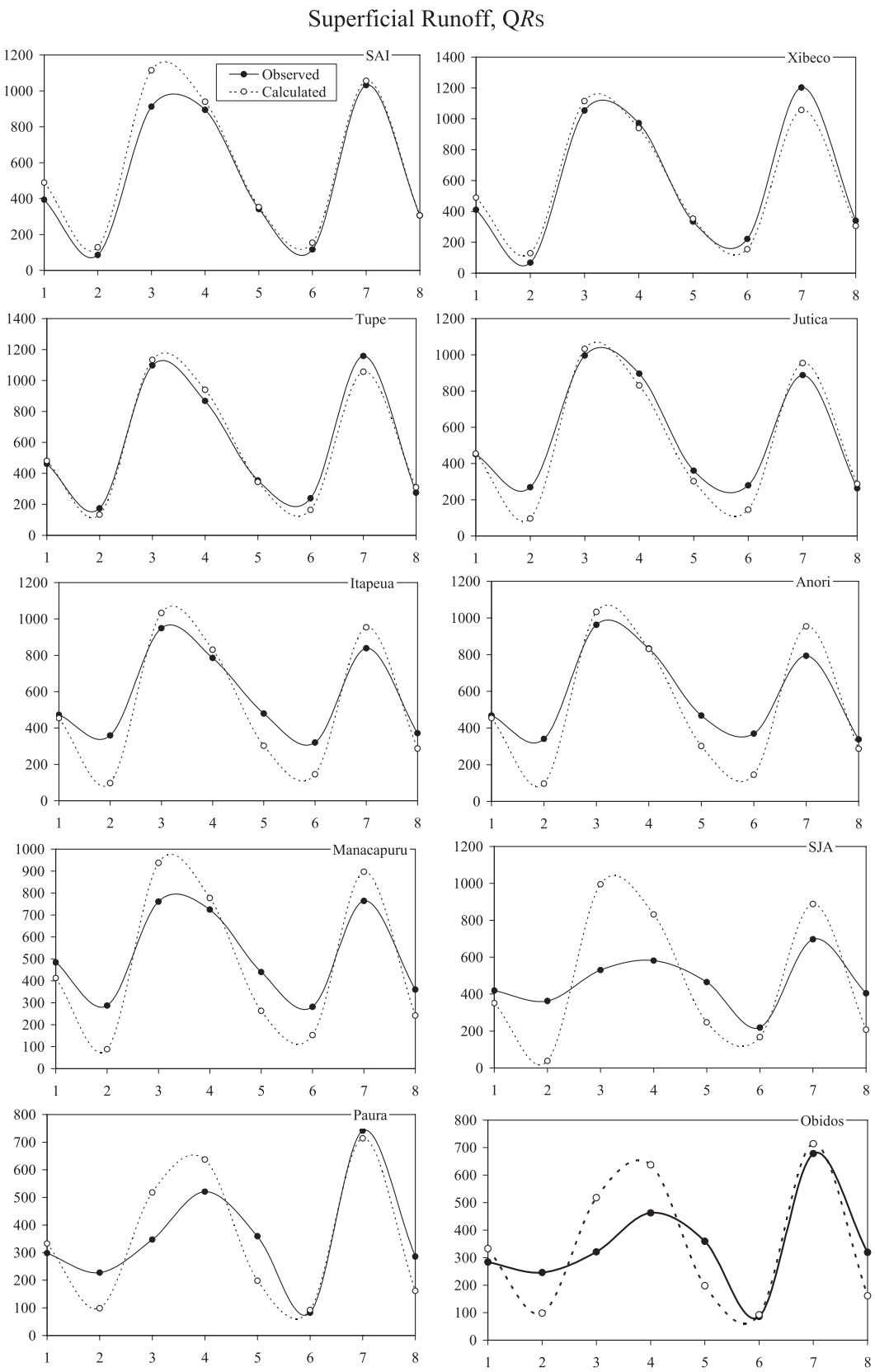

Figure A1. (*Continued*)

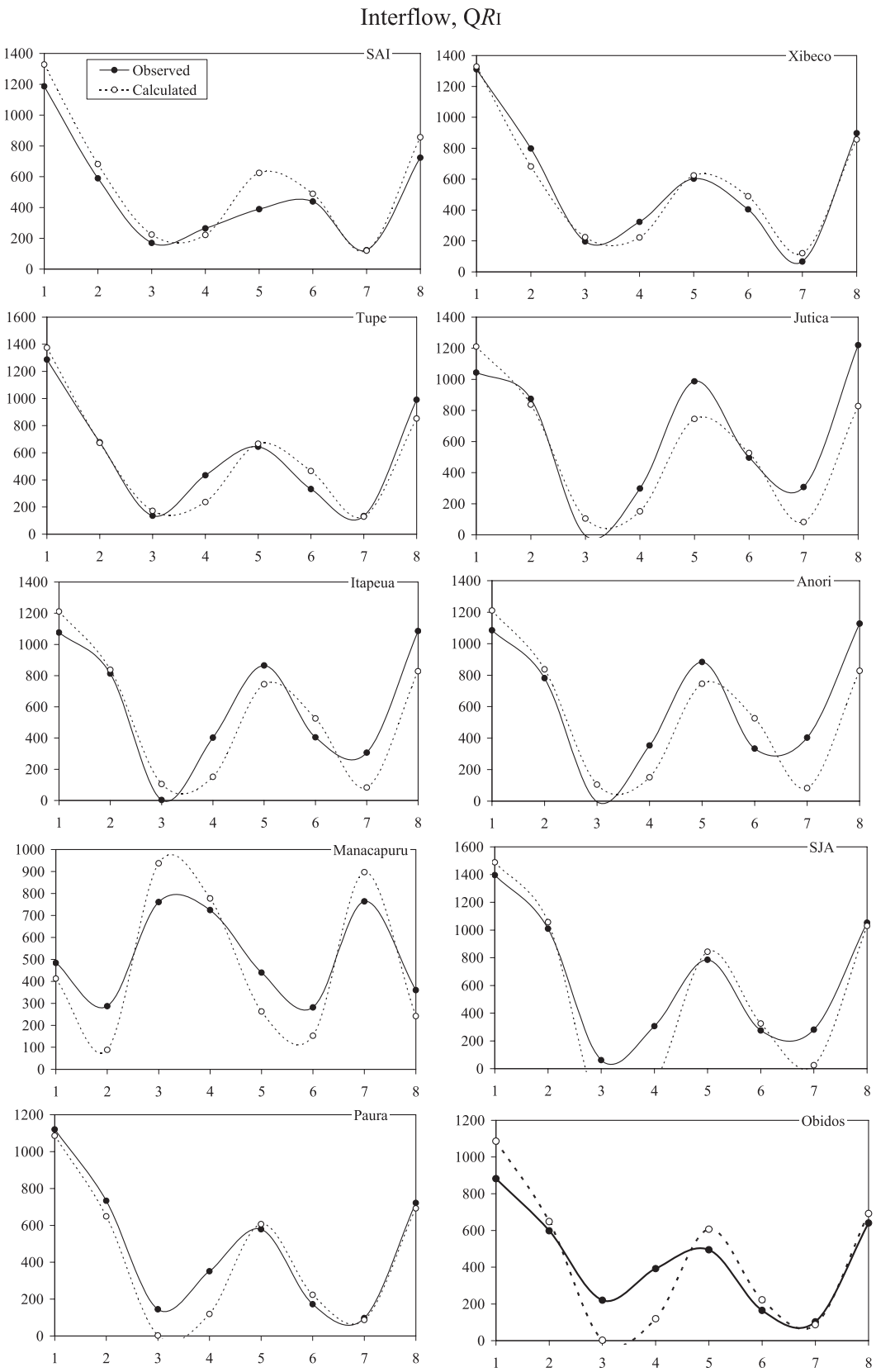

Figure A1. (*Continued*)

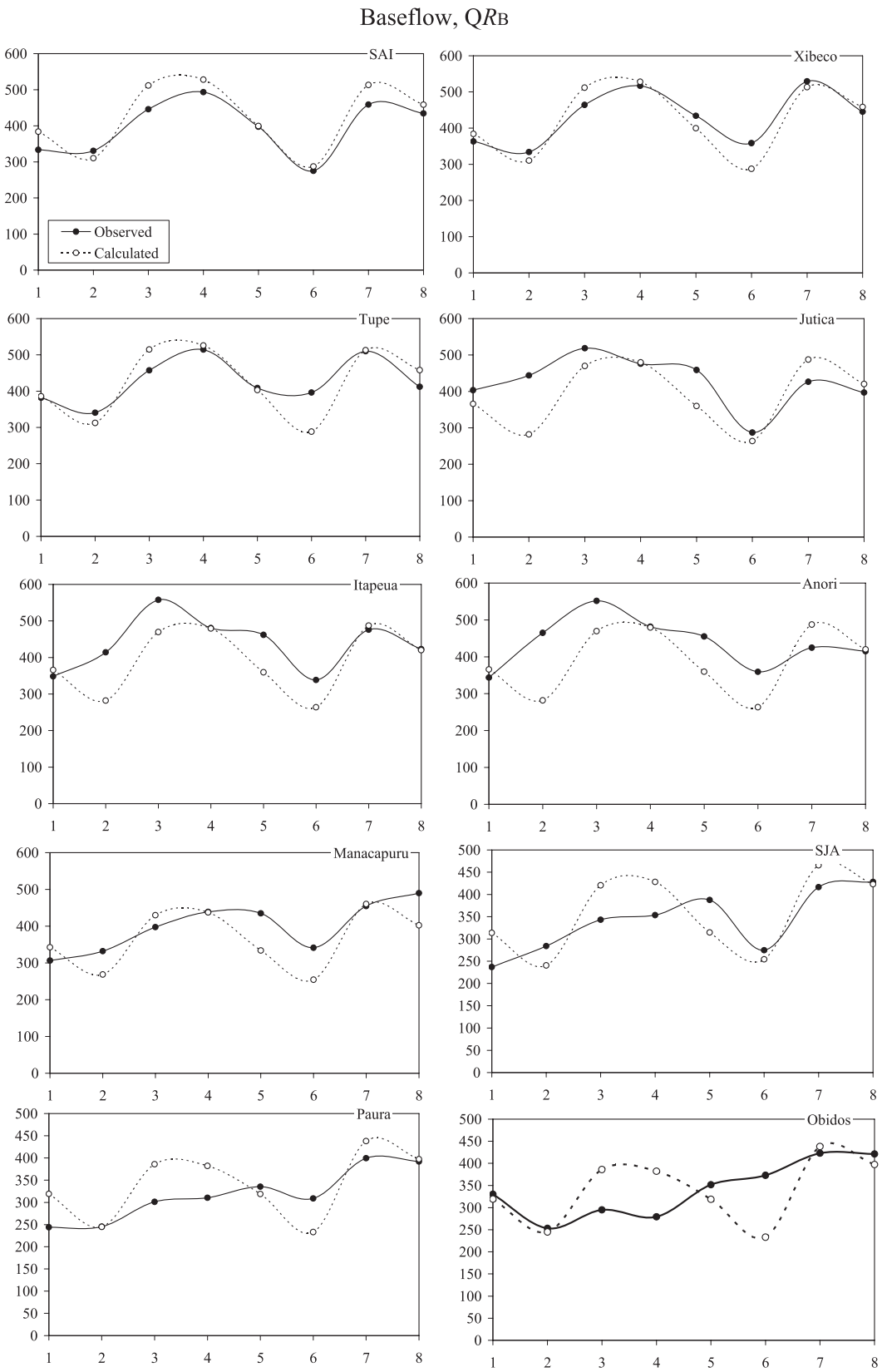

Figure A1. (*Continued*)

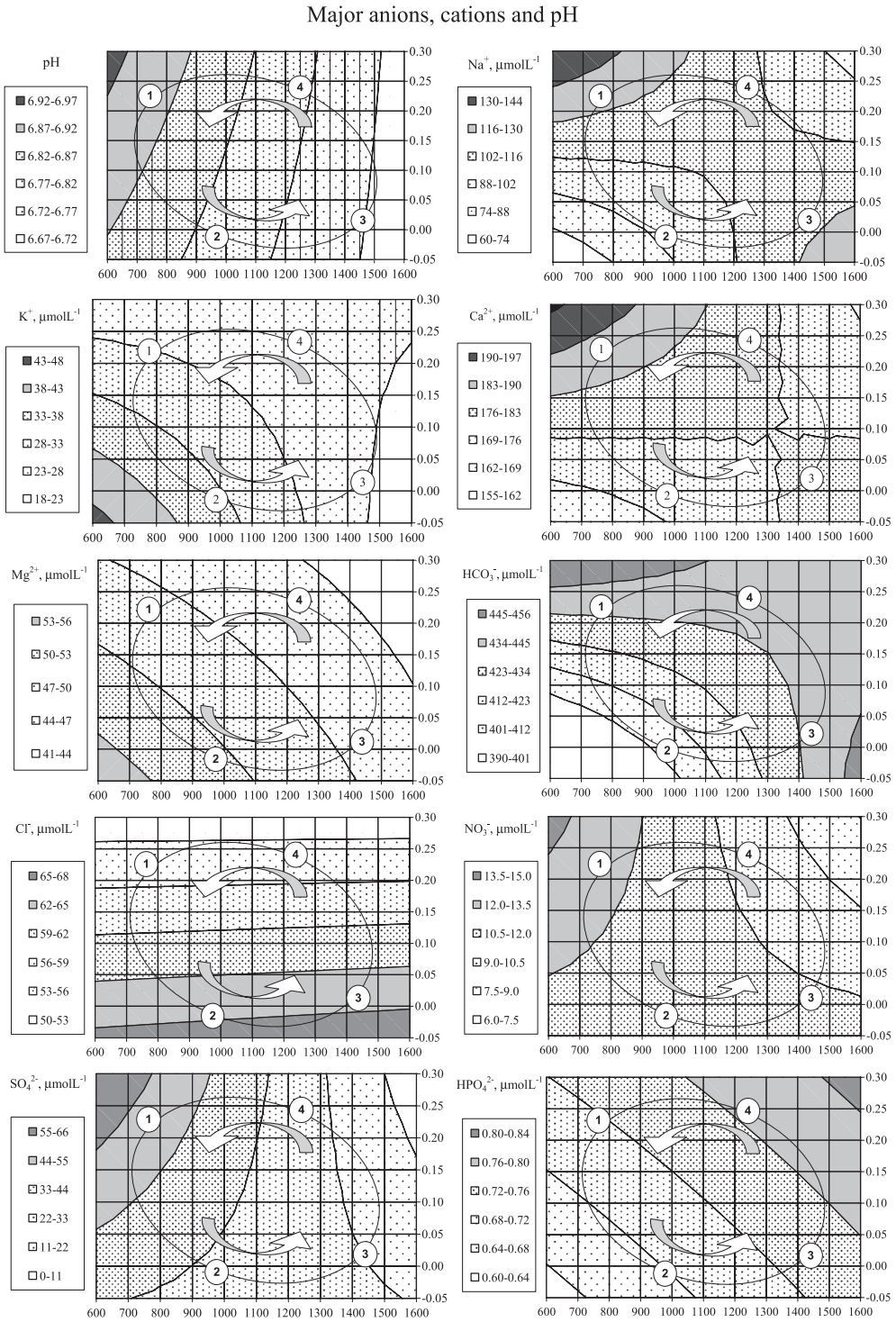

Figure A2. M6 at the station of Óbi. Representation of the compositional variations (for all the parameters) as a function of the river flow (*x* axis) and the water balance of the floodplains appreciated by ΔQ_f (I-O) (*y* axis). The input is supposed to exhibit a constant concentration corresponding to the value at the center of the diagram for which $Q_f = 1122$ mm yr^{-1} and ΔQ_f (I-O) = 0.13. The stages 1, 2, 3, and 4 correspond to the lowest waters, rising waters, peak of discharge, and falling waters, respectively.

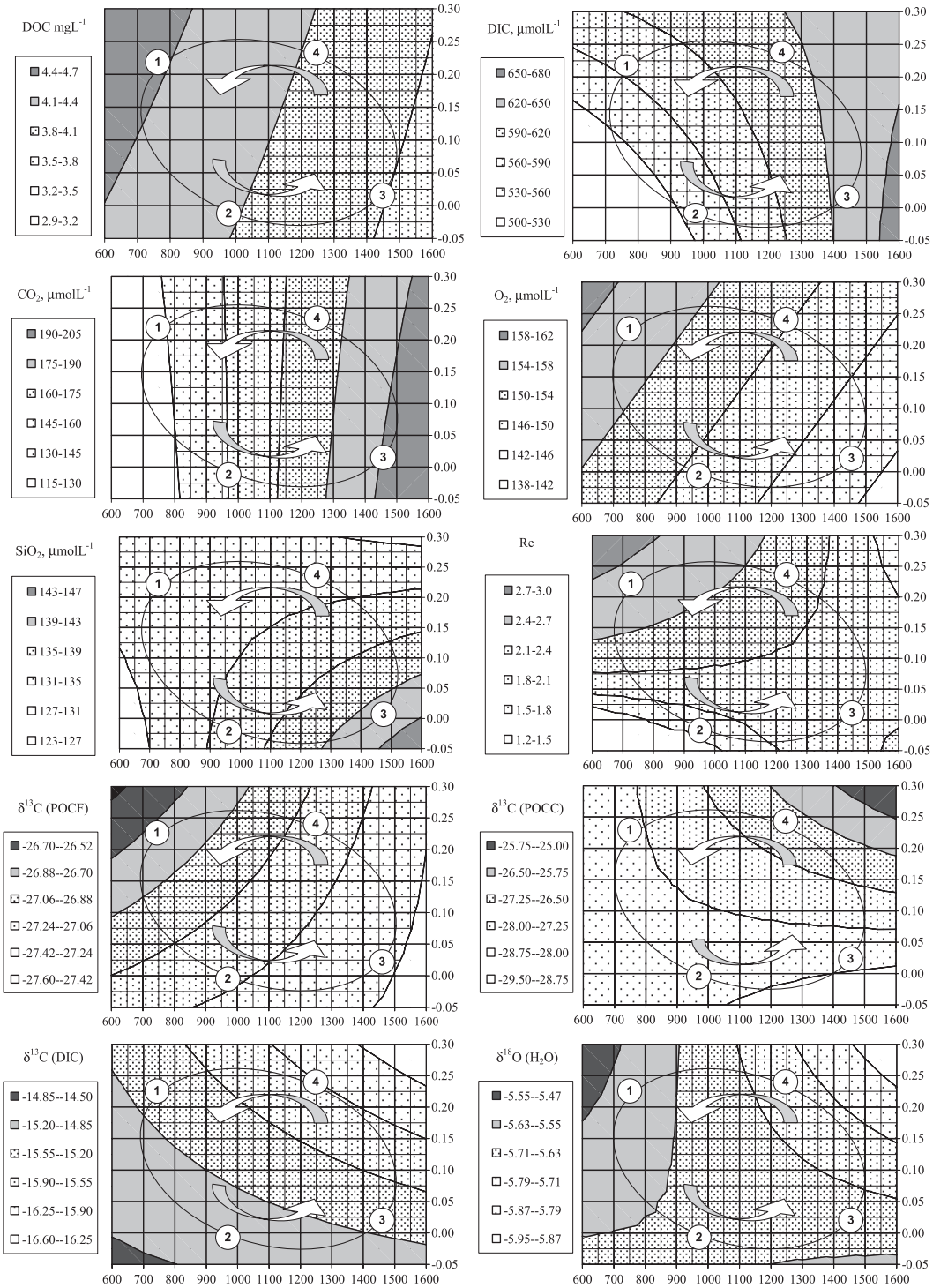

Figure A2. (*Continued*)

Solid load (CSS, FSS), organic carbon (POCC, POCF) and nitrogen (PONF, PONC) and C/N ratios.

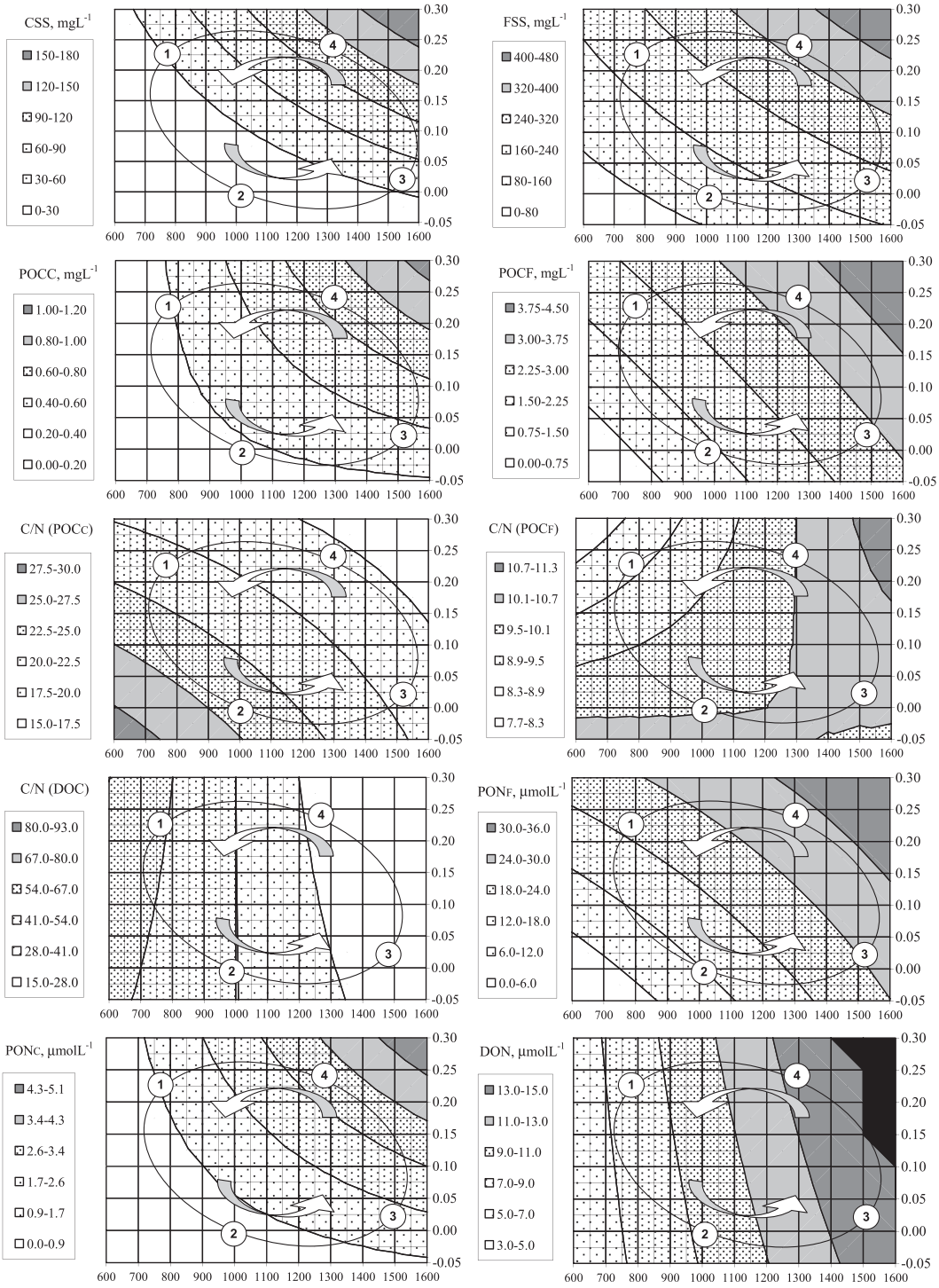

Figure A2. (*Continued*)

Norm of alteration: NaSil, $CaCO_3$, dolomite, components of CO_2 cycle and fluxes (FCO_2, WR)

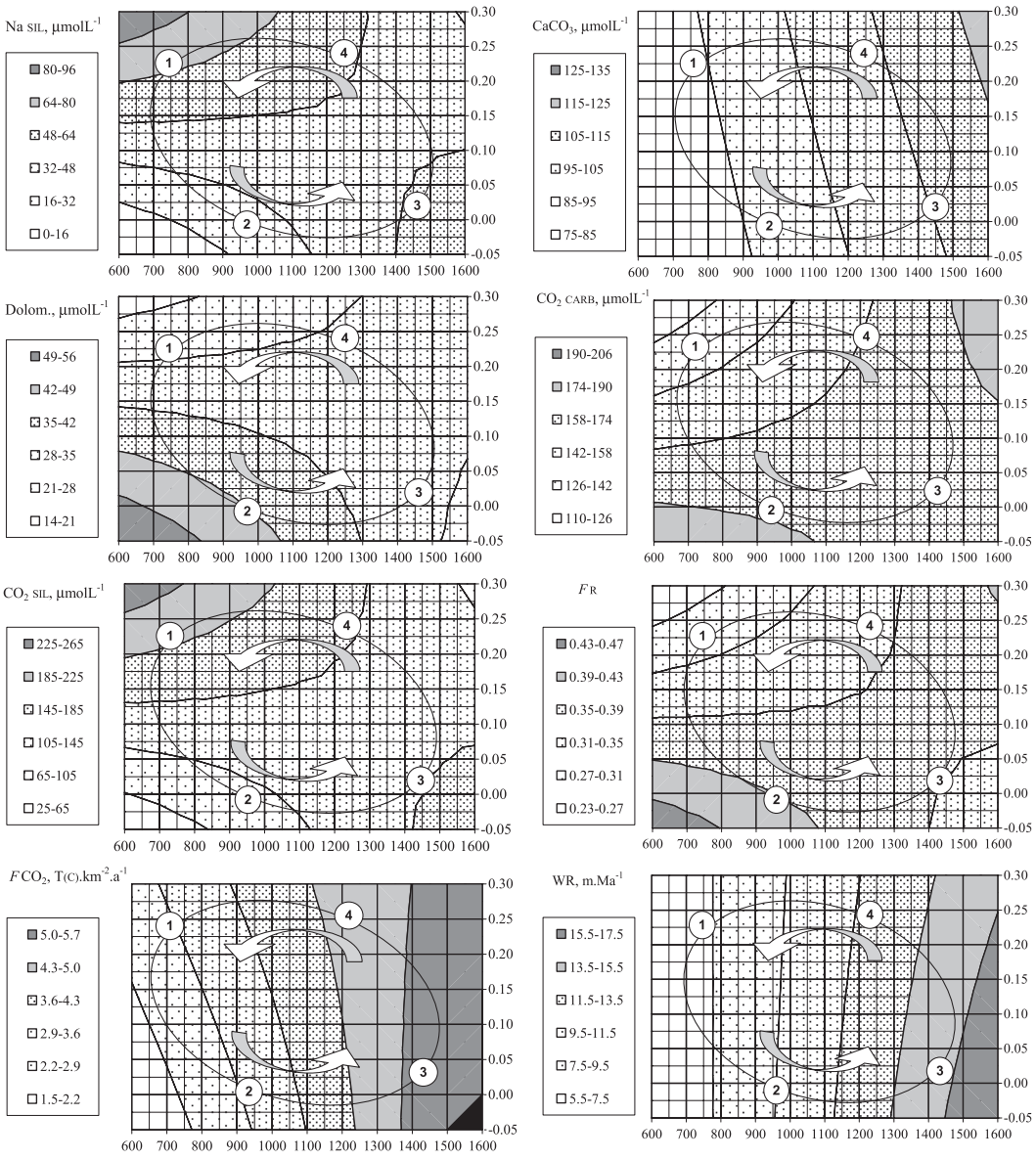

Figure A2. (*Continued*)

References

Amon, R. M. W., and R. Benner, 1996a: Bacterial utilization of different size classes of dissolved organic matter. *Limnol. Oceanogr.,* **41,** 41–51.

——, and ——, 1996b: Photochemical and microbial consumption of dissolved organic carbon and dissolved oxygen in the Amazon River system. *Geochim. Cosmochim. Acta,* **60,** 1783–1792.

Aufdenkampe, A. K., 2002: The role of sorptive processes in the organic carbon and nitrogen cycles of the Amazon River basin. Ph.D. thesis, University of Washington, 164 pp.

——, J. I. Hedges, A. V. Krusche, C. Llerena, and J. E. Richey, 2001: Sorptive fractionation of dissolved organic nitrogen and amino acids onto sediments within the Amazon basin. *Limnol. Oceanogr.,* **46,** 1921–1935.

Bustillo, V., 2005: Hydroclimatologie et Biogéochimie appliquées à l'aménagement des bassins fluviaux. Modèles de mélange. Diagnostic et prévision. PhD thesis, Institut National Polytechnique de Toulouse, 426 pp.

——, 2007: A large-scale synthetic model applied to the hydroclimatology and eco-geodynamics of the Amazonian basin. FAPESP Rep., Post-doctoral fellowship 2005-58884-5, 93 pp.

Dunne, T., L. A. K. Mertes, R. H. Meade, J. E. Richey, and B. R. Forsberg, 1998: Exchanges of sediment between the flood plain and channel of the Amazon River in Brazil. *Geol. Soc. Amer. Bull.,* **110,** 450–467.

Gonzales, A. L., J. Nonner, J. Heijkers, and S. Uhlenbrook, 2009: Comparison of different base flow separation methods in a lowland catchment. *Hydrol. Earth Syst. Sci.,* **13,** 2055–2068.

Guyot, J. L., 1993: *Hydrogéochimie des Fleuves de l'Amazonie Bolivienne*. Editions de l'ORSTOM, 261 pp.

Hamilton, S. K., S. J. Sippel, and J. M. Melack, 2002: Comparison of inundation patterns among major South American floodplains. *J. Geophys. Res.,* **107,** 8038, doi:10.1029/2000JD000306.

Hedges, J. I., W. A. Clark, P. D. Quay, J. E. Richey, A. H. Devol, and U. M. Santos, 1986: Compositions and fluxes for particulate organic material in the Amazon River. *Limnol. Oceanogr.,* **31,** 717–738.

——, G. L. Cowie, J. E. Richey, P. D. Quay, R. Benner, and M. Strom, 1994: Origins and processing of organic matter in the Amazon River as indicated by carbohydrates and amino acids. *Limnol. Oceanogr.,* **39,** 743–761.

Hooper, R. P., N. Christophersen, and J. Peters, 1990: End-member mixing analysis (EMMA): An analytical framework for the interpretation of streamwater chemistry. *J. Hydrol.,* **116,** 321–345.

Irion, G., W. J. Junk, and J. A. S. N. Mello, 1997: The large central Amazonian river floodplains near Manaus: Geological, climatological, hydrological and morphological aspects. *The Central Amazon Floodplain,* W. J. Junk, Ed., Springer-Verlag, 23–44.

Johnsson, M. J., and R. H. Meade, 1990: Chemical weathering of fluvial sediments during alluvial storage: The Macuapanim Island point bar, Solimões River, Brazil. *J. Sediment. Petrol.,* **60,** 827–842.

Junk, W. J., and M. T. Piedade, 1997: Plant life in the floodplain with special reference to herbaceous plants. *The Central Amazon Floodplain,* W. J. Junk, Ed., Springer-Verlag, 147–181.

Marengo, J. A., and R. L. Victoria, 1998: *Pre-Large-Scale Biosphere-Atmosphere Experiment in Amazonia Data Sets Initiative, 3 Vols*. Center for Weather Forecasting and Climate Study, National Institute for Space Research, CD-ROM.

Martinelli, L. A., R. L. Victoria, J. L. I. Dematte, J. E. Richey, and A. H. Devol, 1993: Chemical and mineralogical composition of Amazon River floodplain sediments, Brazil. *Appl. Geochem.,* **8,** 391–402.

——, ——, P. B. Camargo, M. Piccolo, L. Mertes, J. E. Richey, A. H. Devol, and B. R. Forsberg, 2003: Inland variability of carbon-nitrogen concentrations and $\delta^{13}C$ in Amazon floodplain (várzea) vegetation and sediment. *Hydrol. Proc.,* **17,** 1419–1430.

McClain, M. E., J. E. Richey, and R. L. Victoria, 1995: Andean contributions to the biogeochemistry of the Amazon River system. *Bull. Inst. Fr. Etud. Andines,* **24,** 425–437.

Meade, R. H., T. Dunne, J. E. Richey, U. M. Santos, and E. Salati, 1985: Storage and remobilization of sediment in the lower Amazon River of Brazil. *Science,* **228,** 488–490.

Meybeck, M., and C. Vörösmarty, 2005: Fluvial filtering of land-to-ocean fluxes: From natural Holocene variations to Anthropocene. *C. R. Geosci.,* **337** (1–2), 107–123.

Mortatti, J., 1995: Erosão na Amazônia: Processos, modelos e balanço. Ph.D. thesis, University of São Paulo, 150 pp.

Quay, P. D., D. O. Wilbur, J. E. Richey, J. I. Hedges, A. H. Devol, and R. L. Victoria, 1992: Carbon cycling in the Amazon River: Implications from the ^{13}C composition of particles and solutes. *Limnol. Oceanogr.,* **37,** 857–871.

Redfield, A. C., 1958: The biological control of chemical factors in the environment. *Amer. Sci.,* **46,** 206–226.

Richey, J. E., J. I. Hedges, A. H. Devol, P. D. Quay, R. L. Victoria, L. A. Martinelli, and B. R. Forsberg, 1990: Biogeochemistry of carbon in the Amazon River. *Limnol. Oceanogr.,* **35,** 352–371.

——, S. R. Wilhem, M. E. McClain, R. L. Victoria, J. M. Melack, and C. Araujo-Lima, 1997: Organic matter and nutrient dynamics in river corridors of the Amazon basin and their response to anthropogenic change. *Cienc. Cult.,* **49,** 98–110.

——, J. M. Melack, A. K. Aufdenkampe, M. V. Ballester, and L. L. Hess, 2002: Outgassing from Amazonian rivers and wetlands as a large tropical source of atmospheric CO_2. *Nature,* **416,** 617–620.

——, R. L. Victoria, J. I. Hedges, T. Dunne, L. A. Martinelli, L. Mertes, and J. Adams, 2008: Pre-LBA Carbon in the Amazon River Experiment (CAMREX) data. Oak Ridge National Laboratory Distributed Active Archive Center dataset. [Available online at http://daac.ornl.gov/cgi-bin/dsviewer.pl?ds_id=904.]

Tardy, Y., V. Bustillo, and J.-L. Boeglin, 2004: Geochemistry applied to the watershed survey: hydrograph separation, erosion and soil dynamics. A case study: The basin of the Niger River, Africa. *Appl. Geochem.,* **19,** 469–518.

——, ——, C. Roquin, J. Mortatti, and R. Victoria, 2005: The Amazon. Bio-geochemistry applied to the river basin management: Part 1. Hydro-climatology, hydrograph separation, mass transfer balance, stable isotopes, and modelling. *Appl. Geochem.,* **20,** 1746–1829.

——, C. Roquin, V. Bustillo, M. Moreira, L. A. Martinelli, and R. L. Victoria, 2009: *Carbon and Water Cycles: Amazon River Basin, Applied Biogeochemistry.* Atlantica, 479 pp.

Victoria, R. L., L. A. Martinelli, P. C. O. Trivelin, E. Matsui, B. R. Forsberg, J. E. Richey, and A. H. Devol, 1992: The use of stable isotopes in studies of nutrient cycling: Carbon isotope composition of Amazon varzea sediments. *Biotropica,* **24,** 240–249.

Weng, L. P., L. K. Koopal, T. Hiemstra, J. C. L. Meeussen, and W. H. Van Riemsdiejk, 2005: Interactions of calcium and fulvic acids at the goethite-water interface. *Geochim. Cosmochim. Acta,* **69,** 325–339.